الجـــمـــهـــوريـــة الجـــزائـــريـــة
الديمـــقـــراطـــيـــة الـــشـــعـــبـــيـــة
PEOPLE’S DEMOCRATIC REPUBLIC OF ALGERIA
وزارة التـــعـــلـــيـــم العـــالـــي
و البـــحـــث العـــلـــمـــي
MINISTRY OF HIGHER EDUCATION AND SCIENTIFIC RESEARCH
جـــامعة أبي بـــكـــر
بـــلـــقـــايـــد – تـــلـــمســـان –
ABOUBAKR BELKAÏD UNIVERSITY – TLEMCEN –
FACULTY OF TECHNOLOGIE

THESIS

Presented for obtaining the degree of PhD OF SCIENCE
In : mechanical engineering

Option : Energy

By : BELHADJ Omar

Subject

IMPROVING THE THERMO-ENERGETIC PERFORMANCES OF A SOLAR CHIMNEY THROUGH EXPERIMENTAL AND NUMERICAL METHODS

Publicly defended on: October the 14th 2023,

Jury members:

Mr. KORTI Abdelilah Nabil	Prof	Univ. Tlemcen	President
Mr. BENZENINE Hamidou	MCA	Univ. Ain Temouchent	supervisor
Mr. SAIM Rachid	Prof	Univ. Tlemcen	Co-supervisor
Mr. DRAOUI Belkacem	Prof	Univ. Bechar	Examiner
Mr. GUELLIL Hocine	MCA	Univ. Tlemcen	Examiner
Mr. BAHRAM Kaddour	MCA	Univ. Ain Témouchent	Examiner

الملخص

استخدام المدخنة الشمسية للتهوية له تأثير بيئي واقتصادي كبير للغاية .يوضح هذا العمل تأثير نسبة الارتفاع إلى طول القاعدة على كفاءة المدخنة الشمسية شبه المنحرفة على شكل موشور .تكمن الفكرة في إعطاء مزيد من المرونة للتصميم المعماري في المباني وإتاحة إمكانية الدمج مع أنظمة أخرى سلبية أو نشطة .تمت دراسة ثلاثة أشكال مختلفة(الارتفاع إلى طول القاعدة$h / l = 1$ ، $h / l = 1.5$و $h / l = 2$) بشكل تجريبي .تم تطوير واختبار ارتباطين للتنبؤ بمعدل التدفق وكفاءة المدخنة الشمسية ؛ تم إثبات التوافق الجيد مع النتائج التجريبية .أظهرت النتائج أن متوسط الكفاءة الأمثل معطى حيث h / l = 1.65. من أجل تحسين معدل التهوية ، تم أيضًا اقتراح هندسيتين جديدتين لعادم المدخنة الشمسية للحصول على فائدة تأثير الرياح عدديًا بعد التحقق من صحة أداة CFD مع النتائج التجريبية .أظهر نهج باستخدام برنامج RETScreen4 أن مدخنة شمسية بمساحة 1 متر مربع مثبتة في ظروف مواتية يمكن أن تغطي 37 مترًا مربعًا من مساحة المعيشة من حيث التهوية . بالنسبة للمنزل الذي تبلغ مساحته 120 مترًا مربعًا، يوفر نظام المداخن الشمسية ما يعادل 23.9 لترًا من البنزين سنويًا.

الكلمات المفتاحية: مدخنة شمسية، تهوية طبيعية، قوة طفو، مباني، راحة

Abstract

The use of a solar chimney for ventilation has a very significant environmental and economic impact. This work shows the effect of height to base length ratio on the efficiency in trapezoidal prism-shaped solar chimney. The idea is to give more flexibility to the architectural design in buildings and to offer the possibility of combination with other passive or active systems. Three different shapes (height to base length h/l=1, h/l=1.5 and h/l=2) have been experimentally studied. Two correlations to predict the flow rate and the efficiency of the solar chimney were developed and tested; good agreement with experimental results is proved. The results show that the optimum average efficiency is given where h/l=1.65.

In order to improve the ventilation rate, a new exhaust geometry of the solar chimney is also proposed to obtain the wind effect benefit numerically after the validation of the CFD tool with the experimental results.

An approach using RETScreen4 software showed that 1m² solar chimney installed in favorable conditions can cover 37m² of living space in term of ventilation. For a 120m² house, solar chimney system saves the equivalent of 23.9 liters of gasoline per year.

Keywords: solar chimney, natural ventilation, buoyancy force, buildings, comfort

Résumé

L'utilisation d'une cheminée solaire pour la ventilation a un impact environnemental et économique très important. Ce travail montre l'effet du rapport hauteur/longueur de la base sur l'efficacité d'une cheminée solaire en forme de prisme trapézoïdal. L'idée est de donner plus de flexibilité à la conception architecturale des bâtiments et d'offrir la possibilité de combinaison avec d'autres systèmes passifs ou actifs. Trois formes différentes (hauteur sur la longueur de base h/l=1, h/l=1,5 et h/l=2) ont été expérimentalement étudiées. Deux corrélations pour prédire le débit et l'efficacité de la cheminée solaire ont été développées et testées ; un bon accord avec les résultats expérimentaux est prouvé. Les résultats montrent que l'efficacité moyenne optimale est donnée là où h/l = 1,65. Afin d'améliorer le taux de ventilation, une nouvelle géométrie d'échappement de la cheminée solaire est également proposée pour obtenir numériquement le bénéfice de l'effet de vent après la validation de l'outil CFD avec les résultats expérimentaux. Une approche utilisant le logiciel RETScreen4 a montré qu'une cheminée solaire de 1m² installée dans des conditions favorables peut couvrir 37m² de surface habitable en termes de ventilation. Pour une maison de 120m², le système de cheminée solaire permet d'économiser l'équivalent de 23,9 litres d'essence par an.

Mots clés : cheminée solaire, ventilation naturelle, flottabilité, bâtiments, confort

ACKNOWLEDGMENTS

I want to express my gratitude to everyone who helped make my internship a success and who offered assistance to me while I was writing this thesis First and foremost , I would like to express my gratitude to my thesis director ***, Dr BENZENINE Hamidou*** *and* ***Pr SAIM Rachid*** *,for their understanding, their availability, and most importantly, their wise counsel, which fueled mu thinking and who have been a great support in the creation of this thesis, they taught me a lot about the challenges to be met in the educational world and shared their knowledge and experiences in this environment, while giving me their confidence and a large independence in the execution of rewarding missions.*

I also like to thank the University of Tlemcen's complete teaching staff.

Finally, to all those who, from near or far, contributed to the realization of this work ...

Thank you

BELHADJ OMAR

DEDICATION

IN LOVING MEMORY OF MY DEAREST FATHER

Table of Contents

Index of figures

Index of tables

Nomenclature and abbreviations

A	Section area	m^2
ACH	Air change per hour	h^{-1}
c	Sound speed in the gas	$m\ s^{-1}$
C_p	Specific heat	$J\ kg^{-1}\ k^{-1}$
$C_{\varepsilon 1}$, $C_{\varepsilon 2}$, $C_{\varepsilon 3}$, C_{μ}	Empirical constants for the *k-ε* turbulence model	
g	Acceleration due to gravity	$m\ s^{-2}$
H	Mass enthalpy	$J\ kg^{-1}$
h	Heat transfert coefficient	$W\ m^{-2}\ k^{-1}$
h/l	Solar chimney height to bases length ratio	
I	Incident solar radiation	$W\ m^{-2}$
K	Coefficient or constant (as mentioned separately)	
k	Turbulent kinetic energy	$J\ kg^{-1} = m^2\ s^{-2}$
L	Characteristic dimension	m
P	Pressure	$Pa= kg\ m^{-1}\ s^{-2}$
Q	Air volume flow rate	$m^3\ s^{-1}$
S	Absorber area	m^2
T	Temperature	°C or k
T_{ref}	Reference temperature	°C or k
U	Flow mean velocity	$m\ s^{-1}$
U_{wind}	Wind velocity	$m\ s^{-1}$
V	Velocity	$m\ h^{-1}$
v	Total volume of the room	m^3

- ## Greek symbols

α	Thermal diffusivity	$m^2\ s^{-1}$
β	Thermal expansion coefficient	k^{-1}
γ	Isentropic expansion factor (heat capacity ratio C_p/C_v)	
λ	Thermal conductivity	$W\ m^{-1}\ k^{-1}$
ρ	Density	$kg\ m^{-3}$
η	Thermal efficiency	

ν	kinematic viscosity	$m^2\ s^{-1}$
μ	Dynamic viscosity	$kg\ m^{-1}\ s^{-1}$
μ_t	Turbulent or eddy viscosity	$kg\ m^{-1}\ s^{-1}$
φ	Viscous dissipation function	
Γ_t	Eddy diffusivity	
ε	Turbulence kinetic energy dissipation rate	$m^2\ s^{-3}$
u_τ	Friction velocity	$m\ s^{-1}$
τ_w	Wall shear stress	$Pa = kg\ m^{-1}\ s^{-2}$
$\sigma_\varepsilon, \sigma_k$	Empirical constants for the for the *k-ε* turbulence model	

- ## Dimensionless terms

Re	Reynolds number
M	Mach number
Nu	Nusselt number
P_r	Prandtl number
Ra	Rayleigh number
G_r	Grashof number

- ## Abbreviations

ACH	Air change per hour
ASHRAE	American society of heating refrigerating and air-conditioning engineers
BSL	Baseline
CD	Convergent-divergent
CFD	Computational fluid dynamics
DES	Detached eddy simulation
DNS	Direct Numerical Simulation
DSF	Double skin façade
EAHE	Earth to air heat exchanger

GHG	Greenhouse gases
HRV	Heat recovery ventilation
HTD	Heat transfer device
HVAC	Heating, ventilation and air conditioning
IAQ	Indoor air quality
LES	Large eddy simulation
LHS	Latent heat storage
NC	Nocturnal cooling
PCM	Phase change material
PV	Photovoltaic
QUICK	Quadratic Upstream Interpolation for Convective Kinematics
RANS	Reynolds Averaged Navier-Stokes
RNG	Renormalization-group
RSM	Reynolds stress models
SAS	Scale-Adaptive Simulation
SBES	Stress-Blended Eddy Simulation
SC	Solar chimney
SDES	Shielded Detached Eddy Simulation
SIMPLE	Semi-Implicit Method for Pressure Linked Equations.
SST	Shear-stress transport
TDMA	Tri-diagonal matrix algorithm
WMLES	Wall-Modeled LES

Introduction

Introduction

In the future, the energy demand will multiplied, may double or even triple as the population grows and developing countries expand their economies. Energy is necessary for economic and social development and it opens an environmental protection task. In order to prevent energy sources and the environment, The challenge is to explore all aspects of the complex energy supply chain including production, distribution, consumption, waste, and energy efficiency, as well as the global carbon cycle, carbon sources and greenhouse gas emissions and their relationship to climate and environmental impact.

Building sector account today for about 40% of the final energy consumption**.** In view of the fact, designing buildings with very little energy consumption became very important; consequently, the use of passive techniques becomes a good strategy for energy efficiency in buildings. Generally, the energy requirement in buildings is affected by HVAC (Heating, Ventilation and Air Conditioning) systems. This had led to increase the use of sustainable building features like solar chimney, wind catchers, passive cooling and heating systems, Trombe wall, etc. as a technique to save building energy consumption.

Here, we focus on the ventilation that is the flow generated to refresh air in an interior space from the external ambient to provide comfort. The ventilation can be mechanical or natural. Natural ventilation is the flow generated by buoyancy driving force and by the wind through passive systems that become increasingly proposed because of their potential benefits in terms of operational cost, energy requirement and carbon dioxide emission. In addition, natural ventilation can save about 10% of cooling energy requirement and an order of 15% of fan power when climatic and operational conditions are suitable.

Solar chimney is a simple and efficient tool to improve natural ventilation. It transforms solar irradiation into kinetic energy to extract air from the interior space. In this thesis, the goal is to improve the solar chimney as a passive ventilation system through two main parts:

First, we extend the solar chimney geometry to give more flexibility to the architectural design in buildings and offer the possibility of combination with other passive or active systems. The new design proposed is the trapezoidal prim geometry, in some buildings, a solar chimney with this geometry is more aesthetically pleasing, easily to be installed and retrofitted even on existing buildings. An experimental study is performed to show the effect of height to base length ratio on the efficiency.

Second, improve the solar chimney efficiency through the wind effect. At this stage, a CFD tool is used after its validation by the experimental results.

To achieve this task, we propose a research methodology that consist of the following steps:

First, we presented a literature review ordered by the influencing factors on the solar chimney efficiency. Next, in order to understand the performance of solar chimneys, the related theory is offered with the experimental setup as well as the results and discussion. In the third step, The CFD procedure and the simulation results are presented and validated with the experimental data. Once the simulation tool validated, a geometry is designed especially at the chimney exhaust to obtain the wind effect benefits. As it is intriguing to investigate the solar chimney efficiency and ventilation performance and to make this study significant, finally, we presented the economic and environmental impact.

CHAPTER I

Literature Review

CHAPTER 1: LITERATURE REVIEW

I. Introduction

Providing a comfortable and healthy indoor environment for building occupants is the primary concern of HVAC engineers. Comfort and indoor air quality (IAQ) depend on many factors, including thermal regulation, control of internal and external sources of pollutants, supply of acceptable air, removal of unacceptable air, occupants' activities and preferences, and proper operation and maintenance of building systems. Ventilation and infiltration are only part of the acceptable indoor air quality and thermal comfort problem. HVAC designers, occupants, and building owners must be aware of and address other factors as well [1].

Therefore, any home or other space with occupants need to breathe, so it should have a ventilation system. To confirm that the indoor space is properly aerated, there are different sorts of ventilation system mainly:

- Natural Ventilation and
- Mechanical or artificial ventilation

In Natural Ventilation, air changes occur naturally through clearances in doors, windows, louvers, vents …etc, discharge vents should also be provided by this system; the ventilation can be achieved naturally but it depends upon the position of the house and the wind effect, the local climate, house design and human behavior.

Natural ventilation is induced either by thermal buoyancy or by wind. For example, when wind strikes the building, it creates positive pressure on the windward side and negative pressure on the leeward side of the building **[2].**

For its potential advantages in terms of energy requirement, economic and environmental benefits, Natural ventilation is an essential sustainable building design strategy which is known to mankind for ages, and it attracts a strong growing interest till now.

In some buildings, (large buildings, assembly halls, factories, theatres etc.), natural ventilation is insufficient or impossible, so mechanical system arrangement is required to create or increase the rate of airflow. In this case, air movement is generated by a system of fans, vents, and ducts. In this case, ventilation systems are associated with energy consumption. However, under the fact of severe environment problems and energy crises due to the overuse of fossil energy, renewable energy systems are largely developed in buildings, In view of the fact, the using of passive techniques becomes a good strategy for energy efficiency of buildings since the building sector consumes 35.3 % of final energy demand **[3].**

One of the sustainable systems used in buildings to reduce energy consumption and carbon
dioxide emission is to enhance the natural ventilation by solar chimney.

Solar chimney is a reliable passive system used in residential or commercial structure. It is a simple and efficient tool to improve natural ventilation; it transforms solar irradiation into kinetic energy to refresh air in an interior space from the external ambient to provide comfort. It can replace mechanical ventilation systems because of their potential benefits in terms of:

- Operational cost,
- Energy requirement,
- Carbon dioxide emission.

II. Fundamentals of solar chimney

Solar chimney is based on natural convection; the driving mechanism of the airflow inside chimney cavity is thermal buoyancy, which is caused by air density variation under temperature gradient. Between the indoor and chimney cavity air movement is forced by the generated pressure gradient.

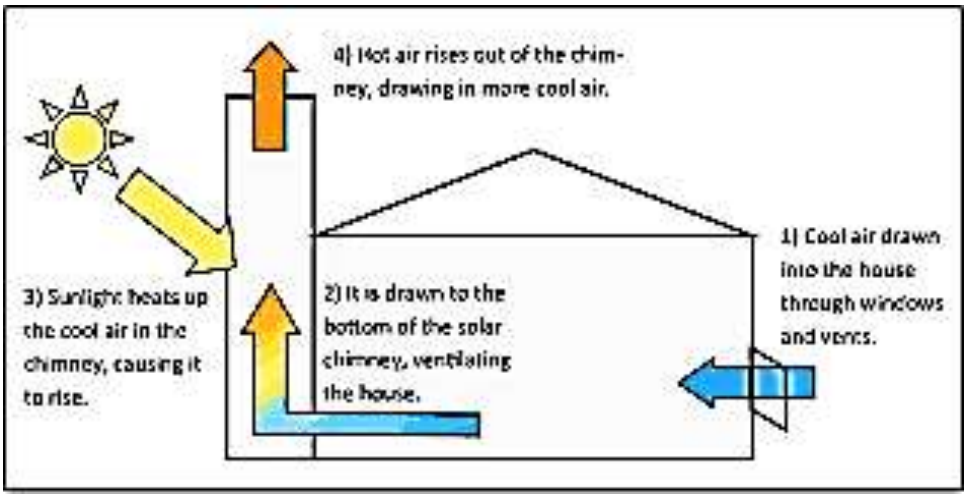

Figure I.1: Ventilation system assisted by solar chimney

Figure I.1 shows the schematic principle of ventilation system assisted by a typical vertical solar chimney. Heated by sunlight, Hot air rises out of the chimney driving the existing air from the interior into the bottom of the chimney, this movement create a pressure drop inside the house forcing fresh air to come into the house through the openings. In A room with an

integrated solar chimney, the ventilation rates is improved by 8–45% in summer and by 1.16–24.89% in winter **[4].**

Similar to a conventional chimney with solar assistance in the south face, solar chimneys gives a significant increase in ventilation rate. **Clito Afonso and Armando Oliveira[5]** compared the behavior of a solar chimney with a conventional one; they developed a thermal model for simulating solar chimneys, taking into account the wind effect. Their results show that solar assistance increases efficiency between 10% and 22%.

As a simple and practical technique, solar chimneys receive considerable attention by researchers in order to improve their performance. The main goal of designing a solar chimney is to optimize its performance with the lowest cost. For this challenge, it is important to identify the factors influencing the efficiency as means to improve it.

In this literature review, we will rather and classify solar chimneys by the main influencing factors, including:

- Installation
- Geometry
- Material usage, and
- Environment (location and meteorological conditions).

III. Influencing factors on solar chimney efficiency

III.1. Installation and position

Solar chimney is fundamentally a solar air heater. It generates air movement under buoyancy forces, when hot air rises and exits from the top of chimney cavity it forces cool air come into the building with continuous cycle. As a part of wall or roof, it can be installed vertically, horizontally or inclined.

III.1.1. Vertical solar chimney

In this case, solar chimney can have the same configuration as a Trombe wall as shown in **figure I.2.** Moreover, it can be installed on the roof or the combination of both roof and wall.

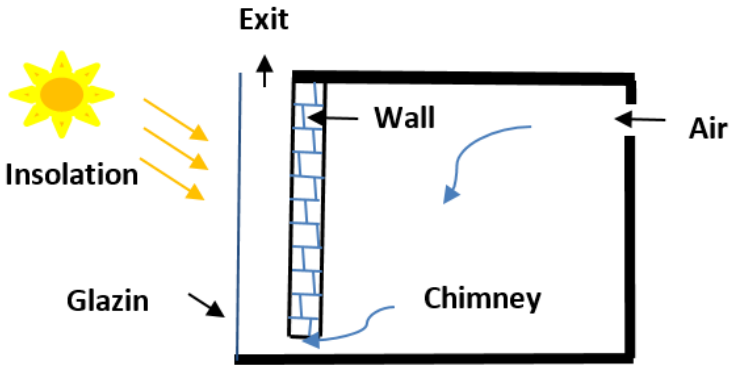

Figure I.2: Schematic diagram of wall-type vertical solar chimney

In this configuration the solar chimney play more than one role. It is a ventilation tool and it cools and heats depending on the climate; at the same time, it isolate the interior from the exterior. **Hoy-Yen Chan et al [3]** illustrate the different operation modes of vertical solar chimney wall integrated. They confirm that the purpose of the solar chimney is to generate airflow through a building, and it provides ventilation not only for cooling but also for heating. When solar chimney is attached to wall, the working mechanism is similar to Trombe wall; it operates as passive heating by supplying warm air, which is heated up by the solar collector into the room. For cold or moderate climate, when the outdoor temperature is lower than the indoor temperature, solar chimney is functioned as passive cooling. However, for hot climate, when the outdoor temperature is higher than the indoor, it operates as thermal insulation of the room. These three different modes are as illustrated in **Figure I.3**

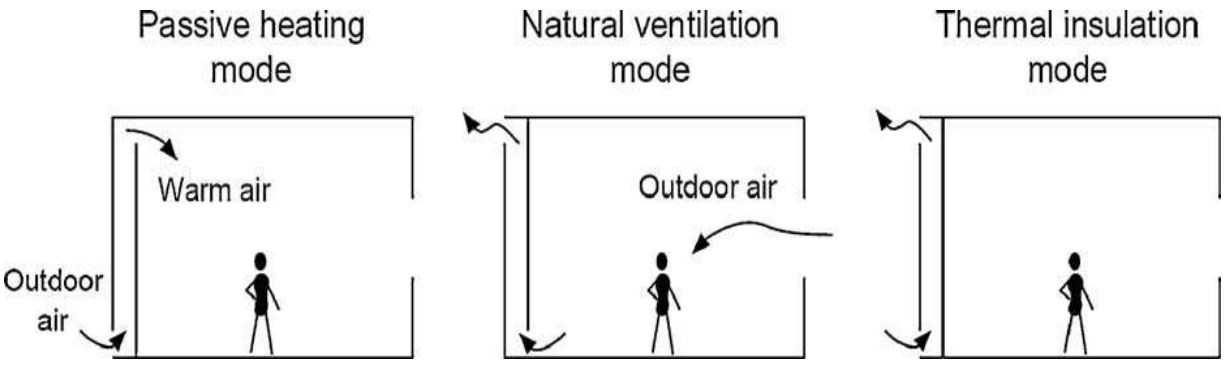

Figure I.3: Solar chimney operation modes

Many researches give attention to this configuration. **Karima E. Amori and Saif Watheq Mohammed [6]** used this configuration to investigate numerically and experimentally heat transfer process and fluid flow, they designed and tested the solar chimney by selecting

different positions of air entrance namely: bottom entrance, side entrance, and both side and bottom entrances. As a result, solar chimney of side entrance has the best thermal performance. They also studied the effect of integrating the chimney with paraffin (phase change material) to extend the ventilation hours after the solar absence or nighttime (by discharging the storage energy).

Wenting Ding et al. [7] used reduced scale model experiments and computational fluid dynamics (CFD) analysis to evaluate the natural ventilation performance of the prototype building as shown in **figure I.4**

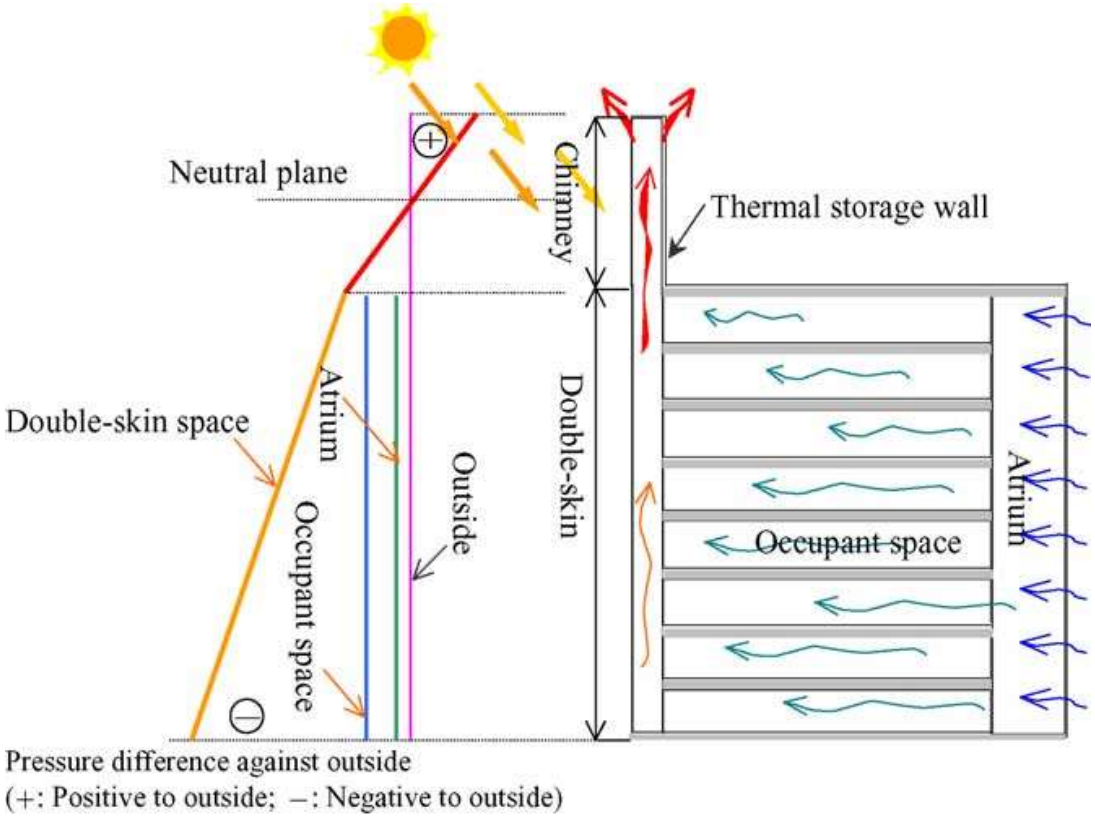

Figure I.4: Wenting Ding et al. **[6]** prototype

The solar chimney is installed vertically on the top of the building because increasing the height of the solar chimney makes more ventilation rate and is profitable to obtain favorable pressure difference distribution. In order to improve the stack effect, installing the solar chimney more than two floor high is recommended.

As shown in **figure I.5**, K.S. Ong **[8]** uses the wall-type solar chimney to develop a simple mathematical model. The physical model is similar to the Trombe wall, Steady state heat transfer equations were set up to determine the boundary temperatures at the surface of the glass cover, the rear solar heat absorbing wall and the air flow in the channel are defined using a thermal resistance technique.

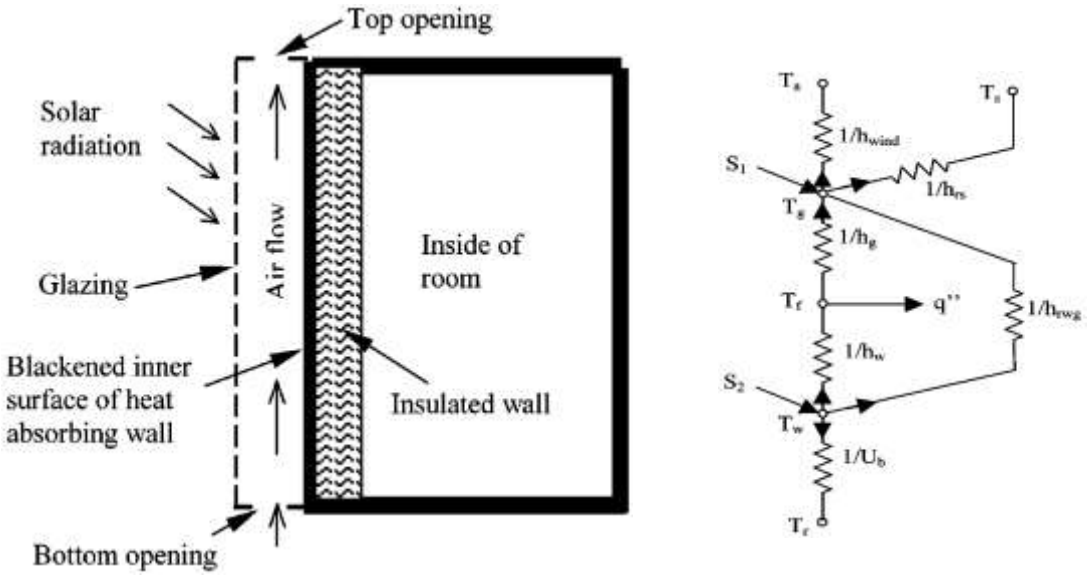

Figure I.5: Schematic diagram of a wall-type solar chimney and thermal network used by K.S. Ong **[8].**

Xinyu Zha et al. **[9]** examines the performance of a full-scale vertical solar chimney in a real building in East-ern China **(Fig. I.6).** It illustrate that the solar chimney is an effective technique to save energy for residential buildings in transition seasons in hot summer and cold winter area; The energy saving rate is around 14.5%

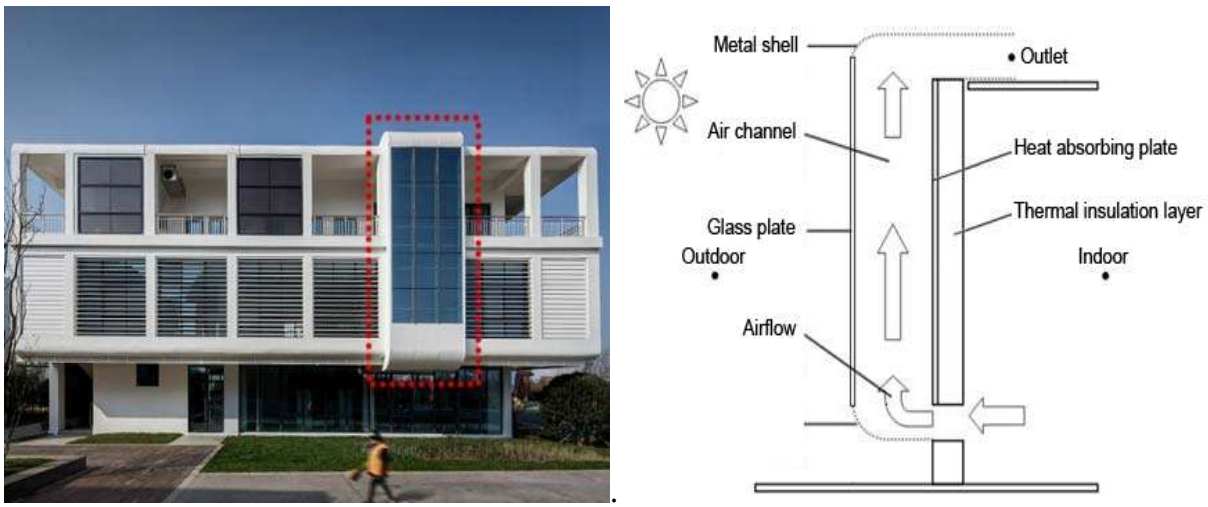

FigureI.6: Full-scale and the sketch of a vertical solar chimney **[9]**

FigureI.7 shows a vertical cutting-edge design in architecture used for ventilation at the Menomonee Valley in USA.

FigureI.7: Solar chimney MENOMONEE VALLEY 3700 W Pierce St Milwaukee, WI 53215, united states **[10]**

Further researchers **[11-17]** were interested by the vertical configuration to study and clarify experimentally or numerically other influencing factors such as the geometry or material usage.

III.1.2. Inclined solar chimney

For many situations, vertical chimney may be not the good architectural arrangement, e.g. when the roof is designed to be a solar chimney, this is why different configuration are studied to obtain the maximum thermal efficiency and flow rate. Wei et al. **[18]** examined numerically a combination of vertical and inclined solar chimneys in series (**Fig.I.8)**; which consisted of an inclined chimney on the roof attached to a vertical wall-type one at the south wall of two floors. They specifically examined the effects of the total length and width of the chimney, the inclined angle of the second floor inlet, the length ratio of the vertical to inclined section, and the chimney inclined angle on the chimney ventilation performance.

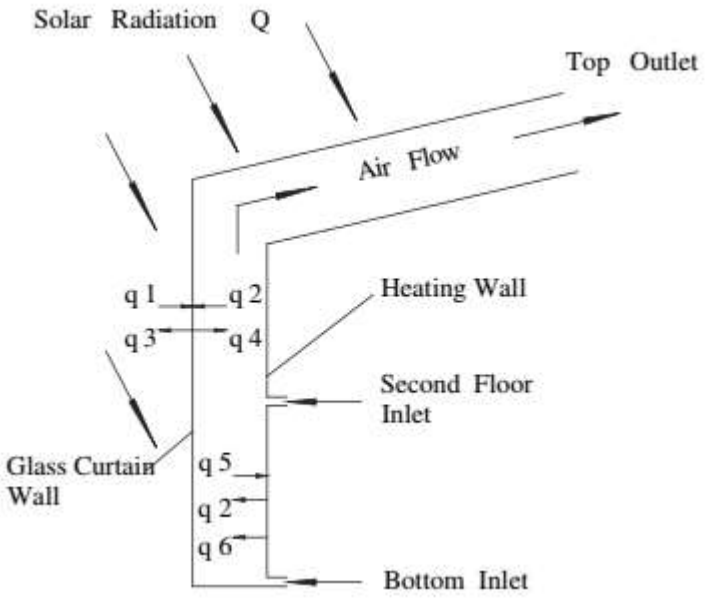

Figure I.8: Schematic configuration of connected inclined solar chimney on the roof and a vertical wall-type section **[18].**

The flow rate inside the chimney decreased with the increase of the length ratio of the inclined section to vertical section, the vertical section height should be as large as possible to increase the flow rate inside the chimney. With the increase of chimney inclined angle, the local resistance caused by the corners from decreases, the velocity distribution inside the chimney is improved and the airflow rate in the chimney increases. The ventilation performance was enhanced with the increase of total chimney length.

Bassiouny et al. **[19]** used the rooftop inclined configuration, as shown in **figure I.9**. by a numerical and analytical investigation, they proposed a correlation to estimate air change per hour depending on inclination angle, solar intensity, and chimney width.

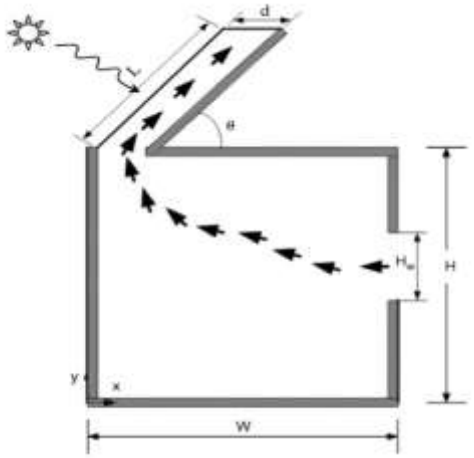

Figure I.9: Rooftop inclined solar chimney studied by Bassiouny et al. **[19]**

Mathur et al. **[20]** shows that the optimum absorber inclination varies from 40° to 60° depending upon the latitude of place; they announce that 45° inclination offers a rate of ventilation 10% higher compared to 60° and 30° inclinations for the location studied.

Jing Kong et al. **[21]** also found that the optimum inclination angle varies from 45° to 60°, depending on the latitude and season of operation.

Figure I.10 shows the experiment arrangement used by Sakonidou et al. **[22]** to develop a mathematical model. The model determine the inclination that maximizes natural airflow inside a solar chimney; it has a good agreement with the 1m solar chimney at different inclination.

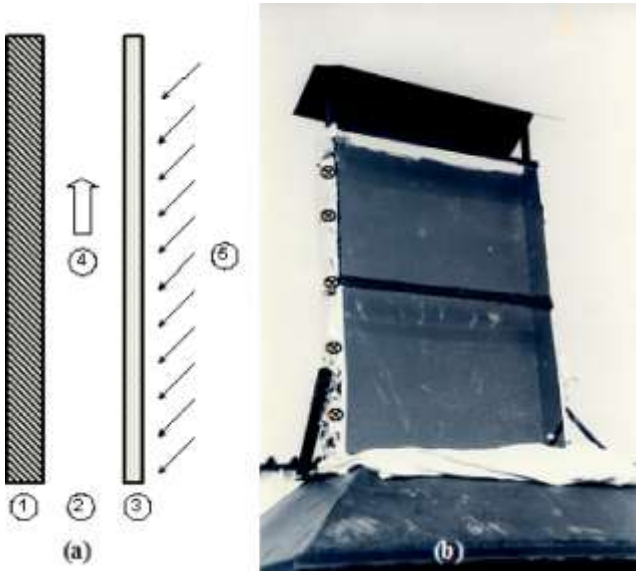

Figure I.10: Solar chimney configuration employed by Sakonidou et al. **[22]**. (a) Schematic of the cross-section of a solar chimney, 1: insulated black-painted absorber, 2: air entry, 3: glazing, 4: airflow direction, 5: incident irradiation and (b) photo of the chimney experiment.

By the experimental system illustrated in **figure I.11**, Chen et al. **[23]** shows that a maximum airflow rate was achieved at an inclination angle around 45° for a 200 mm gap and 1.5m high chimney, and the airflow rate is about 45% higher than that for a vertical chimney.

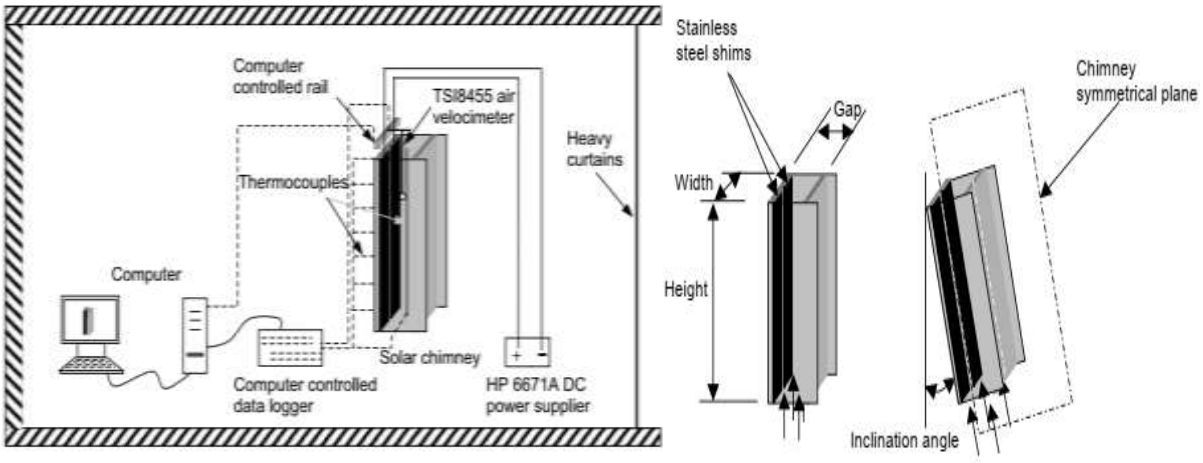

Figure I.11: Schematic view of the solar chimney experimental system Chen et al. **[23].**

Saifi et al. **[24]** confirmed again that the thermal pulling reaches the optimal value at chimney inclination angle of 45°.

The inclination angle is a very important parameter to increase the ventilation rate. In conclusion, airflow and thermal efficiency are like sine and cosine of inclination angle. Contrary to thermal efficiency; airflow increase by increasing the inclination angle, because small inclination angle showed a high flow resistance but greater angle affects irradiation capture and then thermal efficiency **(Fig. I.12).** The optimum angle depends on: geographic situation; time; and day of year. For fixed angle, many researchers agree for 45°.

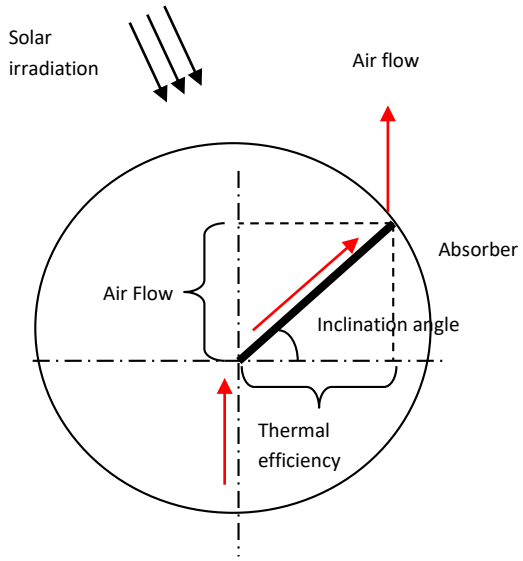

Figure I.12: Schematic optimum inclination angle of the solar chimney

III.2. Geometry

An efficient solar chimney should satisfy the building ventilation, its design must be adjusted in order to increase solar energy collection and air-suction even in low radiation

periods (such as dusk or dawn). **Figure I.13** shows an example of 4-sided (pyramid) design placed on the roof of the building and its CFD analysis. **[25]**

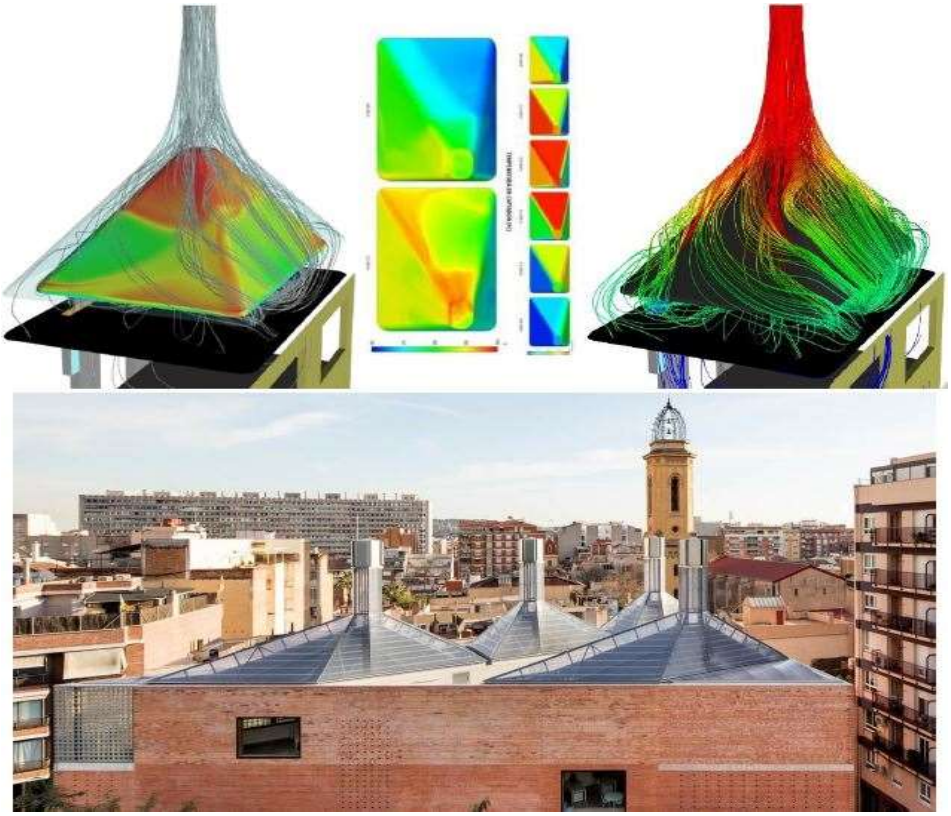

Figure I.13: Rooftop 4-sided solar chimney (pyramid shape) Singapore **[25]**

Except the shape, several other geometry factors impacts the efficiency of a solar chimney such as height, cavity gap, height/gap ratio, inlet area and its position, outlet area and inlet/outlet ratio.

As the chimney height increases, the ventilation rate is enhanced regardless of the locations (average increase rate of 74%); this is because the longer chimney air channel provides a longer path for the convective heat transfer between the absorber wall and the air **[12].** It can be known that the volumetric flow rate is linear to $H^{1/2}$, $H^{0.539}$, $H^{0.6}$, or $H^{2/3}$ **[27]**

Figure I.14 shows the Geometry of two-Stores vertical Solar Chimney models considered by **Hussein J. Mohammed et al. [28];** The results proved that the long vertical solar chimney was able to providing a best natural ventilation but with visible rising into the indoor temperatures.

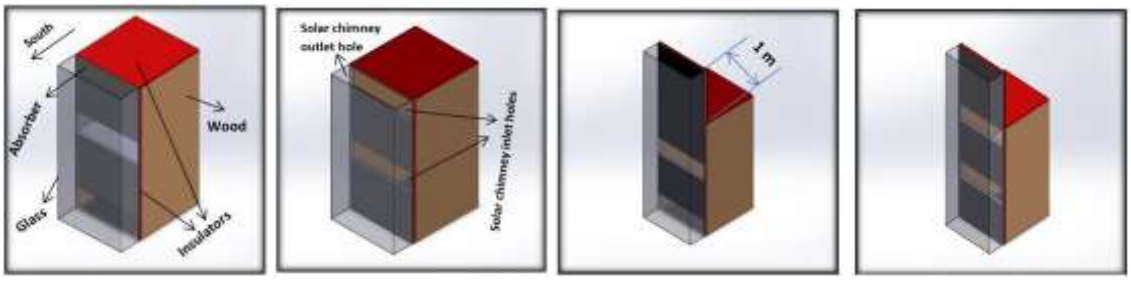

Figure I.14: Geometry models used by **[28]**

In natural convection, the flow behavior depends on Rayleigh number that indicates the strength of the buoyancy-induced flow. It is directly attached to Grashof number that designate the ratio of buoyancy forces to viscous forces.

The Nusselt number identifies if heat transfer is primarily conductive or convective, it represents the ratio of convective heat transfer over conductive heat transfer. Large values of the Nusselt number indicate that the heat transfer is convective and turbulent.

All this numbers and others like Reynolds and Prandtl depends on the geometry of the flow path. This is why the geometry considerations are the subject of many researches.

Other phenomena occur inside the solar chimney that affect the flow rate as well as the ventilation efficacy. The reverse flow is the most important, it occurs at the exit of the channel and the penetration depth on which is dependent the Rayleigh number. In order to enhance the ventilation performance and maximize the flow rate for high Rayleigh number applications, it is necessary to minimize the reverse flow entering from the exit. **Rakesh Khanal and Chengwang Lei [26]** proposed a different solar chimney design with an inclined passive wall (glazing) and a vertical active wall (absorber). In comparison with the vertical passive wall configuration, this design is proposed for maximizing the ventilation performance for high Rayleigh number applications. This improvement is achieved by controlling or suppressing the reverse flow and minimizing its penetration depth.

Guohui Gan [14] compared the results between cavities with horizontal and vertical inlets. He found that the ventilation rate and heat transfer coefficient are dependent on the domain size and inlet position as well as the cavity size and heat distribution ratio. The ventilation rate is larger for cavities with horizontal inlet than those with vertical inlet are.

Yicun Hou et al [17] purpose used a solar chimney with a variable gap-to-height ratio (0.1-0.5) to develop a prediction method. They investigate the induced airflow characteristics such as temperature distribution, velocity distribution, and the reverse flow phenomenon. The results show that the distribution of induced air temperature and velocity were non-uniform and

that the optimum chimney gap-to-height ratio was estimated to be 0.4. The reverse flow phenomenon appeared at the outlet when the chimney gap was 400 mm, and continued to penetrate downward into the chimney as the chimney gap increased.

For the configuration presented in **figure I.8**, the velocity decrease by increasing the chimney channel width. The optimal width corresponding to the maximal flow rate varied with the total chimney length. The optimal ratio of length to width was found to be 12:1. The improvement of the fluid flow as well as the increase in the flow rate can be achieved by decreasing the inclined angle of the second floor chimney inlet. The optimal inclined angle was found to be 4° by a numerical study **[18].**

T V Nguyen and **Y Quoc Nguyen [29]** tested a solar chimney connected to three floors of a three – story building with different inlet locations and sizes with a constant gap of the air channel. The results showed that the location of the air inlet (near the floor or the ceiling), the number of the inlet in each floor, and the size of the inlet strongly influenced the induced flow rate through each room. However, an equal ventilation rate for all floors has not been achieved, so different gaps were designed at different floors. It is deduced that the air gap should increase with the height of the chimney to achieve similar flow rates for each floor. Therefore, they proposed a chimney configuration with larger air gaps at the higher floors as illustrated in **figure I.15.**

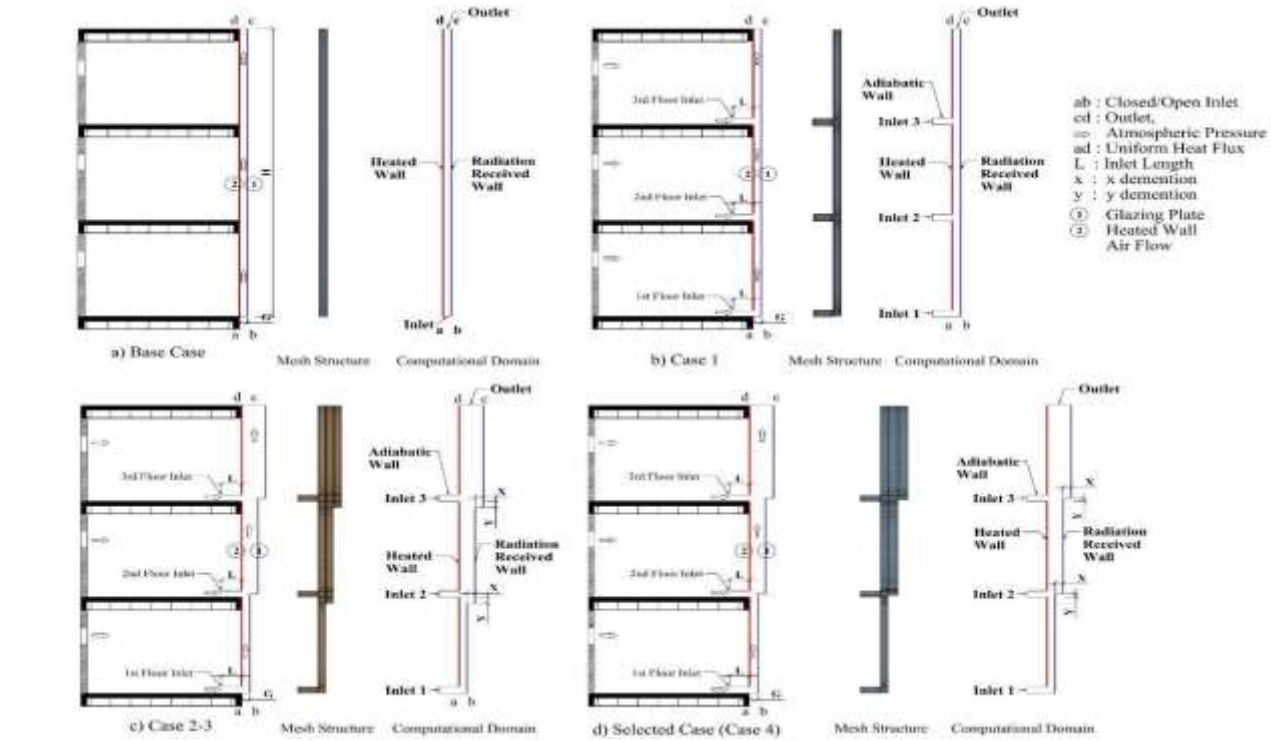

Figure I.15: Schematic of a solar chimney of a three – story building with constant and variable gaps **[29].**

Based on the analysis of the geometry of solar chimney, researchers have widely carried out investigations on solar chimneys to enhance the ventilation performance. Considering different design factors, most of the research goal is to boost the system performance by changing the configuration related to the installation and the geometry of the solar chimney itself as well as the geometric aspect of the room openings. In fact, improving natural ventilation system should consider all the parameters corresponding to the optimum efficiency.

III.3. Material usage

The desired ventilation rate, and thermal behavior of the naturally ventilated building can be achieved by changing the system or building materials; in solar chimney system, optical parameters such as solar transmittance and reflectance of glazing cover, solar absorptivity and emissivity of the absorber and heat storage materials and insolation characteristics are very important as detailed bellow.

III.3.1. Glazing

The glazing is an important component in solar chimney; it aims to enhance thermal buoyancy through the heating processes by the greenhouse phenomenon inside the cavity. For better performances of a solar chimney, several properties of glazing are important, such as transmissivity, reflectivity and absorptivity. An experimental study by **Lee et al. [30]** indicated the influences of several critical parameters on the thermal performance and outlet temperature of solar chimneys; they concluded that a high value of the glazing transmissivity could increase the outlet temperature and the performance. They also observed that influences of the transmissivity of chimney glazing on temperature rise is more obvious than those from reflectivity and absorptivity.

G. Gan and S.B. Riffat [11] investigated the effects of solar heat gain and glazing type on solar chimney performances; it was shown that double or even triple glazing should be used in order to maximize the ventilation rate in a cold winter; this is due to possible condensation or downdraught. The use of single glazing led to moisture condensation on its interior surface. In reality, the negative effect of condensation on the chimney performance is serious because of the latent heat of condensation. In real situations, the condensate on the glass reduces ventilation rates. Condensation would also occur on double-glazing when the outdoor air temperature was reduced to -13°C, resulting in a decrease of the ventilation rate. However, the risk of condensation was, avoided by using triple glazing. In addition, **Harris and Helwig**

[31] indicated that the double-glazing gave a slight improvement in performance, but it was not significant enough to be cost effective.

III.3.2. Absorber

Solar chimney is designed to obtain heat from the sun to enhance ventilation. The system is desired to maximize solar gain and thereby maximize the ventilation effect **Bansal et al [32].** The absorber is the key element in this mechanism; its role is to absorb the maximum of the incoming energy from the sun**. Kwang Ho Lee and Richard K. Strand [12]** indicate that the air flow rates showed improvements of 57%, 42% and 45% as the solar absorptance is improved from 0.25 to 1.0 in three typical United States cities; the maximum absorber surface temperature reaches 114°C under solar absorptance of 1.0 compared to 72°C under 0.25 solar absorptance. The ventilation rate increases as the solar absorptance is enhanced, regardless of the location because the absorber temperature increases with the solar absorptance. In agreement with the common sense, this indicates that absorbers with higher solar absorptance should be used to reach the higher natural ventilation. In addition, the absorber plate with a black-polished surface significantly influence the outlet air temperature and performance of solar chimneys **[30]. Pillai P.K.C and Agarwal R.C [33]** found a linear relationship between the absorptance and the efficiency of solar collector with a more than 0.8 absorptance.

Since the radiative heat transfer is not negligible in solar chimney systems, Emissivity of the absorber is an important parameter because the radiative heat flux is a strong function of the surface emissivity. For many practical materials, the surface emissivity is in the range of 0.7–0.9; **Nouanégué, H. F, and Bilgen, E [34]**

The absorber function can also be boosted by integrating PCM (phase change material) in order to extend the ventilation period. A thermal storage layer with phase change material under the cavity is utilized to absorb as much heat as possible from the hot air in chimney cavity. By integrating PCM, a solar chimney can collect solar energy during sunlight period and discharge heat at night. Thereby improving the solar chimney performances and extend the ventilation period.

Among many studies on improving thermal comfort by integrating PCM in building systems, **Dordelly et al. [35]** investigate the influence of integrating a PCM on the performance of two laboratory prototypes solar chimneys to improve ventilation efficiency; The results obtained show that PCM integration provides a higher ventilation rate and a slower decrease during the discharge period (6 h discharge). By adding fins in PCM as shown in **figure I.16**, a

solar chimney can effectively store solar energy during the day and release heat at night. Thereby improving the solar chimney performances and making the indoor temperature uniform. For the PCM based solar chimney system, the use of fines results in a 20% enhancement in the room's mean temperature and more non-uniform airflow is gained for the case of finned absorber with PCM compared with the non-finned case **[36]**.

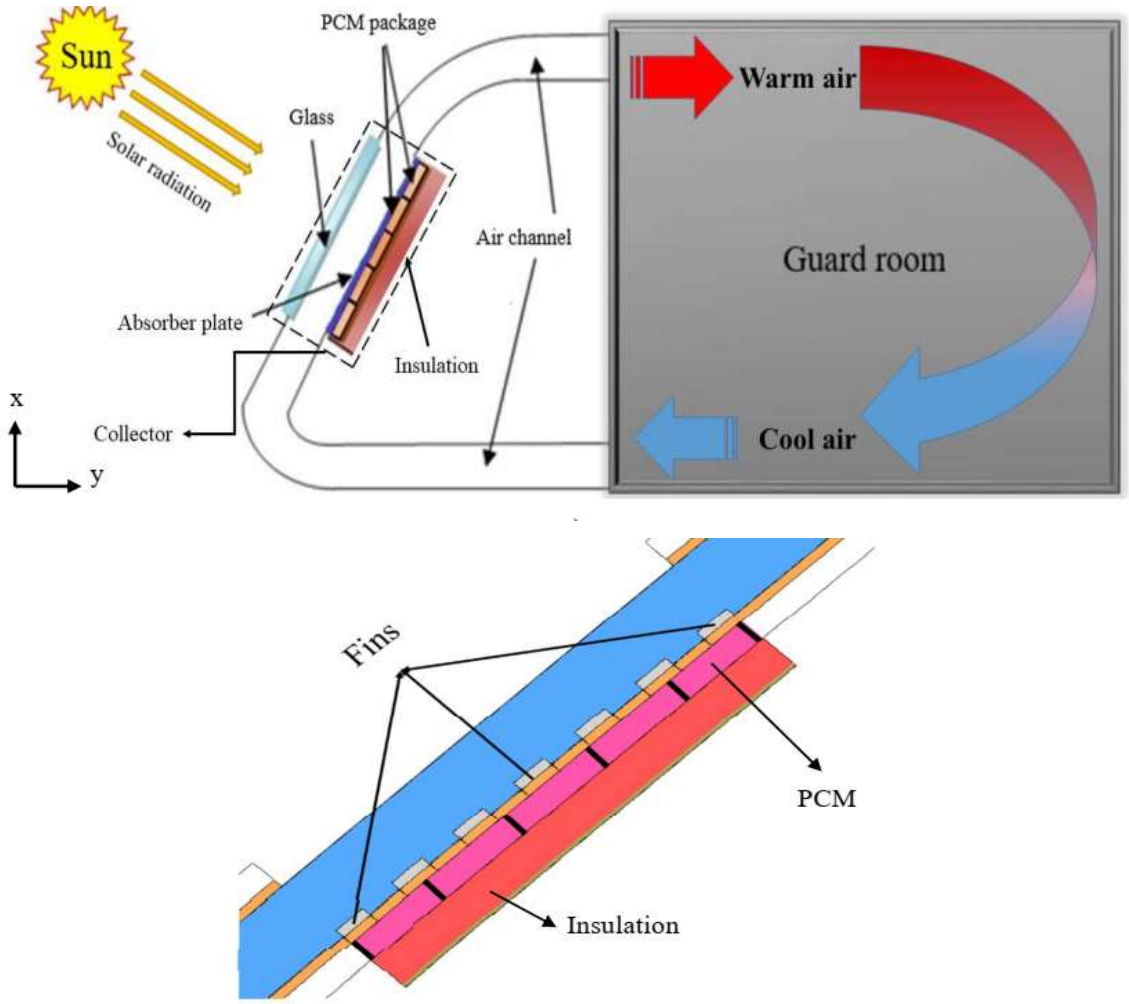

Figure I.16: Guardroom within a solar chimney equipped with fin-based absorber and PCM. **[36]**

The numerical analysis of **B. Buonomo et al. [37]** was proposed to evaluate the thermal and fluid dynamic behavior of the solar chimney integrated with a Latent Heat Storage (LHS) system. A two-dimensional numerical investigation on a prototypal solar chimney system integrated with an absorbing capacity wall in a south facade of a building is presented. The capacity wall is composed of a high absorbing plate and an assigned thickness of Phase Change Material (PCM). The chimney consists of a converging channel with one vertical absorbing

wall and the glass plate inclined of 2° with respect to the vertical. The chimney is 5.0 m high, with the channel height equal to 4.0 m, whereas the channel gap is at the inlet equal to 0.34 m and at the outlet it is 0.20 m. The thermal energy storage system is 4.0 high.

Moreover, most significant research work on applications of the LHS in buildings and PCMs characteristics such as thermo-properties and heat transfer are reviewed by **Souayfane, F et al. [38]**

An illustration of the process of energy storage by PCMs is presented in **Figure I.17** recapitulate the thermal energy storage (TES) systems integration in buildings. Using phase change materials (PCMs) for Thermal Energy Storage (TES) strategies in buildings can meet the potential thermal comfort requirements when selected properly, **Khaireldin. F et al [39].**

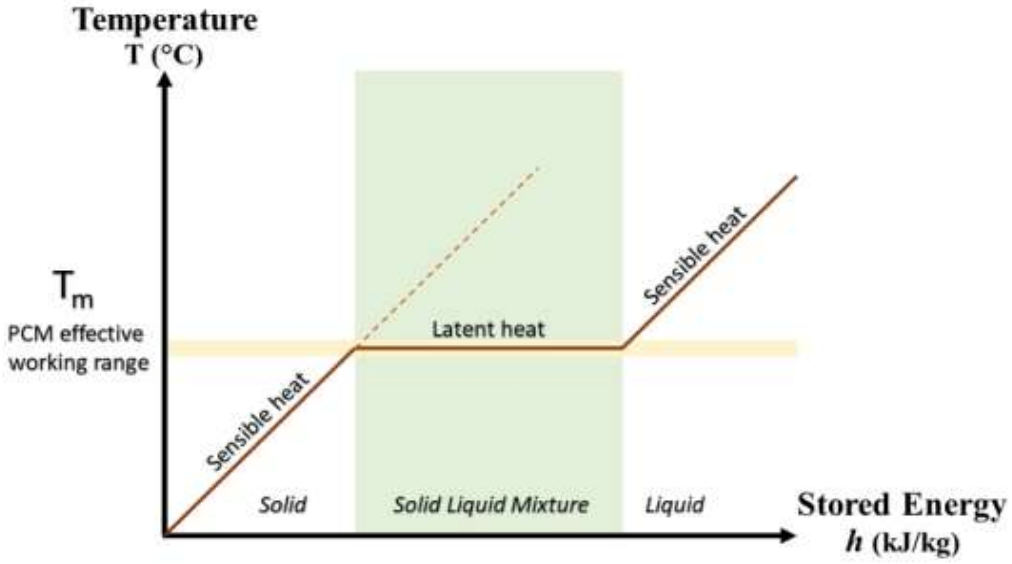

Figure I.17: Latent energy storage by PCM **[39]**

Figure I.18. recapitulate the thermal energy storage (TES) systems integration in buildings. Using phase change materials (PCMs) for Thermal Energy Storage (TES) strategies in buildings can meet the potential thermal comfort requirements when selected properly **[39].**

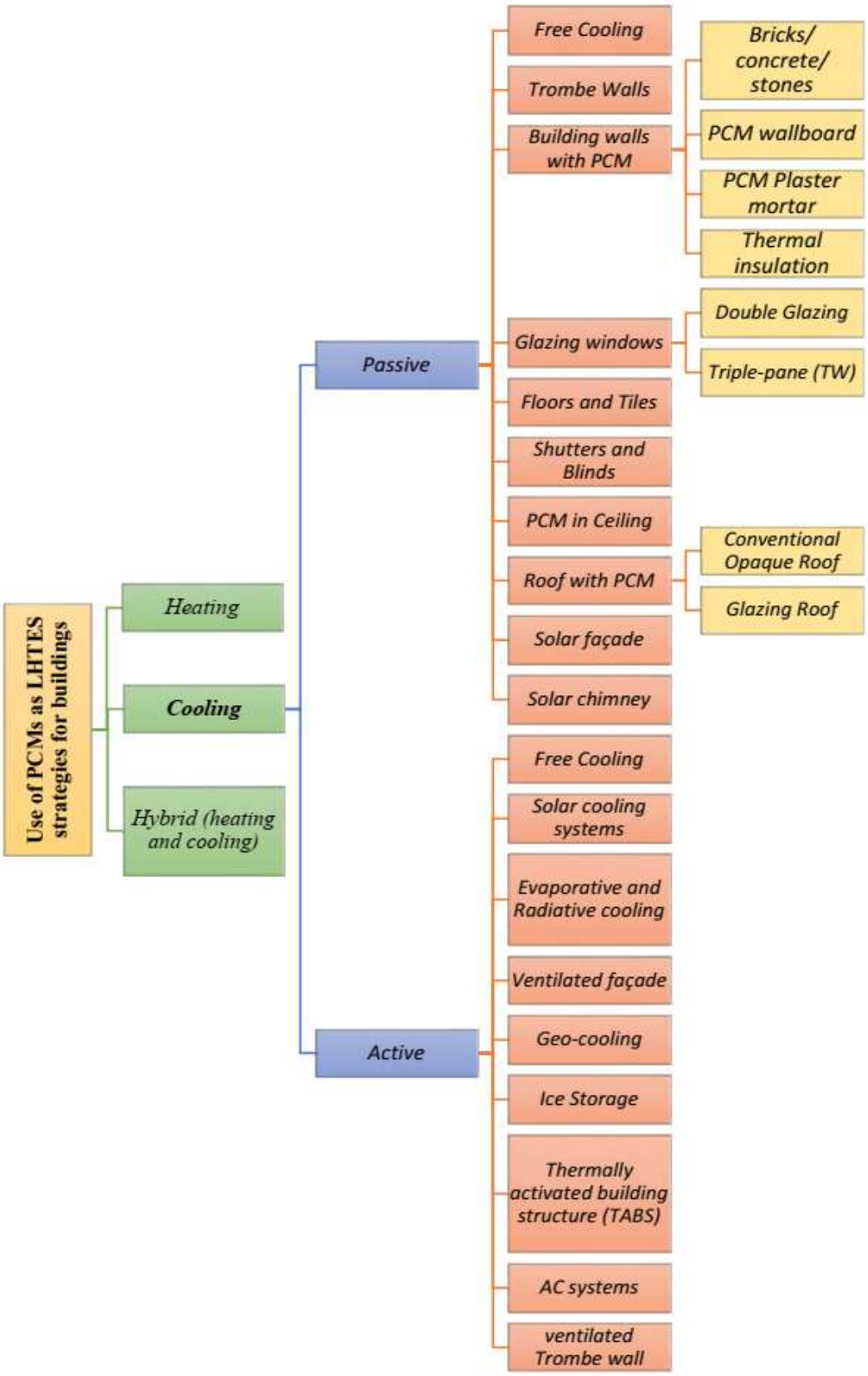

Figure I.18: Schematic for applications of PCM–TES in buildings **[39]**

III.3.3. Thermal insulation materials

Generally, thermal insulation is a very important factor in buildings energy efficiency. In solar chimney applications, **T. Miyazaki et al. [40]** noticed that the improvement of an insulation level of the inner wall of the solar chimney, the ventilation rate was increased. Comparing the case of no solar chimney with 25 mm wall insulation and the case of 1 m solar chimney with 100 mm wall insulation, the global thermal load mitigation throughout the year was estimated as 12%.

Clito Afonso and Armando Oliveira [5] advice to use outside insulation in the brick wall to take advantage of solar gains because if insulation is not used, solar assistance efficiency decreases by more than 60%. They also confirm that a thickness of 5 cm insulation wall of the cavity is optimum and sufficient.

Therefore, to improve the solar chimney performance, it is imperative to take care of the thermal insulation of cavity wall.

III.4. Environment

External environmental conditions and the sensitivity of system performance to these conditions define the system applicability. Evidently, ambient conditions such as radiation intensity, ambient temperature, wind speed and direction, and humidity affect the solar chimney and then the ventilation performance especially when it is used for cooling or heating mode or in combination with other systems. Over all, the performance of a thermal chimney was heavily dependent on the climate of the location **[12].**

III.4.1. Solar radiation

Radiation is the main input of the solar chimney system, so all the outputs especially, the ventilation rate and the exhaust temperature will be affected by the solar radiation variation.

The rise in the received radiation enhances the system performance. In the sunny regions, the implementation of this system is generally economically justified. The latitude and the meteorological conditions are the most determinative factors in the quantity of received solar radiation. In order to receive the maximum flux in a fixed position, the installation is strongly dependent on the geographic latitude; usually, solar chimneys are south facing.

The effect of solar flux on collector performance is very significant, as the incident solar flux increases; the overall collection efficiency also increases **[33].**

On the other hand, an experimental study carried out by **Lee et al. [30]** showed an increase in efficiency only from 20% to 24% when solar radiation rises from 340 to 960 W/m^2.

In solar chimney applications, it is important to collect the maximum of the solar radiation even for poor increase in efficiency because the input energy is free, renewable and sustainable. The most important is to reach the correct ventilation rate. Within this context, the theoretical study of **Arce, J et al. [41]** indicate that when solar irradiance increases from 100 to 700 W/m^2, the maximum instantaneous efficiency of the system varies from 28% to 37%. Correspondingly, the volumetric flow rate increases from 61 to 147 m^3/h. we notice that the efficiency rise by 9%, however, the flow rate increasing is 141%.

III.4.2. Humidity, ambient temperature, and pollution

Humidity, ambient temperature and pollution infect directly the solar radiation that is the most important input factor in solar chimney. **Abdullahi et al. [42]** indicate that high relative humidity is associated with low global solar radiation and low relative humidity is associated with high global solar radiations; high average temperature is associated with high global solar radiations and low average temperature is associated with low global solar radiation. In addition, the influence of humidity on solar radiation is greater.

Global solar radiation is the combination of normal direct and diffuse solar radiation received on a horizontal plane **[43].** Global solar radiation strongly depends on the sky clearness **[44],** which is infected directly by pollution.

III.4.3. Wind effect

External wind shows significant influence on the solar chimney performance **[27]**. In some configuration, other arrangements are included at the exhaust of the chimney in order to enhance the ventilation efficiency. **Figure I.19** shows wind-assisted solar chimneys used to drive natural ventilation through the classrooms of a school in Damascus; The chimneys are designed to use wind to create negative pressure at the top of the chimney which improves the stack air movement inside the chimney **[45].**

Figure I.19: Traditional ventilation and cooling techniques with solar chimneys and wind catchers in a Damascus School **[45]**

In the situation below, the wind acts at the exit of the chimney. The pressure difference generated by the wind near the outlet area of the chimney structure is added to the buoyancy effect; in this way, the driving force for the ventilation is higher.

The wind also act at the suction side. Due to wind, high-pressure is generated from one side of the building pushes air into the building, while the solar chimney is installed on the low-pressure side.

As an answer to residential building where only single-sided ventilation can be performed, chimneys can help enhance the ventilation. They can be mainly buoyancy-driven (e.g. solar chimney) or mainly wind-driven (e.g. windcatcher) **[46].** Mahnoosh.E and Abbas.M **[47]** designed a zero-energy passive system to ventilate the building and provide comfortable conditions ,as shown in **figure I.20**, the solar chimney system is assisted by the wind catcher to improve the ventilation.

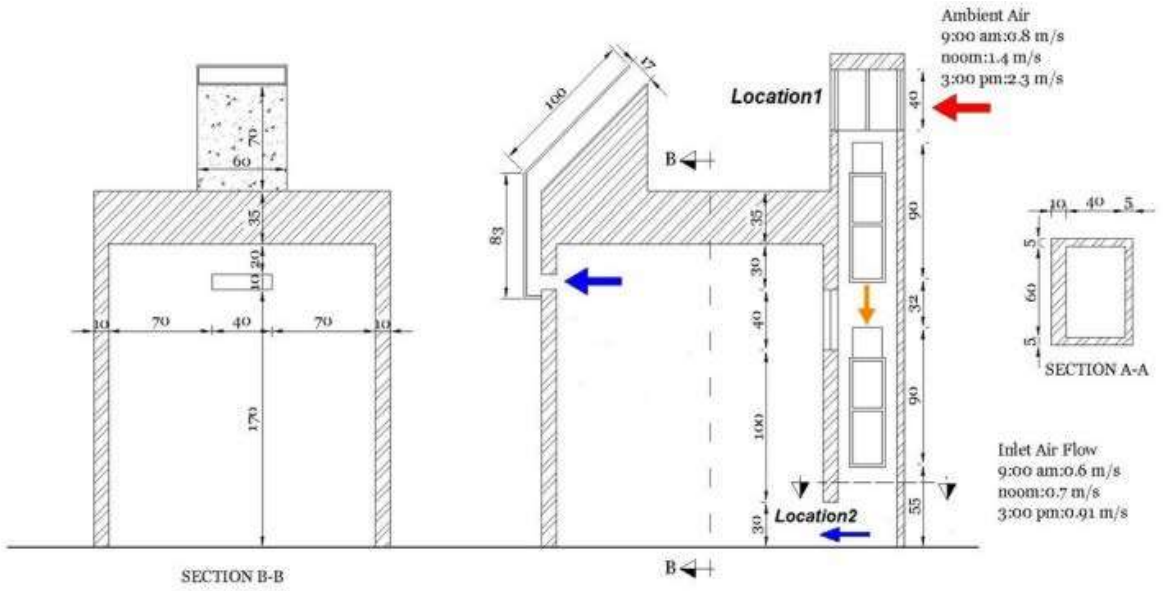

Figure I.20: Solar chimney with wind catcher and evaporative cooling cavity **[47]**

A wind-induced channel was designed and studied by Ning G et al [48] to enhance indoor natural ventilation under a combination of wind and solar energy action as shown in **figure I.21**. It is found that the ventilation rate and indoor air quality is greatly influenced by the external wind speed.

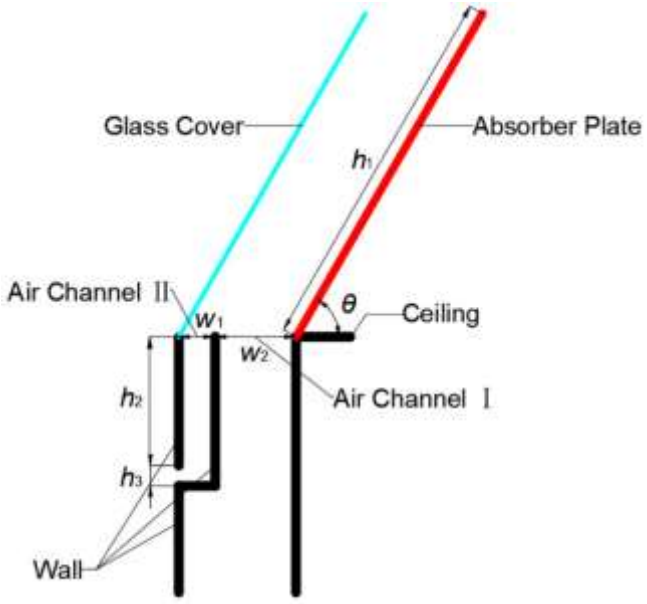

Figure I.21: Solar chimney with induced wind channel **[48]**

Due to the random nature of wind, the design of a solar chimney can be done without considering the wind effect, which will underestimate the real ventilation rates **[5].**

III.4.4. Altitude

Ammar Bouchair [49] shows the relationship between the altitude and the performance of solar chimney. It introduces the basic concepts and governing equations for modelling heat transfer and air flow rates within the solar chimney at various altitudes. The results obtained showed that the altitude has modest influence on the performance of the solar chimney if ambient temperature is supposed constant for all altitudes. However, in real climatic conditions, the ambient temperature is altitude dependent. In these conditions, the altitude significantly influences the performance of the solar chimney.

IV. Combined sustainable systems with solar chimney

Solar chimneys stand out among passive systems not only because of the convenience of their structural features but also because they are used for heating and cooling modes through the installation of dampers and openings or by a combination with other systems which makes the structure more sustainable **Zhang et al. [50]. Figure I.22** presents two modes that a solar chimney can accomplish for cooling and heating.

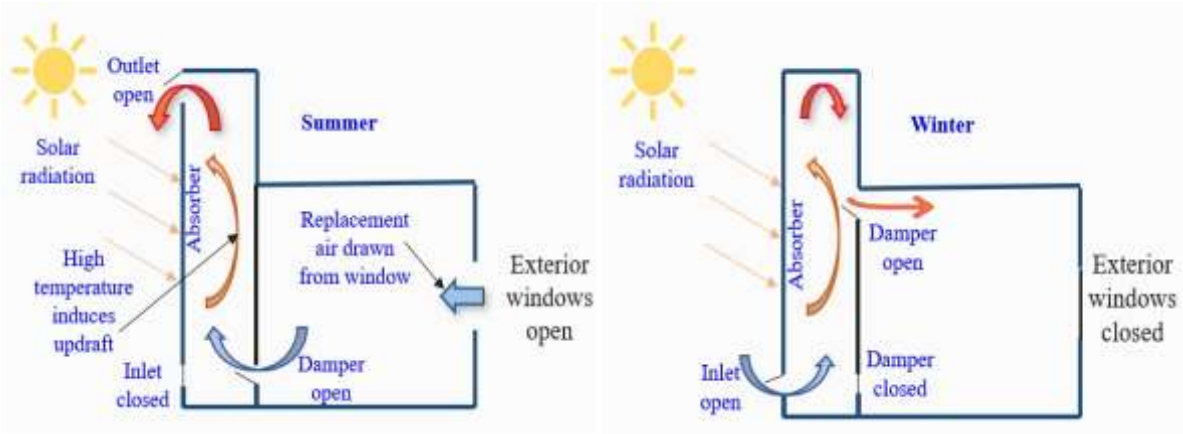

Figure I.22: Schematic of solar chimney under heating and cooling modes Asfour. O, **[51].**

In parallel to the stand-alone passive ventilation system, researchers mostly combined solar chimneys with other systems and applied them to actual structures. **Figure I.23** illustrates the combination possibilities of solar chimney with other sustainable passive systems.

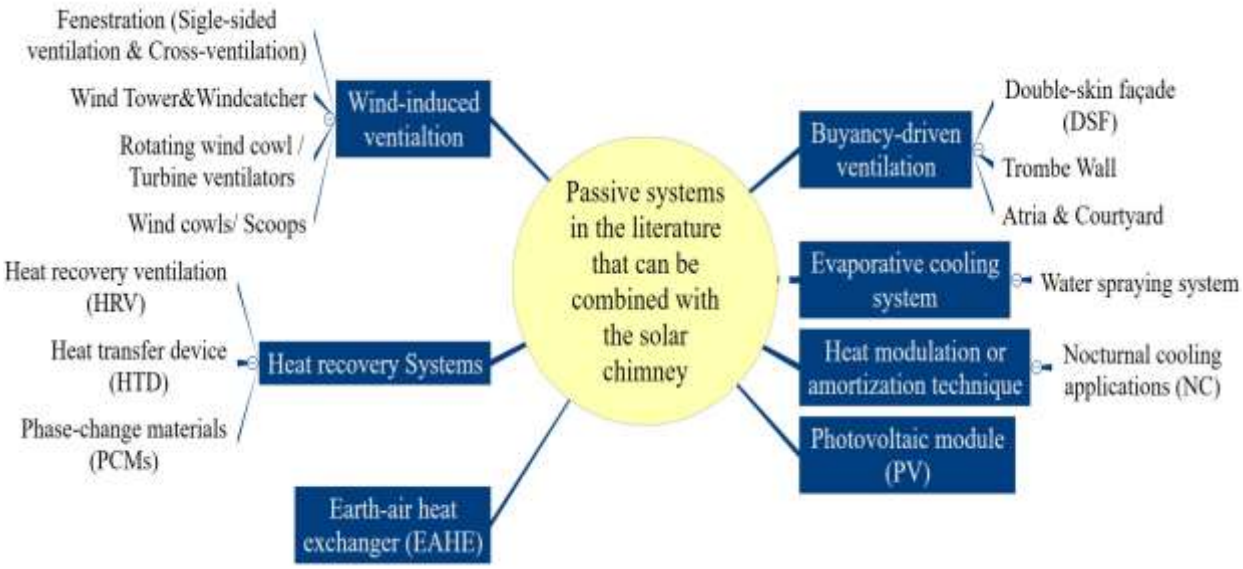

Figure I.23: The coupling of passive systems and a solar chimney **[50]**

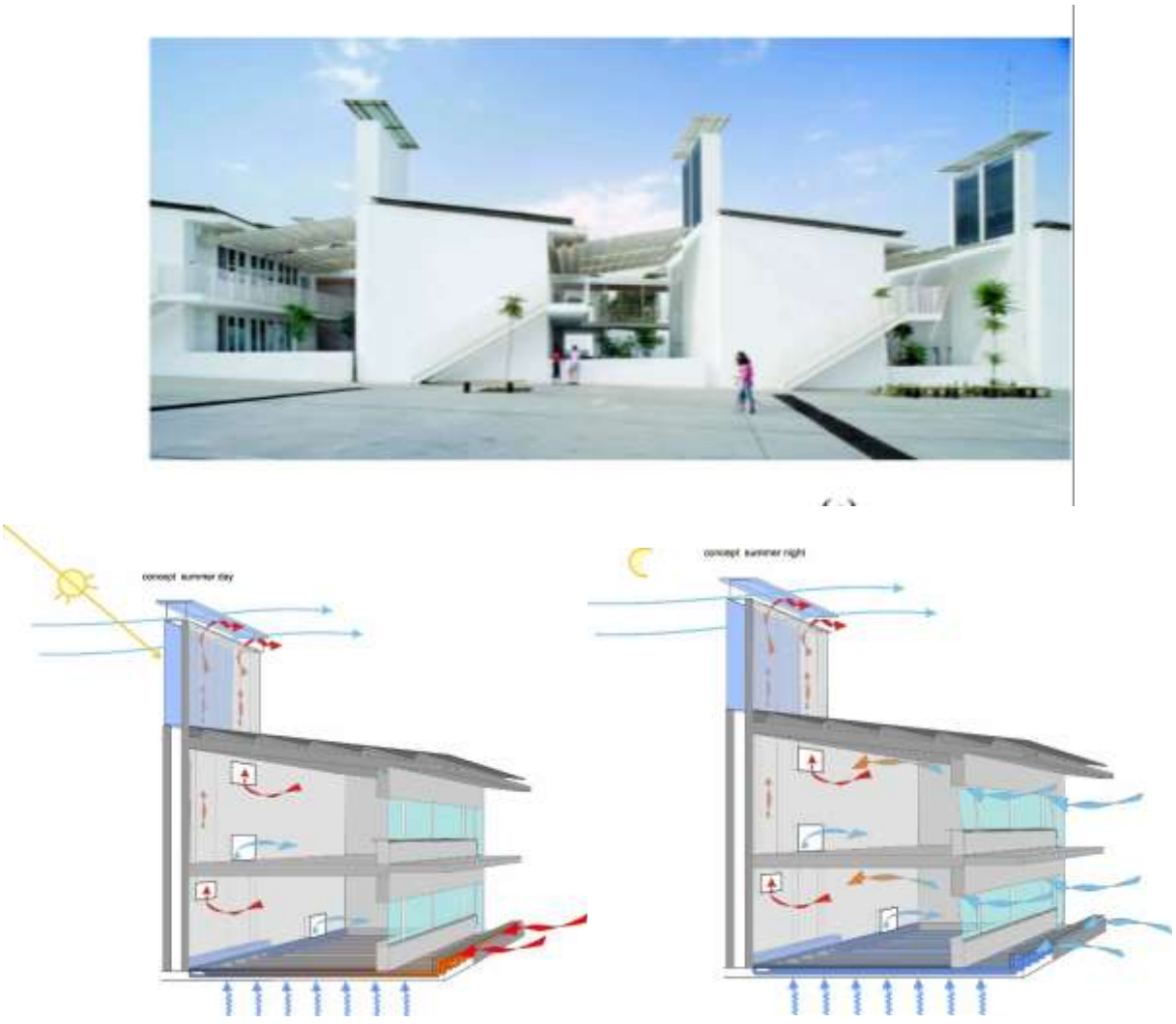

Figure I.24: Ventilation and traditional cooling techniques in a school in Damascus **[45]**

As an example of sustainable passive systems, **Figure I.24** shows the French School in Damascus, a sustainable design is adapted to the local climate conditions. The passive ventilation and cooling of the school's classrooms is achieved through a combination of passive design strategies. The school is made up of small buildings, each with two stacked classrooms, connected via small courtyards. The goal was to find a low-technology solution for ventilation and conditioning of the rooms using local materials as a modern interpretation of the traditional architecture. Syria has a dry desert climate with hot days and cold nights. Wind-assisted solar chimneys are used to drive natural cross-ventilation through the classrooms. The chimneys are south faced with a polycarbonate sheet to trap solar radiation and enhance the stack effect. The wind creates negative pressure at the top of the chimney, which further improves the stack air movement inside the chimney. During the day, outdoor intake air comes either directly from the shaded microclimate of the courtyards or is pre-cooled using miniature earth ducts made up of pipes embedded in the ground floor slab. Operable louvers at the air intake and exhaust provide ventilation control. During nighttime, the thermal mass of the chimney releases heat stored during the day and continues to draw air through the open windows and the earth ducts. Cool night air flushes the classrooms, cooling down the thermal mass and providing comfort for the following day. A shading device above the courtyards provides solar protection during summer days, and is opened for cooling at night by radiation to the sky. In winter, the operation is reversed to capture solar gains and prevent their loss to the clear night sky **[45].**

The underground temperature is less than the annual average air temperature in summer and higher in winter. The average underground temperature below 2-3m depth is 20-25˚C **Shiv L et al [52].** This discard between the geothermal soil and the ambient temperature can be used for heating in winter and cooling in summer. Many researchers use this geothermal heat exchange system called earth to air heat exchanger (EAHE), **Shiv L and Subhash C.K [53],** by a CFD approach, concluded that by integrating EAHE the room temperature can be maintained by 27-30°C, at 5 ACH in peak summer and winter conditions. The cooling gain is 5.30-6.72 kW at 40°C ambient temperature and 400-1000 W/m^2 solar radiations. **Yongcai Li et al [54]** used a full-scale experimental test rig, as shown in **figure I.25**, the results indicate that the buoyant driving force induced by the solar chimney drives 252 m^3/h of air through the EAHE during the daytime. Furthermore, an airflow rate of 50-70 m^3/h was achieved with zero solar radiation intensity due to the building thermal mass. The temperature decreases by 12.5 C

from the inlet to the outlet. Therefore, the maximum total cooling capacity of the EAHE were approximately 1398.0 W.

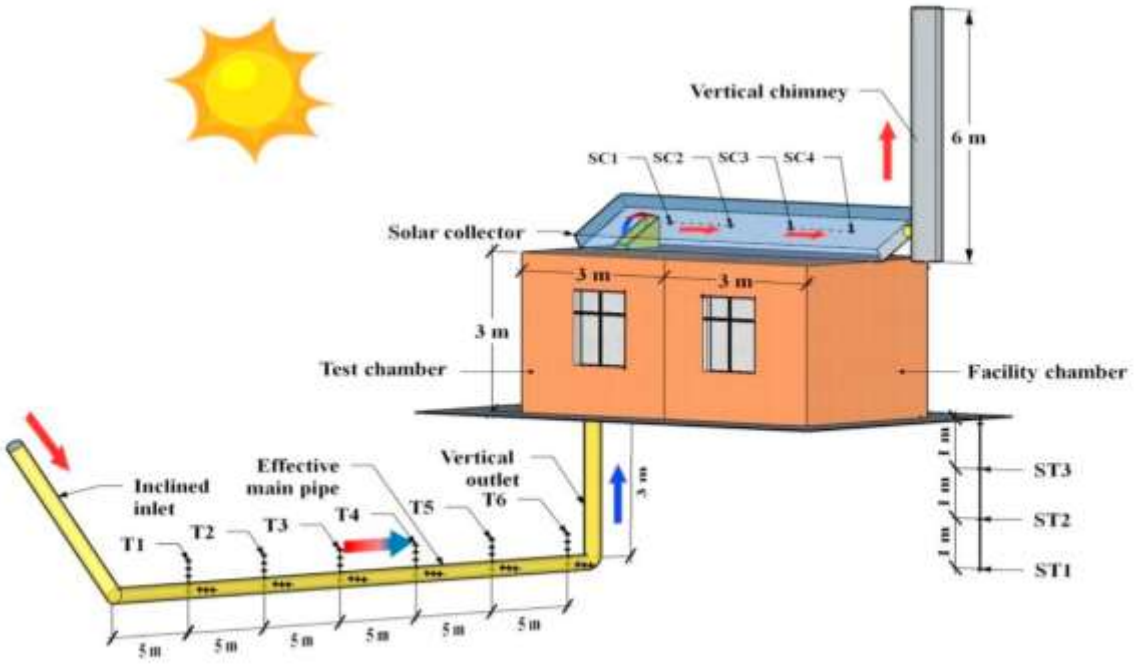

(a) Schematic view of SCEAHE system

(b) Image of solar chimney

Figure I.25: Model of solar chimney and EAHE used by **Yongcai Li et al [54]**

As shown in **figure I.25**, the use of solar chimney (SC) together with earth to air heat exchanger (EAHE) is also introduced by **M. Maerefat and A.P. Haghighi [55];** based on the

required indoor thermal comfort conditions, the numbers of required solar chimneys and EAHEs are calculated and some features of such a system is presented.

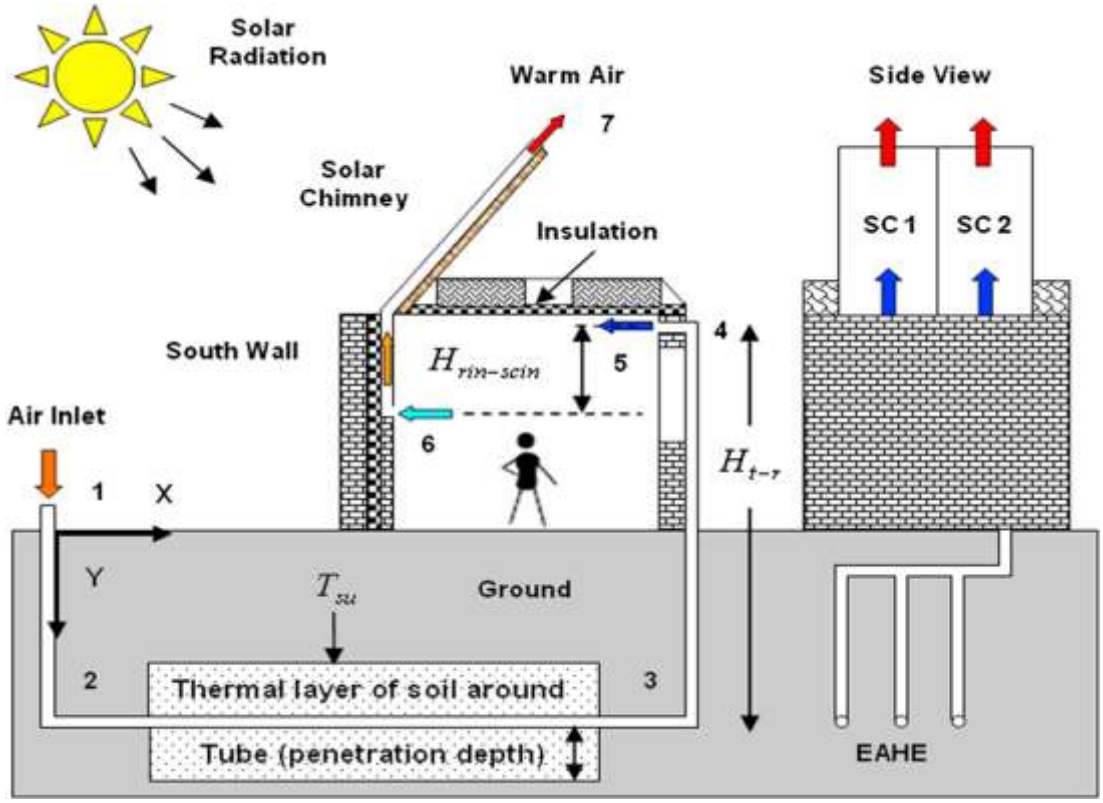

Figure I.26: Schematic diagram of integrated earth to air heat exchanger and solar chimney **[55]**

M. Maerefat and A.P. Haghighi [56] put forward a new solar system configuration, it is a combination of two systems used for cooling and ventilation: a solar chimney and a cooling cavity as illustrated in **Figure I.27**. In the cooling cavity, circulating water is sprayed onto the top of the wall where it flows as a thin film along the wall surfaces of the air passage. The air, near the water film, is at an average temperature of the water spray film. Since partial pressure of water vapor at the interface is higher than air pressure, there is a mass transfer of evaporated water into the air. This is associated with a latent heat transfer and water vaporization. At the same time, convective heat transfer takes place due to the temperature difference between surface of the water and the air. At the end of evaporation process, the cooled falling water is collected in a basin that is provided at the bottom of the evaporative cavity. This water is recycled again to the sprinkler by means of a pump. The water finally achieves an adiabatic saturation temperature of the air naturally after several circulations. Thus, we can call it a direct evaporative passive cooling system. The system operates as follows: the solar energy heats up

the room air flowing through the chimney, and the hot air generates the draft in the chimney. This draft induces air ventilation in the whole system: solar chimney, room, and cooling cavity. The chimney effect causes the air to be drawn through the cooling cavity with wet cool surfaces and to remove heat from this air and brings cooled supply air into the room. Therefore, both cooling and ventilation are provided during daytime by solar energy.

The results show that employing this configuration is capable to provide good indoor conditions at the daytime in a living room even at a poor solar intensity of 200 W/m^2 and high ambient air temperature of 40 °C. Although the performance strongly depends on the ambient air humidity, it is easy to prepare good indoor thermal conditions for ambient air relative humidity lower than 50% even at high ambient temperatures. As such, this technique is suitable to supply the cooling load in the moderate and arid climates.

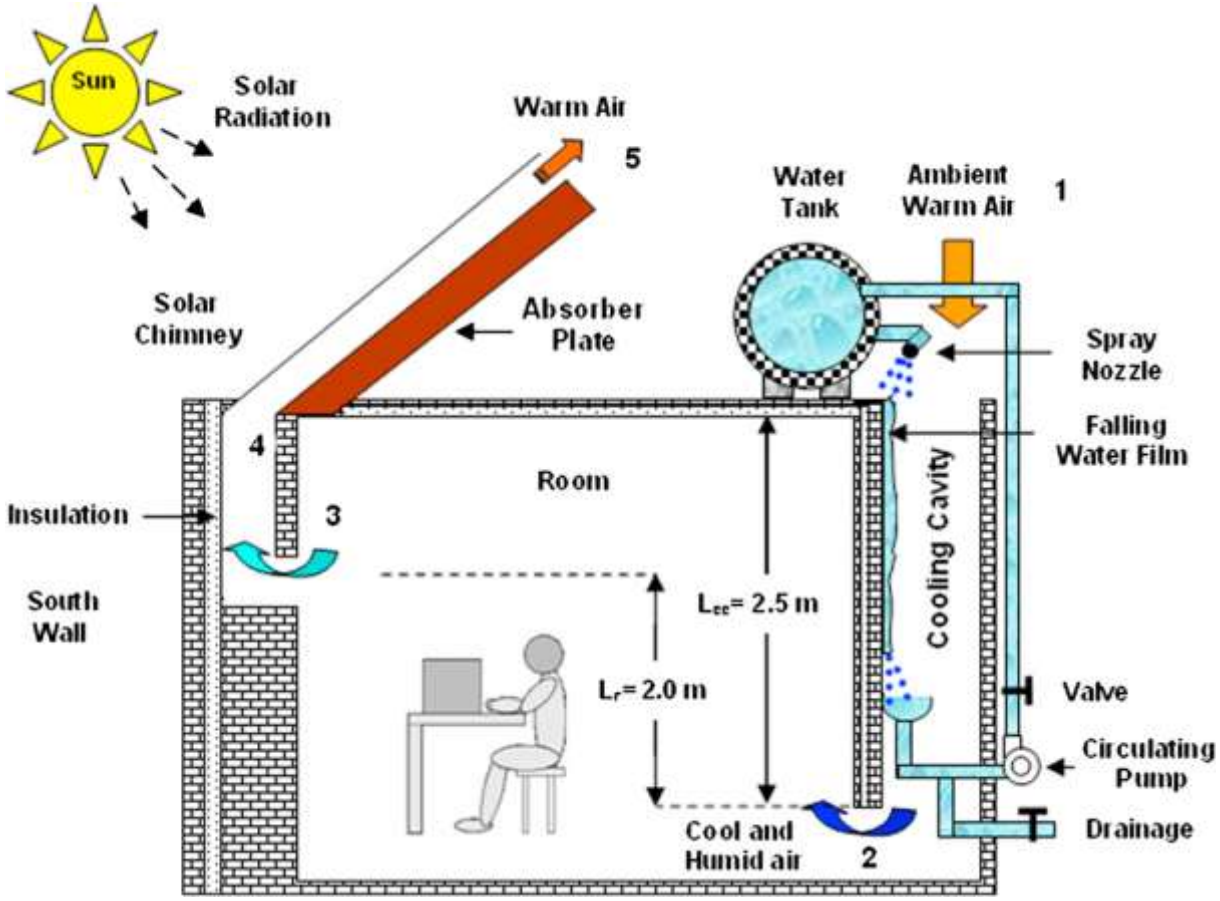

Figure I.27: Schematic diagram of solar chimney and cooling cavity **[56]**

Raman et al. [57] tested a passive solar house based on the incorporation of solar chimneys for heating, cooling and ventilation in composite climates. The model consists of two solar air heaters with (solar chimneys), one placed on the roof and the other placed on the

ground. The roof air heater acts as an exhaust fan, sucking the room air and venting it out during sunshine hours. The bottom collector is used alternatively as a conventional air heater during winter and as an evaporative cooler during summer, with some minor modifications. During winter, the channel is empty of water and is fitted with a glazing so that the unit acts like a solar air heater. During summer, the duct is filled with water, the glazing is removed and a shadow is provided to prevent radiation absorption. The operation of the complete system for winter and for summer operation is shown in **figure I.28.** The air handling capacity of solar chimneys was predicted by computation and verified by measurements. The configuration, performed well for winter, but the summer cooling was not adequate. Regarding the energy costs, the proposed passive system seemed to have good potential.

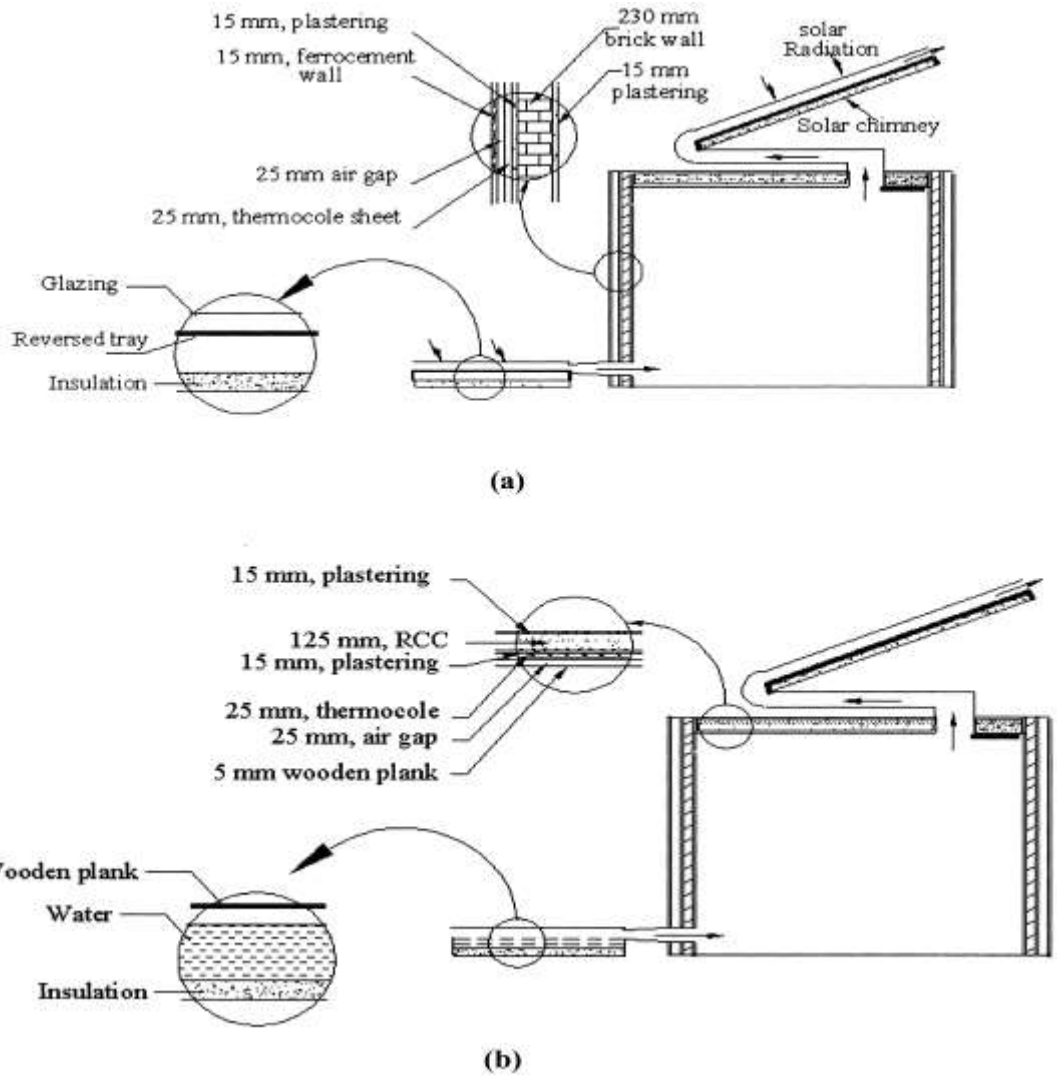

Figure I.28: Schematic diagram of passive system, (a) winter operation, (b) summer operation.

Solar chimneys can be used independently in buildings for improving natural ventilation. However, they are always integrated with other technologies. It is proved that such integrated design approaches can make higher air flow rate and keep more comfortable indoor thermal environment. **X.Q. Zhai [58]** summarized the main configurations and the integrated renewable energy systems based on solar chimneys.

To accomplish, in practical projects, solar chimneys can be integrated into walls or roofs, forming the two main arrangements including both wall solar collector (solar wall or Trombe wall) and roof solar collector. For one thing, they are used in the buildings to improve indoor thermal environment by natural ventilation. For another reason, they are adopted in the buildings with air-conditioning systems.

CHAPTER II

Experimental Study - Formulation and Results

CHAPTER II: EXPERIMENTAL STUDY - FORMULATION AND RESULTS

I. Introduction

Solar energy is a kind of renewable, sustainable and endless source of energy. Suffering from energy shortage, pollution and greenhouse effect, solar energy has become a large research field from 1900s till nowadays. To contribute in this topic, we performed measurements of the key parameters on a scaled-down model of solar chimney installed on the ground. The model is produced considering the similarity between the scaled-down prototype and the full-scale model. The efficiency of the proposed model is experimentally determined by measuring air velocity, solar radiation and air temperature at different locations as well as the weather conditions.

II. Experiment setup

II.1. Description

The experiments are performed in Fellaoucene, Algeria 35°3’28’’ N, 1°35’37’’W, altitude: 280m as shown in **Figure II.1** in a selected clear day, it was April the 14- 2019

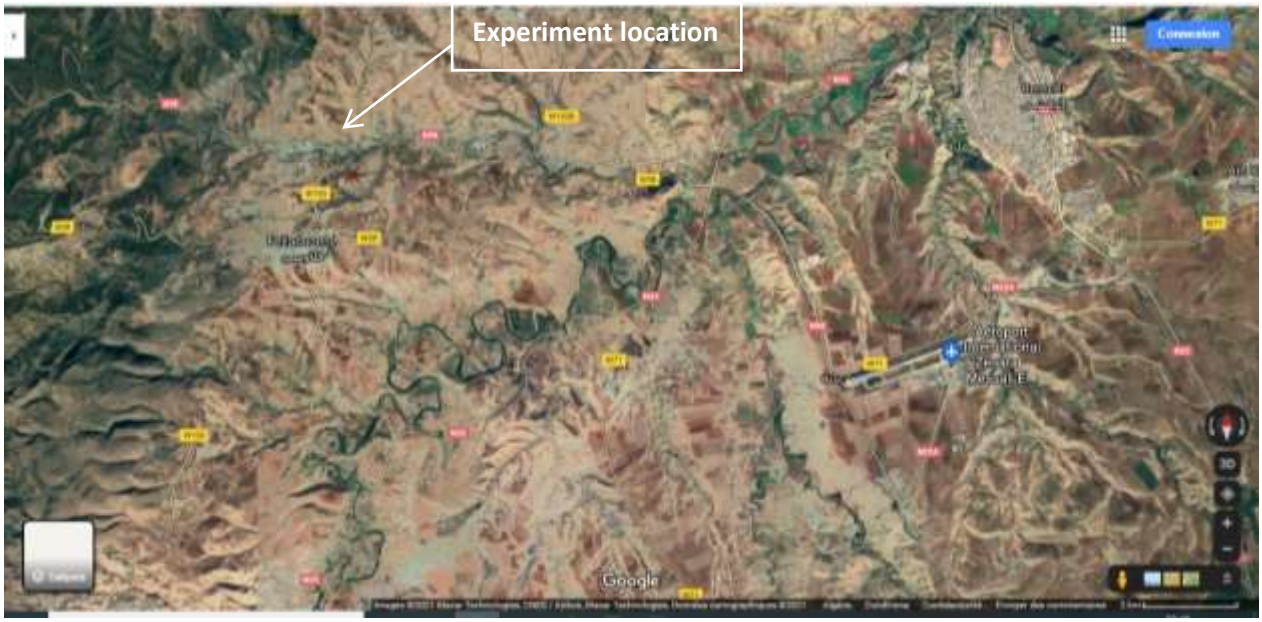

Figure II.1: Satellite image **[61]**

Three chimneys with different heights h=0.5m, h=0.75m and h=1m are used, bases lengths and gaps are the same: 0.5m and 20mm respectively.

Parts of the solar chimneys were: the absorbers made of black painted steel 2mm thickness; Walls were insulated with 20mm expanded polystyrene and commercial glass of 3mm thickness served as the glazing for the chimneys.

The chimneys were positioned to minimize the wind effect; they were installed in a surrounded courtyard of an old house, the height of the entourage is 3m (**FigII.2).**

Chimneys were south facing and inclined 45° to horizontal plan in order to optimize thermal efficiency and air flow.

The cylindrical outlet is used to allow the combination with other systems such as Stack height effect improvement and facilitates adding of other systems like heat recovery or heating by means of a fan to direct hot air to the internal space in future studies. In addition $S_1/S_2=12$, where S_1 and S_2 are inlet and outlet sections. This is to create the Venturi effect with the aim of increasing the air velocity and improve measurement accuracy.

Figure II.2: Solar chimneys and weather station installation

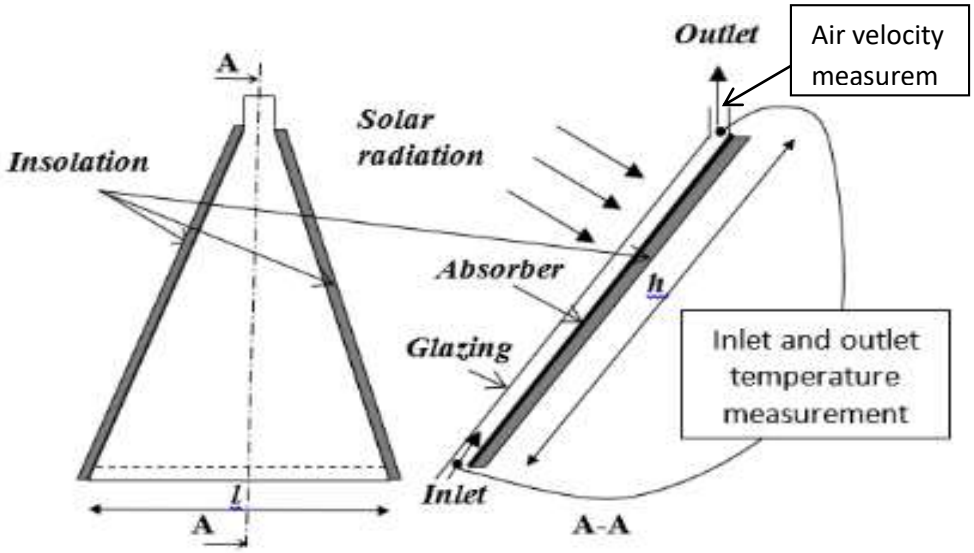

Figure II.3: Schematic experimental setup

II.2. Mesuring equipments

II.2.1. Weather conditions mesurement

Portable weather station (AERCUS INSTRUMENT^{TM} WS2083 PRO WIRELESS WEATHER STATION) was onsite installed. Wireless sensor transmits data to the main unit with LCD screen (FigII.4). The screen displays outdoor and indoor temperatures, humidity, barometric pressure, wind, rainfall, dew point, wind-chill, date/time and short range forecast.

Specifications:

Outdoor temperature: -40.0°C to + 65.0°C (-40°F to +149°F)

Indoor temperature: 0°C to + 50.0°C (32°F to +122°F)

Relative Humidity: 10% to 99% (1% resolution)

Rain volume display: 0 to 9999mm

Wind speed: 0 to 160 km/h

Barometric pressure: 300hPa to 1,100hPa (inHg, mmHg or hPa) with 0.1hPa resolution

Transmission: up to 100m (330 feet)

Transmission frequency: 433MHz

Data storage capacity: 2 weeks at 5 min intervals up to 3 months at 30min intervals

II.2.2. Air velocity mesurement

The velocity of the hot air was measured at the outlet of the chimneys by using multifunctional Hand-held digital anemometer with sensitive wheel; it allows the measurement of the average air velocity and temperature with a maximum error of 5%. Wheel diameter is approximately the same of the outlet of the chimneys.

Specifications

Measuring items : Air velocity (Wind speed), Air temperature

Air velocity units: m/s, Km/h, ft/min, Knots, mph

Range of Air velocity : 0~30m/s, 0~90km/h, 0~5860ft/min, 0~55knots, 0~65mph

Accuracy of Air velocity : ±5%

Range of Air temperature : -10-45C (14-113F)

Accuracy of Air temperature : ±2C (3.6F)

Resolution of Air velocity : 0.1m/s, 0.2C

Thermometer : NTC thermometer

Operating humidity : Less than 90%RH

II.2.3. Solar radiation

Solar radiation was measured by means of a pyranometer model TM-206 with an accuracy of ±10w/m^2.

Specifications

Display: 3½ digits, 2000 readings

Range: 2000 W/m^2, 634BTU / (ft2xh)

Resolution: 0.1 W/m^2, 0.1 BTU/ (ft2xh)

Accuracy: Typically within +/- 10W/m^2 [+/-3 BTU/ (ft2xh)] or +/-
5% whichever is greater in sunlight.

Temperature included error +/- 0.38 W/m^2 / ºC [+/-0.12 BTU/ (ft2xh)] / ºC] deviation from 25 ºC.

Angular accuracy: Cosine corrected

Sampling time: 0.25 second

Operating Temperature and Humidity: 0°C ~ 50ºC below 80% RH

II.2.4. Temperature mesurement

For temperature measurement, six thermocouples with LCD display and the following specifications are installed in the air flow region at the middle of the inlet and outlet area of solar chimneys (**Fig II.3)**.

Specifications

Type: NTC

Range: -50°C to 80°C

Resolution: 0.1°C

Accuracy: ±0.5°C

An infrared camera testo 875-1i was also used to view temperature distribution, Glazing temperature was carried out by means of the software treatment tool (IRsoft) given by the manufacturer of the camera.

Specifications

Image size: 640 x 480 pixels

Minimum focus distance: 0.4 m

Display type: 3.5" LCD with 320 x 240 pixels

Display option: IR image only; real image only; IR image / real image

Number of colors: 10

Video output: USB 2.0

File format image: .bmt; export option in .bmp; .jpg; .png; .csv; .xls

Storage device: SD card 2GB (approx. 2.000 images)

Infrared resolution: 160 x 120 pixels

Thermal sensitivity: < 50 mK at +30 °C

Field of view: 32° x 23°

Minimum focus distance: 0.1 m (Standard lens)

Geometric resolution (IFOV): 3.3 mrad (Standard lens)

Super Resolution (Pixel): 320 x 240 pixels

Super Resolution (IFOV): 2.1 mrad (Standard lens)

Image refresh rate: 33 Hz

Focus: manual

Measuring range: -30 to +100°C; 0 to +350 °C (switchable)

Accuracy: ±2 °C, ±2 % of m.v. (±3 °C of m.v. at -30 to -22 °C)

Figure II.4: Some instrument used for measurements

Other instruments are used for dimensions measurement such as a caliper and a tape measure.

III. Theory

III.1. Main parameters in natural ventilation

In natural ventilation, air changes per hour which is the ratio of the air volume flow rate Q to the total volume of the room *V* can be calculated from the following expression as defined by ASHRAE **[1]**

$$\boldsymbol{ACH = \frac{Q \times 3600}{V}} \quad \textbf{(II.1)}$$

Where Q and V are in (m^3/s) and (m^3) respectively.

Natural ventilation can be provided by wind or buoyancy forces, for the simple case of cross ventilation or wind drive ventilation with an isolated enclosure, the air flow rate can be calculated by the following equation **[32]:**

$$\boldsymbol{Q = K \times A \times V} \quad \textbf{(II.2)}$$

Where Q is the air flow rate in (m^3/h). K is the coefficient of effectiveness. A is the area of the smaller opening in (m^2) and V is the velocity of outside air in (m/h). Wind driven ventilation is solely dependent on wind direction and wind intensity.

In buoyancy driven natural ventilation, the air flow is induced by thermal effect. It can be calculated using the following equation **[32]:**

$$\boldsymbol{Q = K \times A[H(T_{in} - T_{out})]^{1/2}} \quad \textbf{(II.3)}$$

Where Q is the volumetric flow rate in (m^3/h). A is the free area of inlet opening in (m^2). K is a constant depending on the resistance offered by the opening. Tin is the average indoor air temperature, at height H, in (°C) and Tout is the average outdoor air temperature in (°C).

Buoyancy driven natural ventilation is also referred as stack ventilation. It could be mixing or displacement depending upon the position of the openings and the nature of the stack effect **[2]**. The details of wind drive and stack ventilation modeling can be found in **[59].**

A solar chimney generates air movement by buoyancy forces, in which hot air rises and exits from the top of the chimney, drawing air through the building core in a continuous cycle. The driving force on the air column in the chimney is the difference in the density of the air inside and outside the chimney. If the height of the chimney is such that the normal variation of pressure and temperature in the atmosphere can be neglected, together with temperature changes within the chimney due to adiabatic expansion, the pressure difference can be given by **[60]:**

$$\Delta P = 11.67 \left(1 - \frac{T_a}{T_c}\right) h \qquad \textbf{(II.4)}$$

Where h is height of chimney, Ta is ambient air temperature and Tc is temperature inside the chimney.

Neglecting losses in the chimney a reasonable assumption for a chimney of diameter greater than 1/10 of its height, the air velocity at the top of the chimney can be given by:

$$v = \sqrt{\frac{2\Delta P}{\rho_l}} \qquad \textbf{(II.5)}$$

Where ρ_l is the density of the air at chimney temperature. However, this analysis is based upon a simplified model **[60].**

In case of measured average velocity, Air flow rate through the chimney can be calculated as:

$$Q_{vent} = V_{avg} \times A_{out} \qquad \textbf{(II.6)}$$

Where V_{avg} is the average velocity at the exit cross-section of the chimney (m/s), A_{out} is the outlet cross-section area of the chimney in (m^2), Q_{vent} is the flow rate of the hot air (m^3/s).

The thermal efficiency of the solar chimney is calculated by:

$$\eta = \frac{\rho_l Q_{vent} C_p (T_{out} - T_{in})}{I \times S} \qquad \textbf{(II.7)}$$

Where η is the thermal efficiency, ρ_l is the density of the air at chimney temperature, C_p air specific heat (J/kg °K), T_{in} and T_{out} are temperatures at chimney inlet and outlet, I incident solar radiation (W/m^2), S is the absorber area. ρ_l and C_p can be taken from the folowing equations **[19]:**

$$\boldsymbol{\rho_l = 1.1614 - 0.00353(T - 300)} \quad \textbf{(II.8)}$$

$$\boldsymbol{C_p = 1007 + 0.004\,(T - 300)} \quad \textbf{(II.9)}$$

The various important mathematical modeling, including the key parameters are shown in **Table II.1**.The mathematical modelings has been taken from **Shiv L et al [52]**

Table II.1. Mathematical modeling for solar chimney calculations **[52]**

S.No.	Authors	Model size and type	Model	Solution Technique	Results
1.	N. K. Bansal R. Mathur M. S. Bhandari, 1993	Wall mounted Solar chimney 1.5x1.5x0.15m^3 for 3.6 ACH and 4x4x4m^3 room size	Energy balance for absorber plate $(\alpha.\tau).\bar{S}(t) = h_f(T_p - \bar{T}_f) + U_l(T_p - T_a) + U_b(T_p - T_R)$ Energy balance for flowing fluid $m.C_p.\frac{dT_f}{dx}.x = h_f.w.\Delta x.(T_p - T_f)$ Volume flow rate $Q_i = C_d.A_o[2.\left(\Delta T/T_o\right).g.H.sin\beta]^{1/2}.[(1+A_r^2)]^{1/2}$ and $Q_o = C_d.A_o[2.\left(\Delta T/T_i\right).g.H.sin\beta]^{1/2}.[(1+A_r^2)]^{1/2}$		Optimized absorber area 2.25m^2 for ACH-3 to 6 Air flow rate 2.33m/s
2.	K.S. Ong, 2002 K.S. Ong, C.C. Chow, 2003	Wall mounted Solar Chimney 2x0.45x0.48 (Gap varying as 0.1, 0.2, 0.3)	Energy balance Equations $T_g: S_1 + h_{rwg}(T_w - T_g) + h_g(T_f - T_g) = U_t(T_g - T_a)$ $T_f: h_w(T_w - T_f) = h_g(T_f - T_g) + \dot{q}^*$ $T_w: S_2 = h_w(T_w - T_f) + h_{rwg}(T_w - T_g) + U_b(T_w - T_R)$	Solving by matrix inversion method	Air velocity 0.25 to 0.36 m/s
3.	N.K. Bansal, Jyotirmay Mathur, Sanjay Mathur, Meenakshi Jain, 2005	Window Size 1x1x0.13 m^3 Chimney 1x1x1 m^3 Room	For vertical glass cover $S_1A_g + h_{rwg}A_w(T_w - T_g) = h_gA_g(T_g - T_f) + U_tA_g(T_g - T_a)$ For the air in the flow channel $h_wA_w(T_w - T_f) + h_gA_g(T_g - T_f) = q^*$ For the absorber wall $S_2A_w = h_wA_w(T_w - T_f) + h_{rwg}A_w(T_w - T_g) + U_bA_w(T_w - T_R)$	Programming in C++	Flow velocity found 0.24m/s latitude 27° N and altitude 75.82E
4.	E.P. Sakonidou, T.D. Karapantsios, A.I. Balouktsis, D. Chassapis , 2008	Small Chimney 1x0.74x0.11m^3	Model for optimum tilt for maximum air flow $I_T = I_{dir}R_b + I_{diff}\left(\frac{1+\cos s}{2}\right) + I_{rg}(\frac{1-\cos s}{2})$ $v = C_d.\frac{\rho(T_{air})}{\rho(T_o)}.\left[\frac{L.g.(\sin(s))^2.(T_{air} - T_o)}{T_o}\right]^{1/2}$	Compared experimental results with CFD model	Optimum tilt between 65 to 76 degree For latitude 41°70', longitude 23°34', altitude 32 m

III.2. Dimensionless Parameters for natural ventilation

Dimensionless numbers have significant importance in establishing the physics of the flow. In natural ventilation, the following numbers are very significant.

III.2.1. Reynolds number

$$\boldsymbol{Re = \frac{UL}{\nu} \approx \frac{enertial\ forces}{viscous\ forces}} \quad \textbf{(II.10)}$$

U: is the mean velocity of the fluid (m/s)

L: characteristic dimension (m)

ν: (nu) is the kinematic viscosity (ν = μ/ρ) (m^2/s)

In fluid flow, Reynolds number can establish the ratio between inertial force and viscous resistance, the domination of one of these forces indicate the flow behavior. At low Reynolds numbers, flows tend to be laminar. While at high Reynolds numbers flows are turbulent.

III.2.2. Grashof Number

Grashof number is the ratio of buoyancy forces to restraining forces (viscous forces).

$$\boldsymbol{Gr_L = \frac{g\beta(T_s - T_\infty)L^3}{\nu^2} \approx \frac{buoyancy\ force}{viscous\ force}} \quad \textbf{(II.11)}$$

$L \rightarrow$ characteristic length (m)

T_s : surface temperature

T_∞ : bulk temperature

ν: (nu) is the kinematic viscosity (ν = μ/ρ) (m^2/s)

g: Gravity (m/s^2)

ρ: density of fluid (k_g/m^3)

ρ_0: reference density

$\beta \rightarrow$ thermal expansion coefficient (a thermodynamic property of the fluid)

$$\boldsymbol{\beta = -\frac{1}{\rho_0}\left(\frac{\partial \rho}{\partial T}\right)_p} \quad \textbf{(II.12)}$$

For perfect Gases:

$$\boldsymbol{\rho = \frac{P}{RT} \quad \rightarrow \quad \beta = \frac{1}{T}} \quad \textbf{(II.13)}$$

The Grashof number plays the same role in free convection that the Reynolds number plays in inertial fluid flow.

In a mixed convection flow, the contribution of buoyancy forces can be measured by the ratio of the Grashof and Reynolds numbers:

$$\frac{Gr_L}{Re^2} = \frac{g\beta\Delta TL}{\nu^2} \quad \textbf{(II.14)}$$

When buoyancy has strong contributions to the flow, this number approaches or exceeds unity. Conversely, if it is very small, buoyancy forces can be ignored.

III.2.3. Prandtl number

$$\mathbf{Pr} = \frac{c_p\mu}{\lambda} = \frac{\nu}{\alpha} \approx \frac{momentium\ diffusivity}{thermal\ diffusivity} \quad \textbf{(II.15)}$$

P_r: Prandtl number

α: Thermal diffusivity $\alpha = \frac{\lambda}{\rho C_p}$ **(II.16)**

λ: thermal conductivity

C_p: Specific heat of fluid

The Prandtl number represents the ratio of viscous diffusion over thermal diffusion in heat transfer and fluid flow combination.

III.2.4. Nusselt number

$$Nu = \frac{hL}{\lambda} \approx \frac{convective\ heat\ transfert}{conductive\ heat\ transfert} \quad \textbf{(II.17)}$$

The Nusselt number represents the ratio of convective heat transfer over conductive heat transfer. The Nusselt number suggests if heat transfer is primarily conductive or convective. Large values of the Nusselt number indicate that the heat transfer is convective and turbulent, typically in the range of 100-1000

III.2.5. Rayleigh number

$$Ra = Gr\ Pr = \frac{g\beta(T_s - T_\infty)L^3}{\nu\alpha} \quad \textbf{(II.18)}$$

In pure natural convection, Rayleigh number indicates the strength of the buoyancy-induced flow. A buoyancy-induced flow is laminar when Rayleigh numbers is less than 10^8, with transition to turbulence occurring over the range of 10^8<Ra < 10^{10}, **[62]**

III.2.6. Mach number

Compressible flows can be characterized by the value of the Mach number:

$$M = \frac{u}{c} \quad \textbf{(II.19)}$$

u: is the flow velocity

c: is the sound speed in the gas

$$c = \sqrt{\gamma RT} \quad \textbf{(II.20)}$$

$$\gamma = \frac{C_p}{C_v} \quad \textbf{(II.21)}$$

When the Mach number is less than 1.0, the flow is termed subsonic. At Mach numbers much less than 1.0 ($M < 0.1$ or so), compressibility effects are negligible and the variation of the gas density with pressure can safely be ignored in the flow modeling **[62]**.

IV. Results and discussion

Solar radiation was measured during the test period on a selected clear day (April the 14th- 2019). As shown in **figure II.5**, the measurements were taken each 30 minutes between11:45AM and 15:15PM.

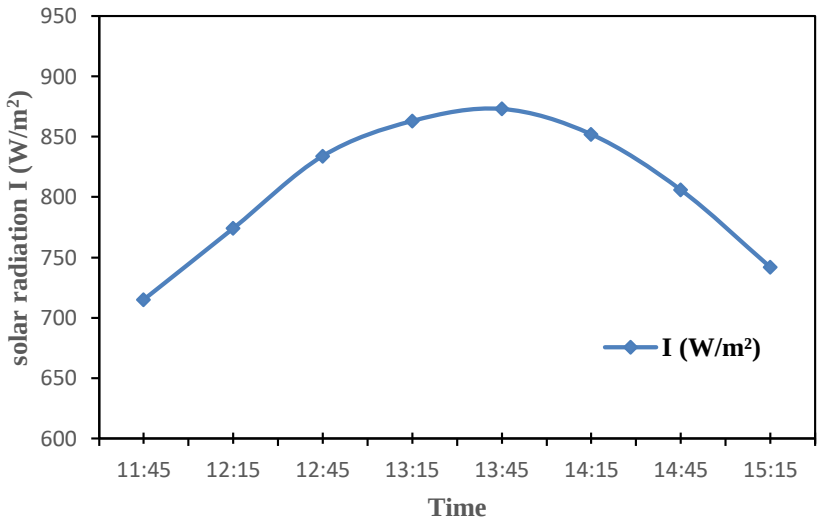

Figure II.5: Solar radiation during the test period in the selected clear day (14th April 2019)

In local conditions of temperature and relative humidity (**Fig.II.6**); chimneys receive the maximum irradiation between 13: 00 and 14: 00; the average ambient temperature was 29.5 °C and 30% of relative humidity. Three chimneys with height to bases length h/l =1, h/l=1.5, and h/l=2 are used, they are south facing and 45° inclined in order to maintain the optimum thermal efficiency and air flow.

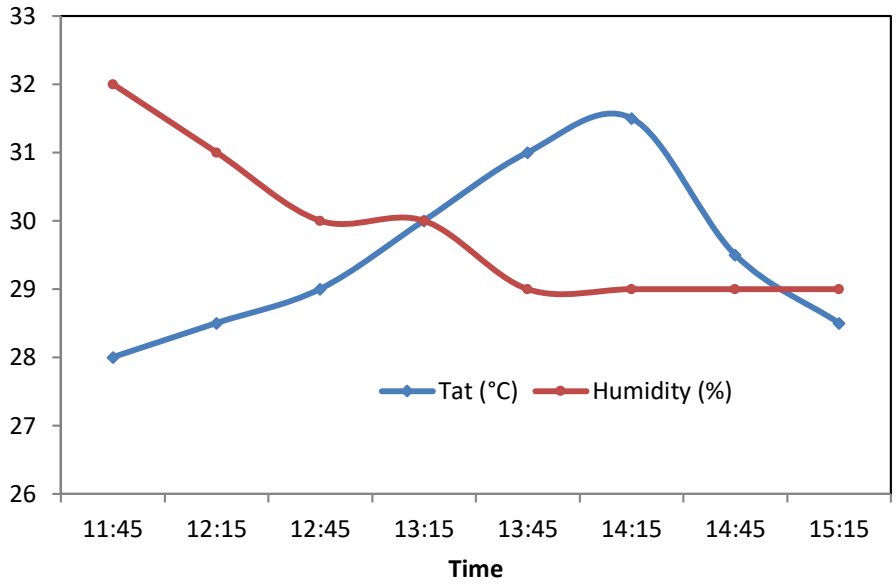

Figure II.6: Ambient temperature and relative humidity during the test period

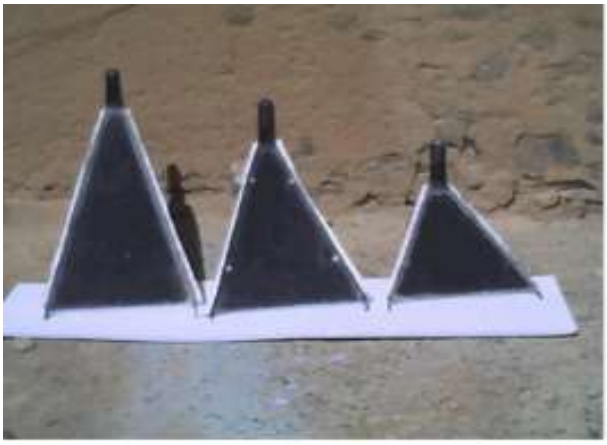

Figure II.7a: Real image (14th April 2019 at 14:40)

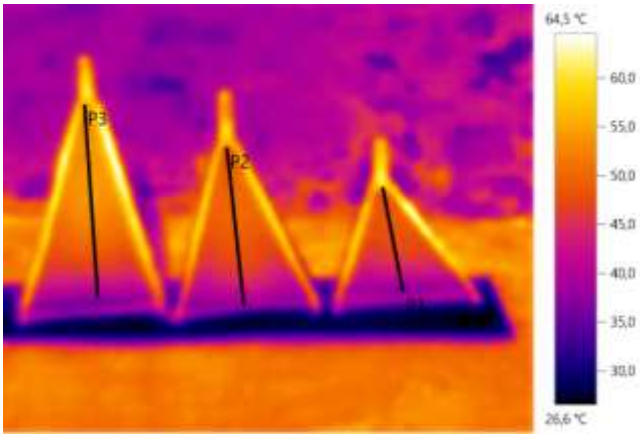

Figure II.7b: Thermal image (14th April 2019 at 14:40)

The infrared camera served to take **Figures (II.7a and II.7b)**. Glazing temperature profiles of the three solar chimneys in **Figure II.7c** was carried out by means of the software treatment tool (IRsoft) given by the manufacturer of the camera. The emissivity of the commercial glass is 0.90 **[6].**

The temperature fields presented in **figure II.7b** by the thermal camera are the reflection of the convective and dynamic structures of the flow. In fact, it is clear that low gradients and temperatures are generated near the inlet of each chimney because fresh air is always sucked. However, the temperature level began to increase ever more from the medium approaching the exit. This is due to the heat exchange between the absorber and air. Heat is generated by the greenhouse effect inside the chimneys; and by

thermal expansion, air density decreases to generate the buoyancy driving force therefore the ventilation process.

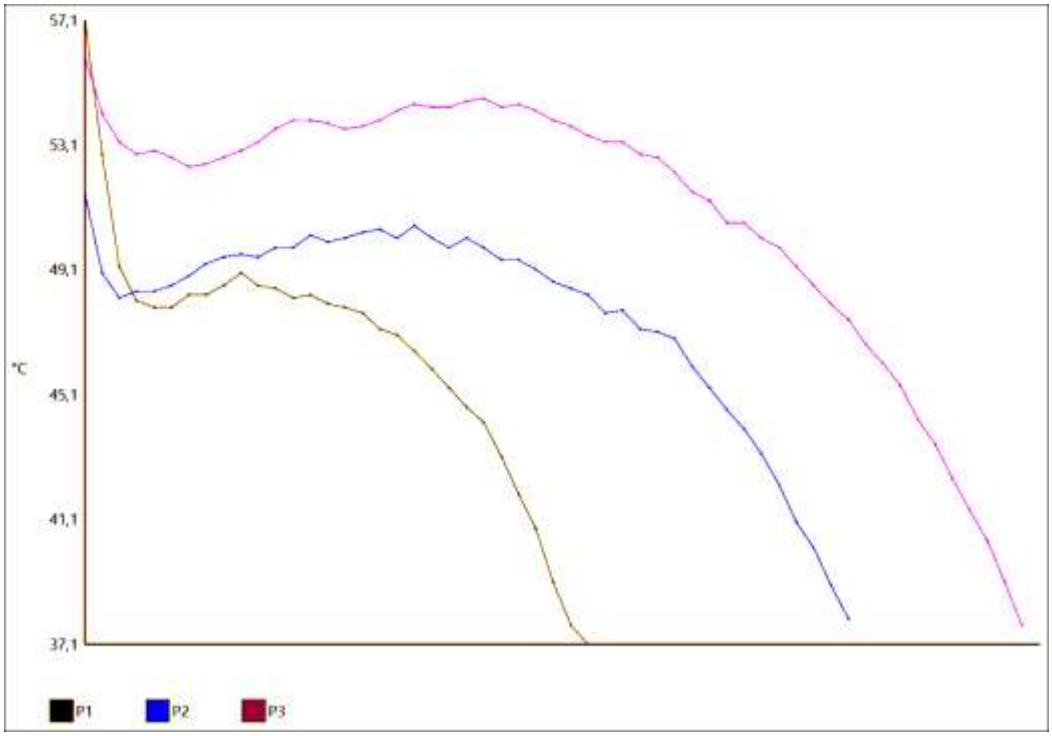

Figure II.7c: Glazing temperature profiles

Figure II.7c presents the glazing temperature profiles in cross sections P1, P2 and P3 (**Fig.II.7b**), temperature values was given by means of the software treatment tool (IRsoft). For the chimneys of ratio (h/l=1), (h/l =1.5) and (h/l=2) respectively, The temperature near the entrances of the three chimneys is around 37.5 °C, and then increases subsequently in the middle until it reaches the maximum near the exit. The highest glazing temperature was 57.1 °C in the longest (h/l=2) and the shortest (h/l=1) solar chimneys, while the maximum glazing temperature presented for the (h/l=1.5) solar chimney is 50°C. Significant temperature difference is observed between the three chimneys, it depends on the absorber area and the air flow. Long chimney (h/l=2) delivers important flow (**Fig.II.9b**) because of the larger absorber surface. The short one gives the same glazing temperature as the long one even it has the smallest absorbing area; this is due to the low flow rate passage (**Fig.II.9b**).

The medium sized solar chimney (h/l=1.5) is the optimum comparing with the studied cases in this work, it has a low glazing temperature but the best thermal efficiency (**Fig.II.11**) so the desired heat exchange inside.

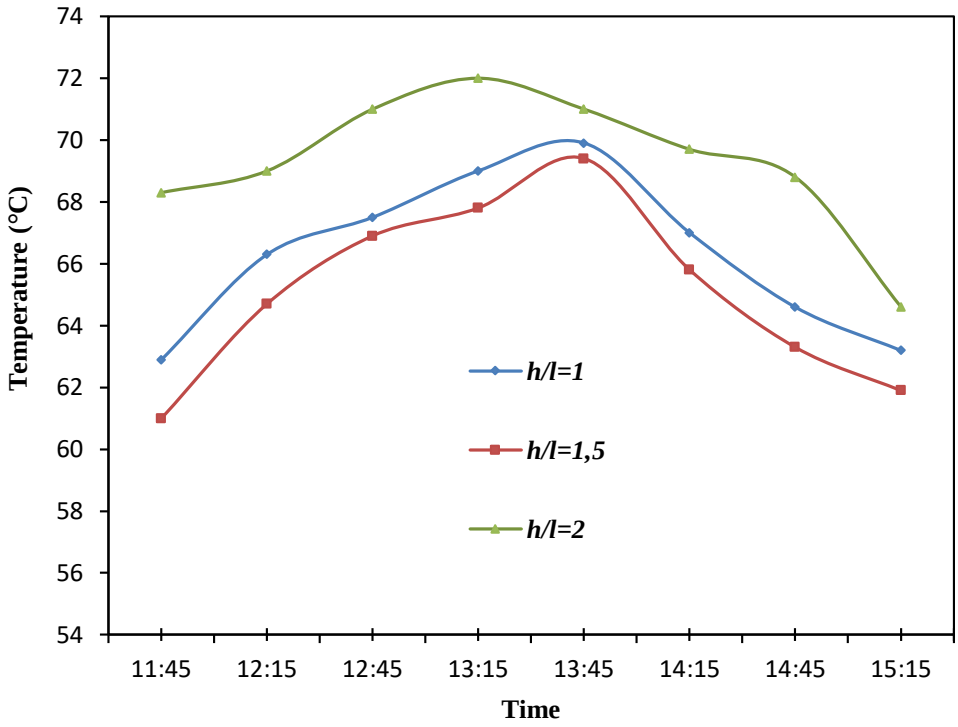

Figure II.8: Outlet temperature for different chimneys

Figure II.8 shows the air temperatures at the exit of chimneys. They are changing with the intensity of solar radiation, the maximum air temperature recorded is 72°c at 13:15 in the longest chimney (h/l=2). During the test period; outlet air temperatures in h/l=1 solar chimney are highest than these of (h/1=1.5). Discharge flow was obtained from eq. (6) and measured air velocity.

Results in **figures II.9a and II.9b** indicate that the lowest airflow at the outlet corresponds to the shortest solar chimney (h / l = 1). For the same dimensions of the base, the use of this small height gives rise to a resistance to the air flow inside the solar chimney. This generates more exchange time and subsequently, a higher temperature of the air at the outlet as shown in **figure II.8**.

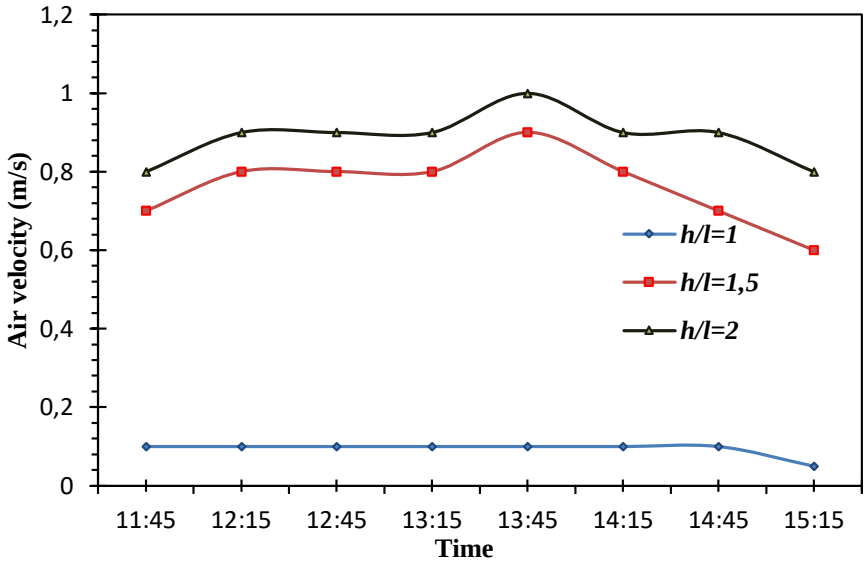

Figure II.9a: Outlet air velocity for different chimneys

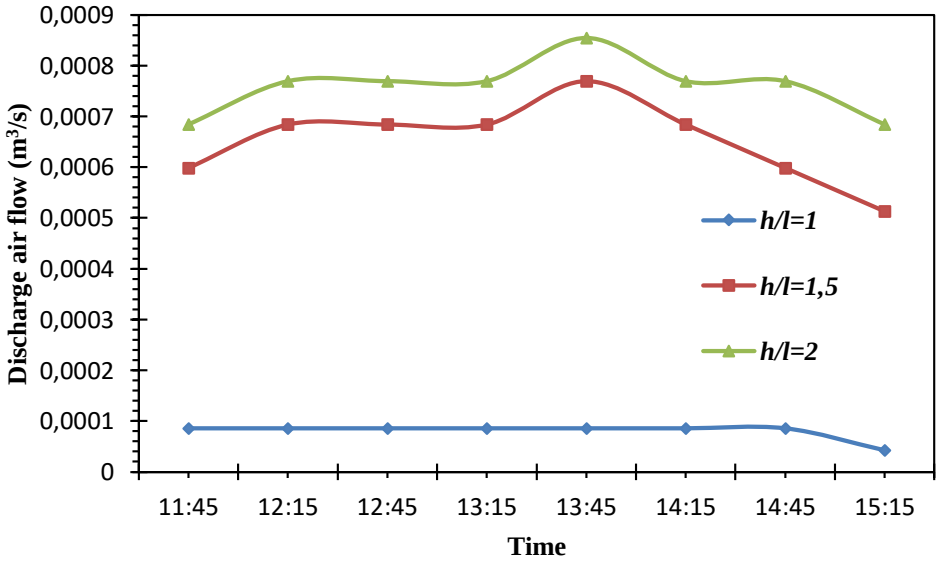

Figure II.9b: Discharge volumetric flow from solar chimneys cases

In **figure II.9b,** discharge air flow is illustrated, It takes the same curving of exit air velocity because of the constant inlet and outlet sections in all chimneys cases.

Outlet air velocity reach the maximum value (1m/s) in the longest chimney (h/l=2). The chimney with (h/l=1) deliver hot air slowly. In this case, the velocity didn't exceed (0.1m/s) during the test period. The peak velocity value in case of (h/l=1.5) chimney was (0.9m/s).

Figure II.10 shows the variation of the average air velocity at the exit of chimneys by their height to base length ratio (h/l). The velocity increase by increasing the (h/l), the evolution has a logarithmic tendency.

A correlation is developed to estimate the air velocity at the outlet of trapezoidal prism chimneys, with inlet by outlet section ratio equivalent to (S_1/S_2=12).

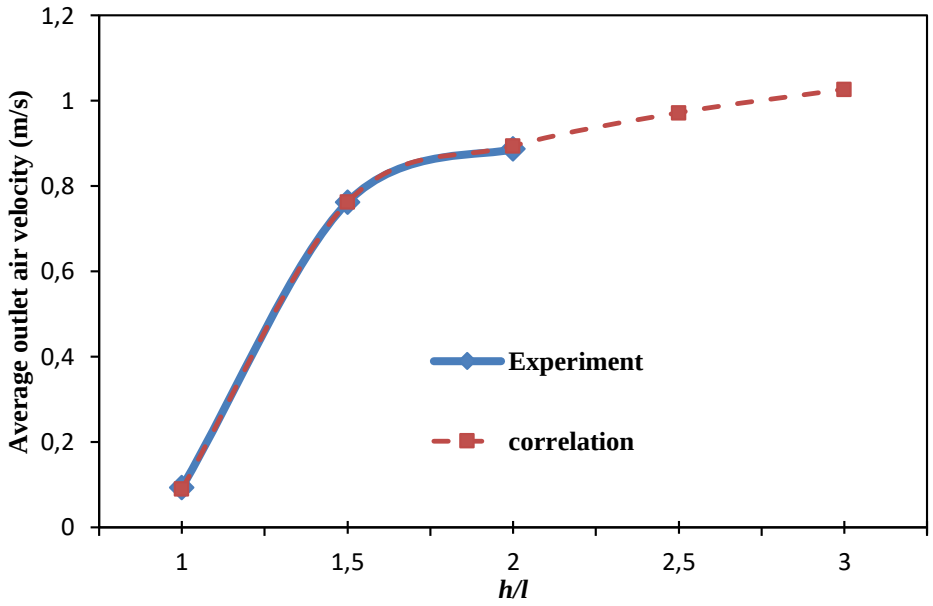

Figure II.10: Average outlet air velocity for different chimneys during the test period and developed correlation

$$V = 0.09 + [0.75 \ln(\frac{h}{l})]^{1/3} \qquad \text{with } h/l \geq 1 \qquad \text{(II.22)}$$

Estimated results by the developed correlation (22) in **figure II.10** show a maxim error of 0.7% at the present experiment conditions. Correlation (22) can be multiplied by a coefficient of correction (k) in order to add the effect of climatic conditions, geographic location and time of year. Therefore, it becomes:

$$V = k[0.09 + [0.75 \ln(\frac{h}{l})]^{\frac{1}{3}}] \qquad \text{(II.23)}$$

Where h and l are the chimney height and base length respectively, k is the coefficient of correction.

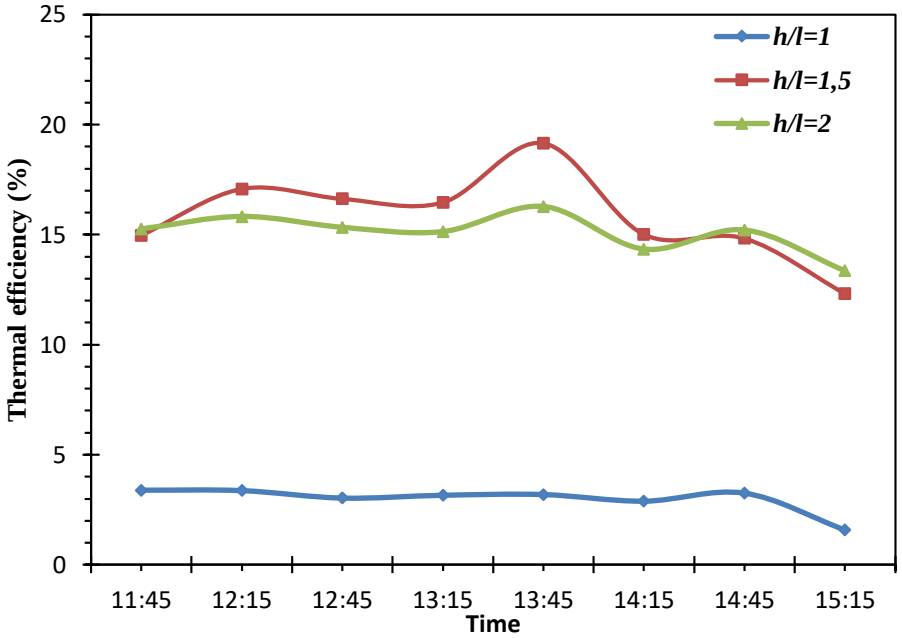

Figure II.11: Thermal efficiency from solar chimneys cases during the test period.

Thermal efficiency was calculated using eq. (7), (8), (9) and experiment results. **Figure II.11** indicates the thermal efficiency of chimney cases for the test period; the solar energy transferred into the air movement to improve the ventilation reach its higher rate in the h/l=1.5 chimney mainly for solar intensity higher than 800W/m^2. Between 700 and 800 W/m^2 the efficiencies are similar in h/l=1.5 and h/l=2 scenarios.

Experimental results show that the optimum value of the average thermal efficiency, **figure II.12**, is obtained by the chimney with h/l=1.5, in h/l=1 chimney case, the thermal efficiency didn't exceed 3.36%.

Another correlation is developed to estimate the thermal efficiency of trapezoidal prism chimneys as:

$$\eta = 3 + 70\frac{\ln(h/l)}{(h/l)^2} \qquad \text{With} \quad h/l \geq 1 \qquad \textbf{(II.}24\textbf{)}$$

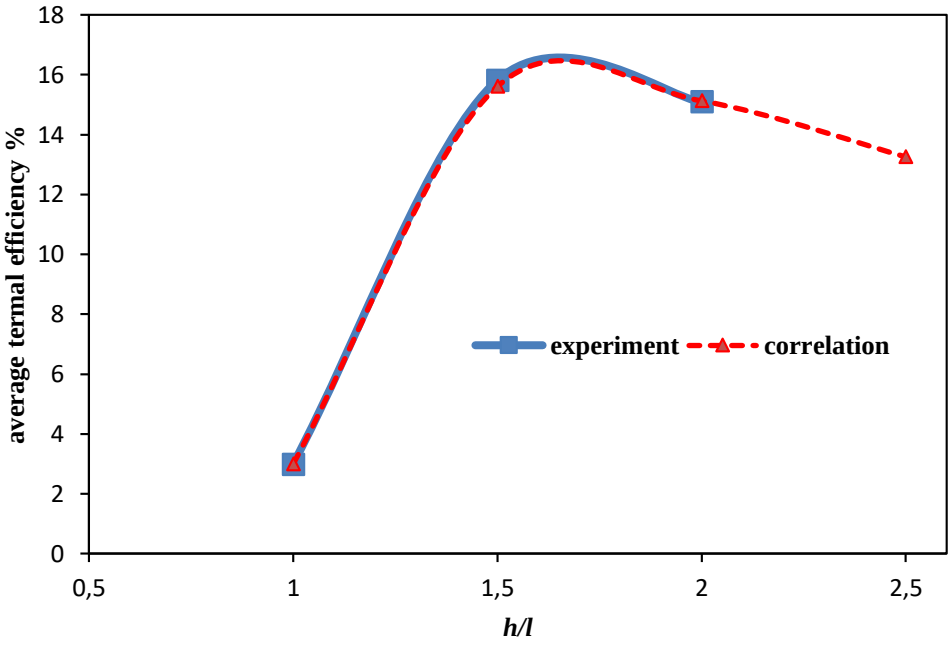

Figure II.12: Average thermal efficiency and developed correlation

As shown in **figure II.12**, the developed correlation gave very close results compared to the experiment. The maximum recorded error is 0.2 in the efficiency value. Using correlation (24), the efficiency reaches its maximum by **h/l=1.65**

CHAPTER III

Numerical Study- Formulation and Results

CHAPTER III: NUMERICAL STUDY – FORMULATION AND RESULTS

I. Introduction

Computational fluid dynamics CFD has the advantage to provide the flow details and temperature distributions throughout the computed space, and the calculations can include all the likely physical processes such as heat transfer from surfaces and transient behavior. CFD can also, deal with the complex geometry of a space.

II. Mathematical modeling

II.1. Hypothesis

In order to reduce the model complexity and computing time, the following assumptions are adopted:

- The flow is steady.
- Fluid is Newtonian and incompressible: Compressibility can be characterized by the value of the Mach number: When the Mach number is less than 1.0, the flow is termed subsonic. At Mach numbers much less than 1.0 ($M < 0.1$ or so), compressibility effects are negligible and the variation of the gas density with pressure can safely be ignored in the flow modeling **[62]**. In our case study, the peak Mach number is much less than 0.1; so we can consider that the flow is incompressible.
- The Boussinesq approximation is applied: density variations are ignored except in the gravitational term ***"****buoyancy term",* By this approach, we get faster convergence than by setting up the problem with fluid density as a function of temperature.

II.2. Governing equations of fluid mechanics and heat transfer

The fundamental equations are based on universal laws of conservation:

- Conservation of mass
- Conservation of momentum
- Conservation of energy

When applying the conservation of mass law to a fluid flow, it results the continuity equation; the conservation of momentum is the Newton's Second law: the rate of change of momentum equals the sum of forces acting on the fluid. When this law is applied to a fluid

flow, it becomes a vector equation known as the momentum equation. The conservation of energy is the same to the first law of thermodynamics: the rate of energy equals the sum of rate of heat addition to and the rate of work done on the fluid, and the resulting fluid dynamics equation. In order to close the system of equations developed from universal laws, it is necessary to establish relationships between fluid properties, such as the equation of state which relate the thermodynamic variables: pressure, density and temperature.

For a conservative flow of a Newtonian fluid governed by the law of perfect gases, these equations are written as:

Continuity $$\frac{\partial U_i}{\partial x_i} = 0 \qquad \textbf{(III.1)}$$

Momentum $$\frac{\partial}{\partial x_j}\left(\rho U_i U_j\right) = -\frac{\partial P}{\partial x_i} + \frac{\partial}{\partial x_j}\left[\mu\left(\frac{\partial U_i}{\partial x_j} + \frac{\partial U_j}{\partial x_i}\right) - \frac{2}{3}\mu\frac{\partial U_l}{\partial x_l}\delta_{ij}\right] + \rho g_i \qquad \textbf{(III.2)}$$

$$\delta_{ij}\begin{cases} 0 & if \quad i \neq j \\ 1 & if \quad i = j \end{cases} \qquad \text{(Kronecker delta)}$$

Energy $$\frac{\partial}{\partial x_j}\left(\rho U_j h\right) = \frac{\partial}{\partial x_j}\left(\lambda\frac{\partial T}{\partial x_j}\right) + U_j\frac{\partial P}{\partial x_j} + \varphi \qquad \textbf{(III.3)}$$

$$\varphi = \frac{\partial U_j}{\partial x_j}\left[\mu\left(\frac{\partial U_i}{\partial x_j} + \frac{\partial U_j}{\partial x_i}\right) - \frac{2}{3}\mu\frac{\partial U_l}{\partial x_l}\delta_{ij}\right]$$

Where:

φ is the viscous dissipation function.

h is the mass enthalpy; the relation (III.4) relates it to the temperature:

$$h = \int_{T_{ref}}^{T} c_P dT \qquad \textbf{(III.4)}$$

T_{ref} : is the reference temperature, is often equal to 0°C.

In the Eqs (III.1)-(III.4) appear the density ρ, the dynamic viscosity μ, the thermal conductivity λ, and the specific heat C_p.

II.3. Reynolds Averaged Navier-Stokes

The Navier-Stokes equations describe the physics of fluid motion, they are the most important in fluid mechanics. However, analytical solutions for the Navier-Stokes equations are only available for very simple laminar flows. Most real life flows are turbulent and three-dimensional. Hence, an analytical solution may not be achievable. The Navier-Stokes equations can be solved using Direct Numerical Simulation (DNS), which solves Navier-Stokes equations as is; however, it would require extensive computational resources and time, and this is not a feasible approach in general. In view of the great complexity of turbulence, we often use statistical methods. ReynoldsAveraged Navier-Stokes (RANS) are time-averaged equations of motion for fluid flow. The idea is to decompose turbulent quantity g into two components G and g', which are the mean and fluctuating components Eq (III.5). This is called Reynolds decomposition.

$$g = G + g' \qquad \textbf{(III.5)}$$

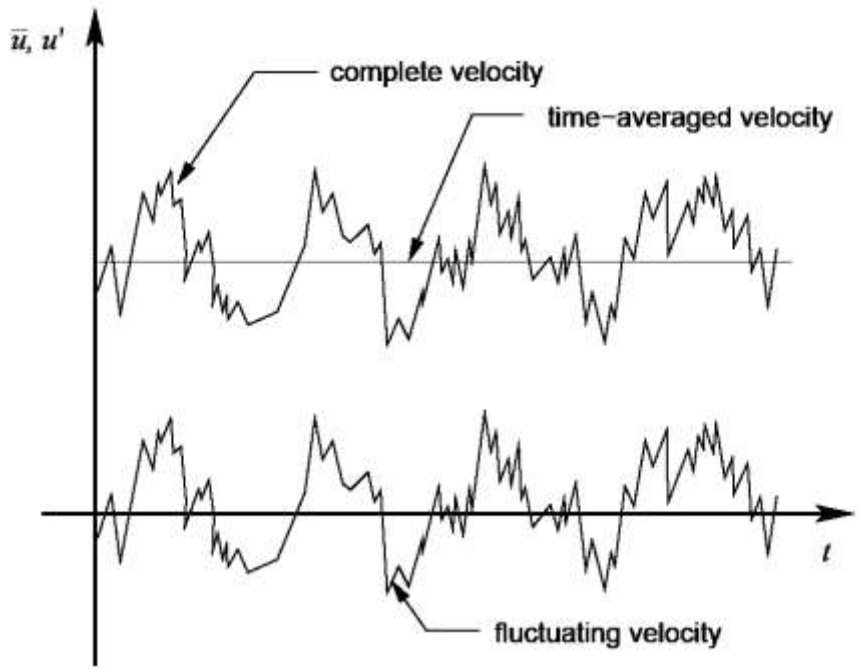

Figure III.1: Reynolds decomposition

The average of two quantities f and g confirms that:

$$\overline{g'} = 0 ;$$
$$\overline{f+g} = F+G ;$$
$$\overline{ag} = aG ; \qquad a \text{ is a constant}$$
$$\overline{fg} = FG ;$$
$$\frac{\overline{\partial g}}{\partial x} = \frac{\partial G}{\partial x}$$

There are other decompositions such as the mass-average or Favre's average, Eq (III.6), partially adapted to compressible flows

$$G = \frac{\overline{\rho g}}{\rho} \qquad \textbf{(III.6)}$$

However, Favre's decomposition generates relatively complex equations, and for slightly compressible flows, we can often assume that only the mean value of the density varies and neglect the fluctuations **[63].**

The Navier-Stokes equation (III.7) are the direct consequence of the momentum conservation:

$$\mathrm{U_j}\frac{\partial \mathrm{U_i}}{\partial \mathrm{x_j}} = -\frac{\partial}{\partial \mathrm{x_i}}\left(\frac{\mathrm{P}}{\rho}\right) + \frac{\partial}{\partial \mathrm{x_j}}\left(\nu \frac{\partial \mathrm{U_i}}{\partial \mathrm{x_j}}\right) \qquad \textbf{(III.7)}$$

The mass conservation (continuity) for an incompressible flow is written as:

$$\frac{\partial U_i}{\partial x_i} = 0 \qquad \textbf{(III.8)}$$

If we apply the Reynolds decomposition Eq (III.5) to the Navier-Stokes Eq (III.7), and continuity Eq (III.8) we obtain the following relations for the mass and momentum conservation; this formalism (by averaging each equation) leads to the Reynolds equations:

$$\overline{\mathrm{U_j}}\frac{\partial \overline{\mathrm{U_i}}}{\partial \mathrm{x_j}} = -\frac{\partial}{\partial \mathrm{x_i}}\left(\frac{\overline{\mathrm{P}}}{\rho}\right) + \frac{\partial}{\partial \mathrm{x_j}}\left(\nu \frac{\partial \overline{\mathrm{U_i}}}{\partial \mathrm{x_j}} - \overline{\mathrm{u'_i\ u'_j}}\right) \qquad \textbf{(III-9)}$$

$$\frac{\partial \overline{U_i}}{\partial x_i} = 0 \qquad \textbf{(III.10)}$$

The terms $\overline{u'_i u'_j} = \tau_{ij}$ give rise to the Reynolds stresses, which come from the nonlinearities of the Navier equations and govern the interaction between the mean flow and the fluctuating motion.

The system of Eqs (III.9)–(III.10) contains more unknowns than equations, so it is an open system. To close the system, physical hypothesis has to be reintroduced. Introducing closure hypotheses allows us to obtain a number of equations equal to the number of unknowns and consequently these equations can be solved numerically.

In order to close the system, the components of the Eq. (III.9) must be solved. Generally, this is known as the turbulence closure problem. An ideal turbulence model should be capable of being applied to a wide range of problems; it should have reasonable accuracy, and must be computationally inexpensive

II.4. Boussinesq Hypothesis "Eddy viscosity hypothesis"

The Boussinesq hypothesis also called eddy viscosity hypothesis (***note that this is not related to Boussinesq approximation used for simplification of free-convection flows***) is a widely used simplification to relate the Reynolds stresses to the mean velocity gradients in order to obtain two-equation turbulence models closure. It hypothesizes that the momentum transfer, due to turbulent eddies, can be modeled using an "eddy viscosity". For an incompressible flow, the Reynolds stresses can be modeled using the following equation,

$$\rho\tau_{ij} = \mu_t\left[\frac{\partial U_i}{\partial x_j} + \frac{\partial U_j}{\partial x_i}\right] - \frac{2}{3}\delta_{ij}\rho k \qquad \textbf{(III.11)}$$

The Boussinesq hypothesis is used in the Spalart-Allmaras one equation model, the ***k-ε*** and the ***k-ω*** two equations models, the advantage of this approach is the relatively low computational cost.

Where k is the turbulent kinetic energy per unit mass, μ_t is the eddy viscosity and U_i is the mean velocity component. Using the Boussinesq hypothesis, the six Reynolds stresses are reduced to two unknowns, μ_t and k. This is established by defining the turbulent kinetic energy k as:

$$k = \frac{1}{2}\overline{u'_i u'_j} \qquad \textbf{(III.12)}$$

The average root mean square velocities divided by the reference mean velocities defines the turbulent intensity T_i

$$T_i = \frac{\frac{2}{3}k^{1/2}}{U_{ref}} \quad \textbf{(III.13)}$$

By identifying the turbulence intensity, the turbulent kinetic energy per unit mass can be determined. The specification of the turbulence intensity is based on how intense the turbulence is. Turbulence transport of scalar quantities Φ such as mass, density etc. can also be modeled similarly, as show in Eq. (III.14)

$$-\overline{\rho u_i' \varphi'} = \Gamma_t \frac{\partial \Phi}{\partial x_i} \quad \textbf{(III.14)}$$

Where Γ_t is the eddy diffusivity. Both momentum turbulence transport as well as scalar transport modeling of turbulence is done using similar procedure; therefore, the eddy diffusivity Γ_t and turbulent viscosity μ_t are nearly equal. Two-equation turbulence models are widely used in the industry and academia. The Boussinesq hypothesis is generally used in CFD solvers.

For more detail of turbulent flow modeling, we recommend referring to [64]-[75]

II.5. Standard k-ε model

Standard k-ε model was used in numerical simulation of solar chimneys by several researchers [13], [15], [22] and compared with other turbulence models,[16]; Robustness, economy, and reasonable accuracy are attested.

Proposed by Launder and Spalding [77] and [80], the standard k-ε model is a two-equation turbulence closing system. It allows the determination of both, a turbulent length and time scale by solving two transport equations. The standard k-ε model has become the workhorse of practical engineering flow calculations in the time. It is a semi-empirical model, and the derivation of the model equations relies on phenomenological considerations and empiricism.

The standard k-ε model is based on model transport equations for the turbulence kinetic energy (k) and its dissipation rate (ε). The model transport equation for k is derived from the exact equation, while the model transport equation for ε was obtained using physical reasoning and bears little resemblance to its mathematically exact counterpart.

II.5.1. Transport Equations for the standard k-ε model

The turbulence kinetic energy $\boldsymbol{k}$ and its rate of dissipation ε are obtained from the following transport equations:

$$\frac{\partial}{\partial t}(\rho k) + \frac{\partial}{\partial x_i}(\rho k u_i) = \frac{\partial}{\partial x_j}\left[\left(\mu + \frac{\mu_t}{\sigma_k}\right)\frac{\partial k}{\partial x_j}\right] + G_k + G_b - \rho\varepsilon - Y_M + S_k \quad \textbf{(III.15)}$$

$$\frac{\partial}{\partial t}(\rho \varepsilon) + \frac{\partial}{\partial x_i}(\rho \varepsilon u_i) = \frac{\partial}{\partial x_j}\left[\left(\mu + \frac{\mu_t}{\sigma_\varepsilon}\right)\frac{\partial \varepsilon}{\partial x_j}\right] + C_{1\varepsilon}\frac{\varepsilon}{k}(G_k + C_{3\varepsilon}G_b) - C_{2\varepsilon}\rho\frac{\varepsilon^2}{k} + S_\varepsilon \quad \textbf{(III.16)}$$

μ_t is the turbulent (or eddy) viscosity, it is the combination of *k* and *ε* by:

$$\mu_t = \rho C_\mu \frac{k^2}{\varepsilon} \quad \textbf{(III.17)}$$

$\boldsymbol{G_k}$ Characterizes the generation of turbulence kinetic energy due to the mean velocity gradients, calculated as:

$$G_k = -\rho\overline{u'_\iota u'_J}\,\frac{\partial u_j}{\partial x_i} \quad \textbf{(III.18)}$$

To evaluate $\boldsymbol{G_k}$ in a manner consistent with the Boussinesq hypothesis:

$$G_k = \mu_t S^2 \quad \textbf{(III.19)}$$

Where $\boldsymbol{S}$ is the modulus of the mean rate-of-strain tensor, defined as:

$$S \equiv \sqrt{2S_{ij}S_{ij}} \quad \textbf{(III.20)}$$

The model constants have the following values

$$C_{1\varepsilon} = 1.44, C_{2\varepsilon} = 1.92, C_\mu = 0.09, \sigma_k = 1.0, \sigma_\varepsilon = 1.3$$

Note that $\mu_{eff} = \mu + \mu_t$ is used instead of $\mu_t$in equation (III.19) when using high Reynolds number *k*-*ε* model.

$\boldsymbol{G_b}$is The generation of turbulence due to buoyancy defined by:

$$G_b = \beta g_i \frac{\mu_t}{Pr_t}\frac{\partial T}{\partial x_i} \quad \textbf{(III.21)}$$

$\boldsymbol{Pr_t}$ is the turbulent prandtl number

$\boldsymbol{g_i}$ is the component of the gravitational vector in i^{th} direction

$\boldsymbol{\beta}$ is the thermal expansion coefficient $\boldsymbol{\beta = -\frac{1}{\rho}\left(\frac{\partial \rho}{\partial T}\right)_p}$

For ideal gases, equation (III.21) becomes:

$$\boldsymbol{G_b = -g_i \frac{\mu_t}{Pr_t}\frac{\partial \rho}{\partial x_i}} \quad \textbf{(III.22)}$$

In ANSYS Fluent, the effects of buoyancy on the generation of *k* are always included when you have both a nonzero gravity field and a nonzero temperature (or density) gradient [62]

The buoyancy effects on ε are neglected simply by setting G_b to zero in the transport equation for ε. However, the buoyancy effect on ε can be included. In this case, the value of G_b is given by equation (III.22) considering air as an ideal gas.

$C_{3\varepsilon}$ determines the degree to which ε is affected by the buoyancy, it is calculated by:

$$\boldsymbol{C_{3\varepsilon} = tanh\left|\frac{v}{u}\right|} \quad \textbf{(III.23)}$$

v Is the component of velocity parallel to the gravitational direction.

u is the component of velocity perpendicular to the gravitational direction.

So $C_{3\varepsilon}$becomes unity (1) when the flow is parallel to the gravity direction and zero (0) when the flow is perpendicular to the gravitational vector.

Y_M Indicate the compressibility effect; it can be neglected in modelling incompressible flows.

S_k and S_ε are source terms.

II.5.2. Energy equation in k-ε model

By the same analogy to turbulent momentum transfer; heat transport is modeled using the concept of Reynolds; the energy equation is therefore

$$\boldsymbol{\frac{\partial}{\partial t}(\rho E) + \frac{\partial}{\partial x_i}[u_i(\rho E + p)] = \frac{\partial}{\partial x_j}\left[K_{eff}\frac{\partial T}{\partial x_j} + u_i(\tau_{ij})_{eff}\right] + S_h} \quad \textbf{(III.24)}$$

E is the total energy of a fluid obtained by adding its internal energy per unit mass, e, to its kinetic energy per unit mass $\frac{|\vec{v}|^2}{2}$, so we can write for the total energy [69]

$$E = e + \frac{|\vec{v}|^2}{2} = e + \frac{u^2+v^2+w^2}{2} \quad \textbf{(III.25)}$$

Usually, the energy equation (III.24) is written in a slightly different form. For that purpose, we will utilize the following general relation between the total enthalpy, the total energy and the pressure [69]

$$H = h + \frac{|\vec{v}|^2}{2} = E + \frac{P}{\rho} \quad \textbf{(III.26)}$$

K_{eff} Is the effective thermal conductivity

$$K_{eff} = \lambda + \frac{c_p+\mu_t}{Pr_t} \quad \textbf{(III.27)}$$

Pr_t Is the turbulent Prandtl number, the default value in ANSYS Fluent is 0.85. Its value can be changed in the viscous model dialog box.

The turbulent Prandtl number is in general assumed to be constant in the flow field (Pr_t= 0.9 for air) **[69]**

$(\tau_{ij})_{eff}$ Is the deviatoric stress tensor, defined as:

$$(\tau_{ij})_{eff} = \mu_{eff}\left(\frac{\partial u_j}{\partial u_i} + \frac{\partial u_i}{\partial u_j}\right) - \frac{2}{3}\mu_{eff}\frac{\partial u_k}{\partial u_k}\delta_{ij} \quad \textbf{(III.28)}$$

The term involving $(\tau_{ij})_{eff}$ represents the viscous heating, and is always computed in the density-based solvers. It is not computed by default in the pressure-based solver [62].

S_h Is the source therm.

III. Boussinesq approximation in buoyancy-driven flow

Natural-convection flows or "*buoyancy-driven flow"*, can be computed by

1. Setting up the problem with fluid density as a function of temperature
2. Treats density as a constant value in all solved equations, except for the buoyancy term in the momentum equation.

The second approach is proposed by Joseph Valentin Boussinesq; it ignores density variations except in the gravitational term ***"****buoyancy term"*. The principle of this approximation is that the difference in inertia is negligible but gravity is sufficiently strong to make the specific weight significantly different.

By this approach, we get faster convergence than by setting up the problem with fluid density as a function of temperature.

The continuity equation is:

$$\boldsymbol{\nabla.(\rho u) = 0} \qquad \textbf{(III.29)}$$

If density variations are ignored, eq. (III.29) reduces to:

$$\boldsymbol{\nabla.U = 0} \qquad \textbf{(III.30)}$$

The general expression for conservation of momentum (Navier-Stokes equations) is:

$$\boldsymbol{\nabla.(\rho UU) = -\nabla P + \nabla.\left(\mu\left((\nabla U) + (\nabla U)^T\right)\right) - \frac{2}{3}\mu(\nabla.U)I + \rho g} \qquad \textbf{(III.31)}$$

$\boldsymbol{I}$ replace the kronecker delta

The gravitational term $\boldsymbol{\rho g}$ is the body force (buoyancy force).

Assuming that density have a fixed part (reference density$\boldsymbol{\rho_0}$) and fluctuation$\boldsymbol{\Delta\rho}$

$$\boldsymbol{\rho = \rho_0 + \Delta\rho}$$

Navier Stokes equation becomes:

$$\underbrace{\boldsymbol{\nabla.((\rho_0 + \Delta\rho)UU)}}_{\boldsymbol{convection}} = \boldsymbol{-\nabla P + \nabla.\left(\mu\left((\nabla U) + (\nabla U)^T\right)\right) - \frac{2}{3}\mu(\nabla.U)I + \underbrace{(\rho_0 + \Delta\rho)g}_{\boldsymbol{bouyancy}}} \qquad \textbf{(III.32)}$$

- Considering the density as a constant ($\boldsymbol{\rho \approx \rho_0}$) in the convection terms.
- Assuming that the density changes affect only in buoyancy term, Navier Stokes equations are now:

$$\underbrace{\boldsymbol{\rho_0(\nabla.(UU))}}_{\boldsymbol{approximation}} = \boldsymbol{-\nabla P + \nabla.\left(\mu\left((\nabla U) + (\nabla U)^T\right)\right) - \frac{2}{3}\mu(\nabla.U)I + \underbrace{\rho g}_{\boldsymbol{no\ change}}} \qquad \textbf{(III.33)}$$

For incompressible flows, further simplification now yields (divide eq (III.33) by $\boldsymbol{\rho_0}$ and take in the continuity equation (III.30))

$$\boldsymbol{\nabla.(UU) = -\frac{1}{\rho_0}\nabla P \pm \nu\nabla^2 U + \frac{\rho g}{\rho_0}} \qquad \textbf{(III.34)}$$

In incompressible flow solvers, it is a standard practice to use kinematic pressure

$$\boldsymbol{P_k = \frac{P}{\rho_0}} \quad \textbf{(III.35)}$$

The Navier Stokes equations are now:

$$\begin{cases} \boldsymbol{\nabla . U = 0} \\ \boldsymbol{\nabla . (UU) = -\nabla P_k \pm \nu \nabla^2 U + \frac{\rho g}{\rho_0}} \end{cases} \quad \textbf{(III.36)}$$

We also need to remove density from the buoyancy term.

The coefficient of thermal expansion is defined as:

$$\boldsymbol{\beta = -\frac{1}{\rho_0}\left(\frac{\partial \rho}{\partial T}\right)_p} \quad \textbf{(III.37)}$$

By the following linear approximation:

$$\boldsymbol{\beta \approx -\frac{1}{\rho_0}\left(\frac{\rho - \rho_0}{T - T_0}\right)} \quad \textbf{(III.38)}$$

$$\boldsymbol{\rho - \rho_0 \approx -\beta \rho_0 (T - T_0)} \quad \textbf{(III.39)}$$

$$\boldsymbol{\rho \approx \rho_0 [1 - \beta (T - T_0)]} \quad \textbf{(III.40)}$$

The buoyancy term is now:

$$\boldsymbol{\frac{\rho g}{\rho_0} \approx [1 - \beta (T - T_0)] g} \quad \textbf{(III.41)}$$

By replacing the buoyancy term in Navier Stokes equations **(III.36),** we have:

$$\begin{cases} \boldsymbol{\nabla . U = 0} \\ \boldsymbol{\nabla . (UU) = -\nabla P_k \pm \nu \nabla^2 U + \underbrace{[1 - \beta (T - T_0)] g}_{bouyancy}} \end{cases} \quad \textbf{(III.42)}$$

By this approach, the degree of non-linearity and the memory requirement are reduced.

The Boussinesq approximation is valid when $\boldsymbol{\Delta \rho \ll \rho_0}$

IV. Near wall treatment

IV.1. Theory of boundary layer

Close to the wall, the turbulence field is affected by numerous and complex effects; mainly,

- The reduction in the length scales.
- The wall reflection contribution in the pressure-strain correlations.
- The development of a thin layer adjacent to the wall (viscous sublayer) in which the molecular viscosity is dominant.
- The anisotropic character of the turbulence near the wall.
- The strongly non-homogenous character of the turbulence field.

All these effects have important consequences on the transfer properties of the flow, in particular on the wall friction and thermal diffusion.

In the presence of a wall with a no-slip condition, the flow is reduced to laminar due to the viscous effects. The velocity near the wall changes rapidly within a small distance. For high-Reynolds flows, the boundary layer is very thin, and in order to capture the effects of the boundary layer, many nodes may be required. This will result in an expensive computation.

Very close to the wall, viscous damping reduces the tangential velocity fluctuations, while kinematic blocking reduces the normal fluctuations.
The appropriate selection of a wall treatment is hence essential for correct modeling of the physics.

Concerning the outer part of the near-wall region, the turbulence is rapidly developed by the production of turbulence kinetic energy due to the large gradients in mean velocity.

As shown in figure (III.2) the near-wall region can be subdivided into three layers:

- The "viscous sublayer", $\boldsymbol{y^+ < 5}$ where the flow is almost laminar, and the viscosity plays a dominant role in momentum and heat or mass transfer
- The outer layer, $\boldsymbol{y^+ > 30}$ called the fully turbulent or log-law region, the turbulent shear dominates.

- The buffer layer located in the intermediate region between the viscous sublayer and the fully turbulent layer, $\mathbf{5 < y^+ < 30}$ where the effects of molecular viscosity and turbulence are both important.

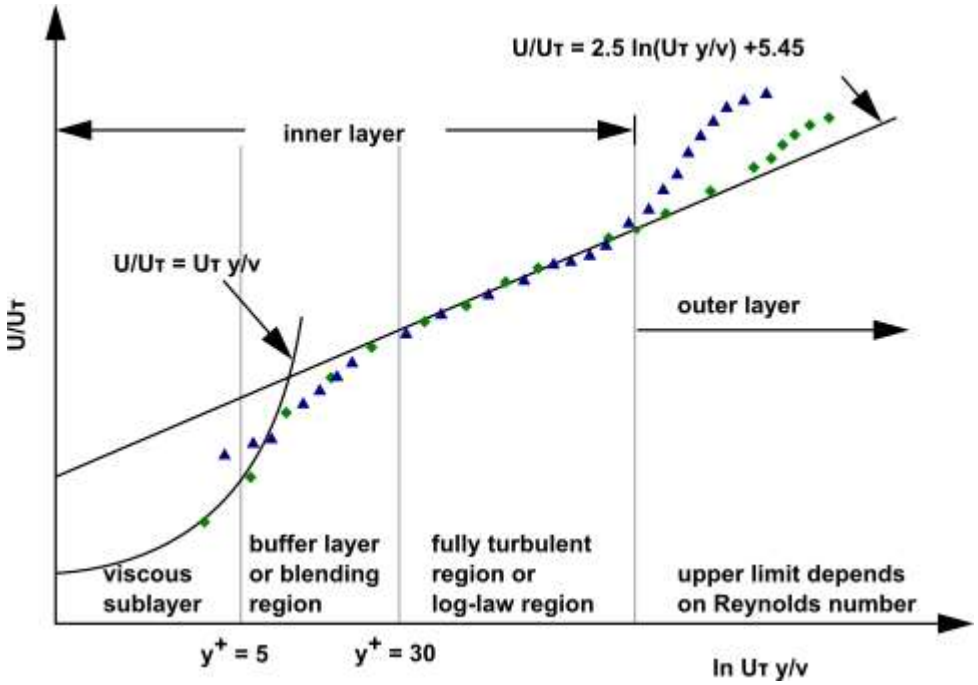

Figure III .2: Near wall regions

In figure (**III** .2)

$$y^+ \equiv \rho u_\tau y/\mu \qquad \textbf{(III.43)}$$

u_τ Is the friction velocity defined as:

$$u_\tau = \sqrt{\tau_w/\rho} \qquad \textbf{(III.44)}$$

τ_w Is the wall shear stress

$$\tau_w = \mu \left.\frac{du}{dy}\right|_{wall} \qquad \textbf{(III.45)}$$

There are two approaches to modeling the near-wall region

IV.2. "Near-wall modeling" approach (Low Reynolds Number Models)

Turbulent model with an appropriate near wall treatment can be applied all the way until the wall. The turbulence models are modified to enable the viscosity-affected region to be resolved with a mesh all the way to the wall, including the viscous sublayer. Close to the wall, gradients of scalars are large; so a fine grid resolution is required to accurately resolve the gradients.

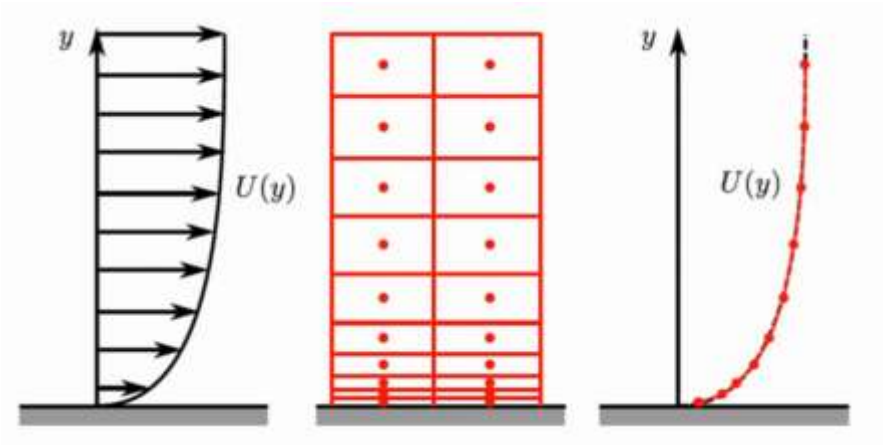

Figure III.3: Inflation layer of mesh cells to capture the steep velocity gradient in a boundary layer [78]

However, by refining meshes down to the smallest scales to resolve boundary layers may exert new issues that effect on mesh quality and cell account and consequently calculation performance.

IV.3. "Wall functions" approach (High Reynolds Number Models)

In this approach, the viscous sublayer and buffer layer are not resolved. As an alternative, semi-empirical formulas called "wall functions" are used to bridge the viscosity-affected region between the wall and the fully-turbulent region. The use of wall functions avoids the need to modify the turbulence models near the wall to compute flow scalars. (**Fig. III .4)**

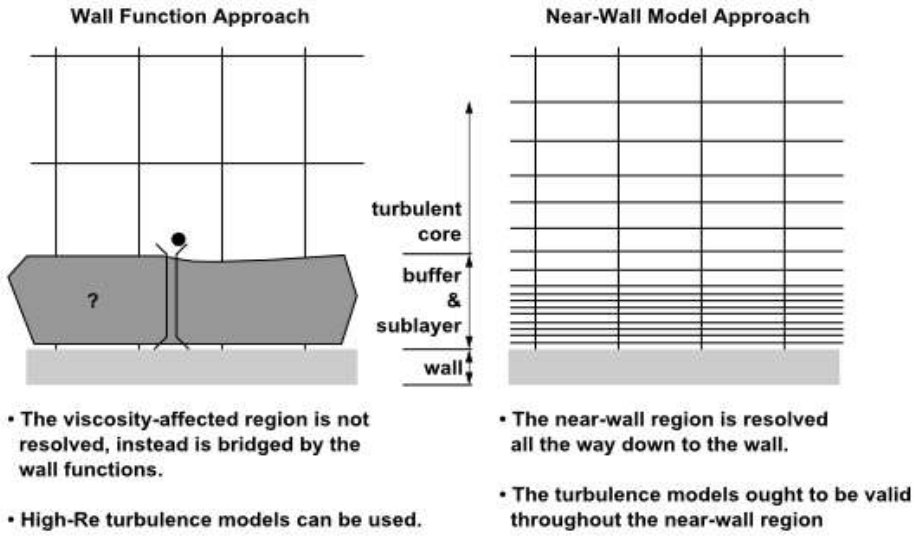

Figure III .4: Near-Wall Treatments in ANSYS Fluent [62]

IV.4. Wall functions

Wall functions are semi-empirical formulas and functions that link the solution variables at the near-wall cells and the corresponding quantities on the wall. They consist of:

- law-of-the-wall for the mean value of scalars
- formulae for the near-wall turbulent quantities

Depending on the choice of turbulent model, ANSYS Fluent offers the following choices of wall-function approaches [62]:

- Standard Wall Functions
- Scalable Wall Functions
- Non-Equilibrium Wall Functions
- User-Defined Wall Functions

IV.5. Standard Wall functions

In 1931, Theodore von Kármán **[81]** noticed that there were a common behavior patterns repeated among different boundary layers in a wide range of flow scenarios.

The so-called Law of the Wall based on the following non-dimensionalization of flow variables, such as velocity (U^+), and distance to the wall (y^+):

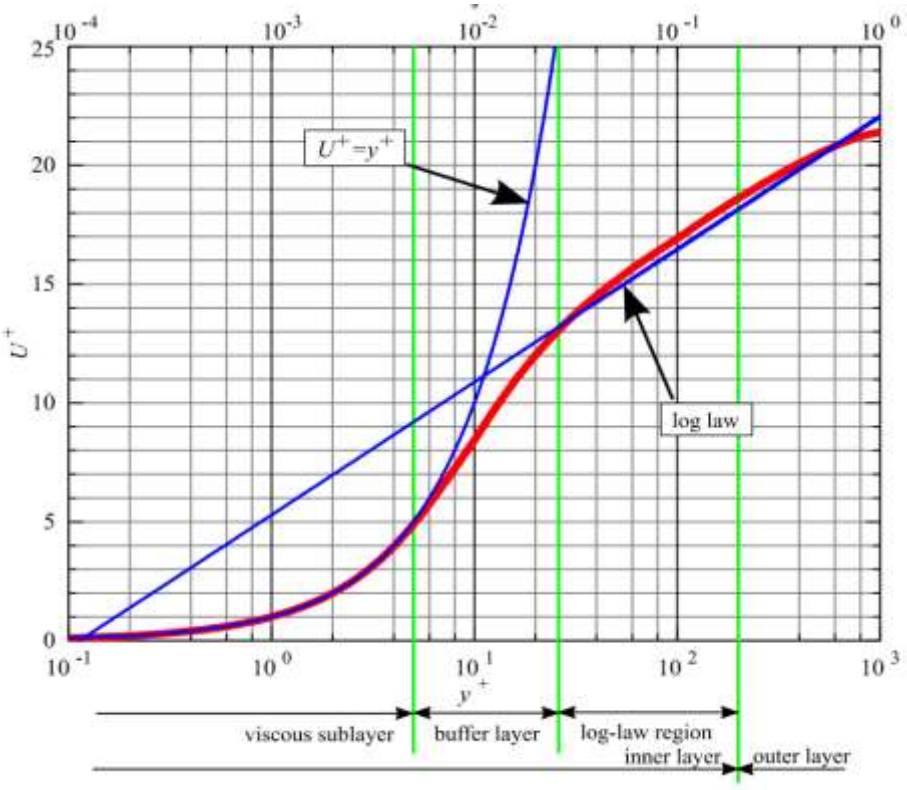

Figure III .5: Schematic standard wall function

These functions are:

$$\begin{cases} \boldsymbol{U^+ = y^+} & \boldsymbol{y^+ < 5} \\ \boldsymbol{U^+ = \frac{1}{k}\log(Ey^+)} & \boldsymbol{30 < y^+ < 200} \end{cases} \quad \textbf{(III.46)}$$

$\boldsymbol{k = 0.4187\ and\ E = 9.793}$ Are von Kårmån and empirical coefficients respectively.

$$\begin{cases} \boldsymbol{y^+ \equiv \frac{\rho u_\tau y}{\mu}} \\ \boldsymbol{U^+ = \frac{U}{u_\tau}} \end{cases} \quad \textbf{(III.47)}$$

$\boldsymbol{u_\tau}$ Is the friction velocity defined in equation **(III.44)**

The wall functions intersect at $\boldsymbol{y^+ = 11.25}$

Hence, the model that can be used is:

$$\boldsymbol{U^+ = \begin{cases} y^+ & y^+ < 11.25 \\ \frac{1}{k}\log(Ey^+) & y^+ > 11.25 \end{cases}} \quad \textbf{(III.48)}$$

This approach gives large errors in the buffer region $\boldsymbol{5 < y^+ < 30}$ **;** for this reason, it is not recommended to place cells in this region.

V. Computational fluid dynamic of solar chimney

For new buildings design, the use of CFD in calculating ventilation systems becomes an increasingly common practice. In the present work, the main aim of the numerical simulation is to allow flow visualization for qualitative evaluation, while the experimental measurements provided quantitative evaluation. CFD analysis allow defining properties in the computational domain. The model is validated with the small-scale test solar chimney so as to be used for the evaluation and measurement of the thermal behavior and efficiency of any other design improving natural ventilation and solar chimneys in particular.

Techniques of numerical solution are finite difference, finite element, finite volume and spectral methods. We are concerned with only the finite volume method. In summary, the numerical algorithm consists of the following steps:

• Integration of the governing equations of fluid flow over all the finite control volumes of the domain

• Discretization: conversion of the resulting integral equations into a system of algebraic equations

• Solution of the algebraic equations by an iterative method

The first step, the control volume integration, the resulting statements express the conservation of relevant properties for each finite size cell. This clear relationship between the numerical algorithm and the basic physical conservation principle forms one of the main attractions of the finite volume method and makes its concepts more simple. The conservation of a general flow variable$\emptyset$, e.g. a velocity component or enthalpy, within a finite control volume can be expressed as a balance between the various processes tending to increase or decrease it. Therefore, we have:

$$\begin{bmatrix} rate\ of \\ change \\ of\ \emptyset \\ in\ time \\ into\ the \\ control\ volume \end{bmatrix} = \begin{bmatrix} net\ rate\ of \\ increase \\ of\ \emptyset \\ due\ to \\ convection \\ into\ the \\ control\ volume \end{bmatrix} + \begin{bmatrix} net\ rate\ of \\ increase \\ of\ \emptyset \\ due\ to \\ diffusion \\ into\ the \\ control\ volume \end{bmatrix} + \begin{bmatrix} net\ rate\ of \\ creation \\ of\ \emptyset \\ inside\ the \\ control\ volume \end{bmatrix}$$

CFD codes contain discretization techniques suitable for the treatment of the key transport phenomena, convection (transport due to fluid flow) and diffusion (transport due to variations

of ∅ from point to point) as well as for the source terms (associated with the creation or destruction of ∅) and the rate of change with respect to time. The underlying physical phenomena are complex and non-linear so an iterative solution approach is required. The most popular solution procedures are by the TDMA (tri-diagonal matrix algorithm) line-by-line solver of the algebraic equations and the SIMPLE algorithm to ensure correct linkage between pressure and velocity. Commercial codes may also give the user a selection of further, more recent, techniques such as Gauss–Seidel point iterative techniques with multigrid accelerators and conjugate gradient methods **[83].**

In **Figure III .6,** the organizational chart illustrates steps followed in the present simulation using **ANSYS Fluent**.

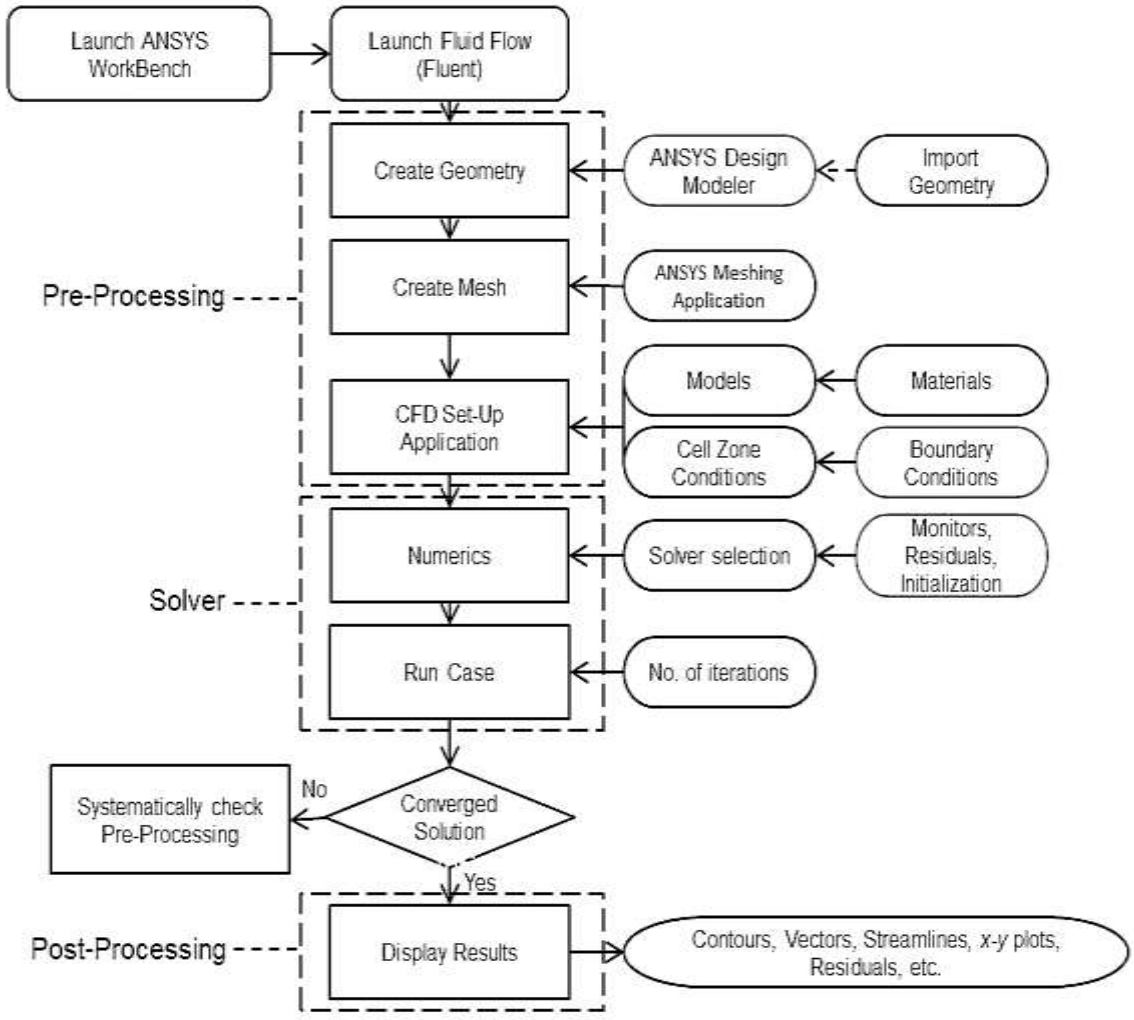

Figure III .6: Steps chart of the numerical simulation

V.1. 5.1 CFD set up

V.1.1. Geometry

A 3D three-dimensional geometry of solar chimney used in the experimental work is developed in Design Modeler (DM) of ANSYS workbench (version R19.1, **Fig III .7**) Dimensions of the solar chimney are the same used in the experimental system.

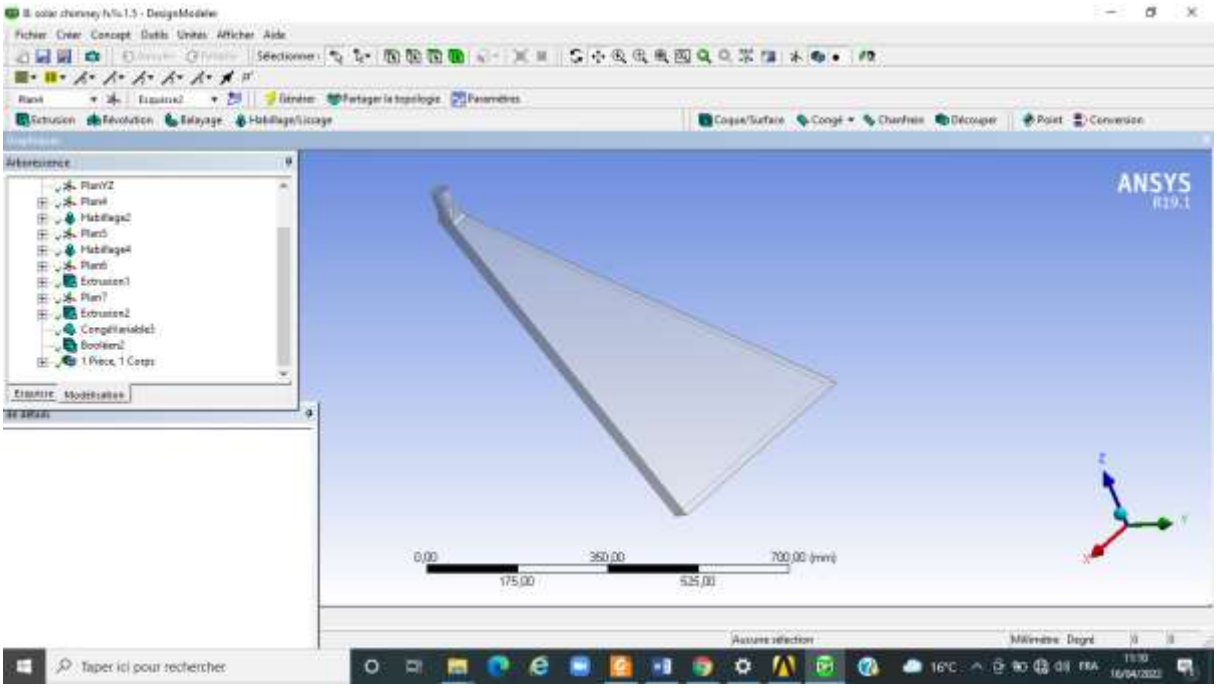

Figure 3.7: Geometry of the h/l=1.5 solar chimney

V.2. Mesh

The computational domain is split into smaller finite volumes; this process is called meshing; it is done using the mesher of ANSYS R19.1. The scheme is unstructured that uses hexahedral elements and quadratic order with coarser grids in the central region of the air channel and refined no uniform grids near the outlet boundary **(Fig. III .8 a and b).**

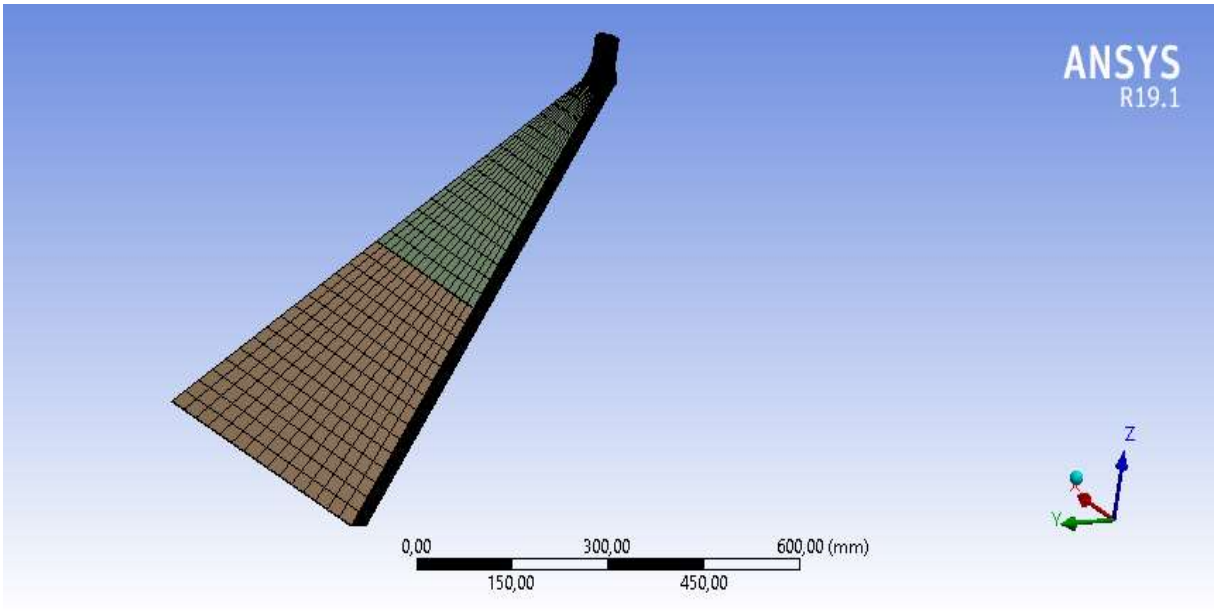

Figure III .8.a : Computational domain grid

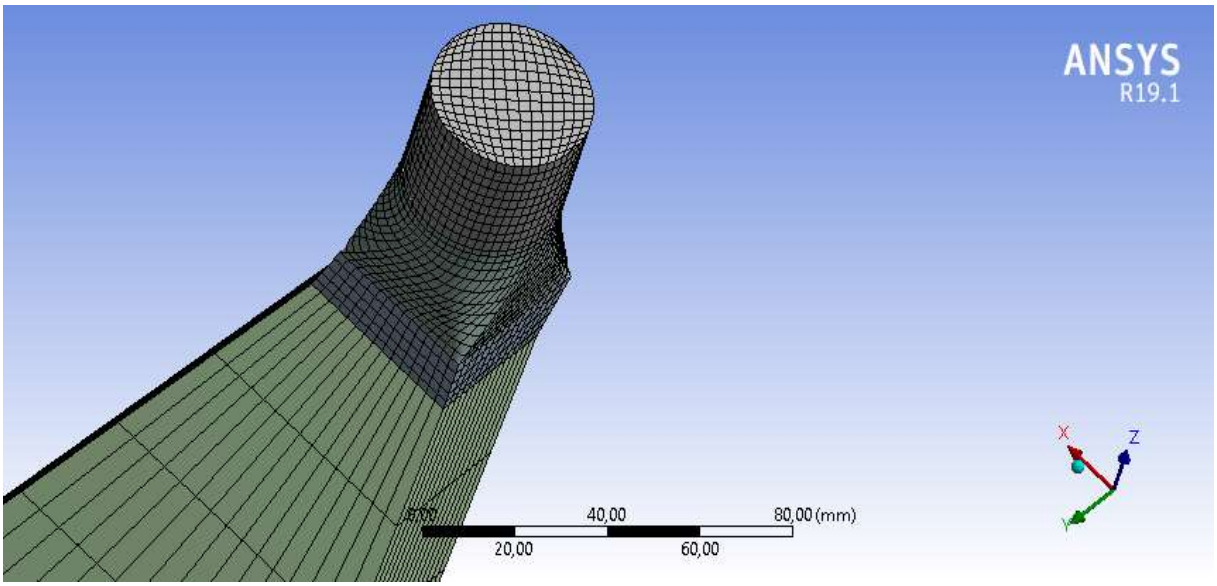

Figure3.8.b: Outlet region treatment

Special attention is given to the air exit region, since capturing the physics here is essential. The expansion rate of the mesh size in the wall normal direction is 1.2. A mesh sensitivity test is performed.

V.2.1. Mesh import and check

The mesh is checked after reading in Fluent, in order to detect any mesh trouble before starting with the problem setup.

The mesh check examines the topological information, beginning with the number of faces and nodes per cell. A tetrahedral cell should have four faces and four nodes, and a hexahedral cell should have six faces and eight nodes. Polyhedral cells will have an arbitrary number of faces and nodes. In addition, the face handedness and face node order for each zone is checked. The zones should contain all right-handed faces, and all faces should have the correct node order.

The last topological verification is checking the element-type consistency. If a mesh does not contain mixed elements (quadrilaterals and triangles or hexahedral and tetrahedral), ANSYS Fluent will determine that it does not need to keep track of the element types. By doing so, it can eliminate some unnecessary work.

V.2.2. Mesh Sensitivity Analysis

The accuracy of calculation is dependent on the number of cells used to represent the domain. If few cells are used small scale may not be resolved and if too many cells are used the computational cost will be incredibly high in term of time and memory. A mesh sensitivity study was carried out to have the best compromise between accuracy and time. The number of cells is optimized by means of a grid independence test via a parametric analysis. The interesting value is the average velocity at the outlet of the computational domain **Fig. III .9.**

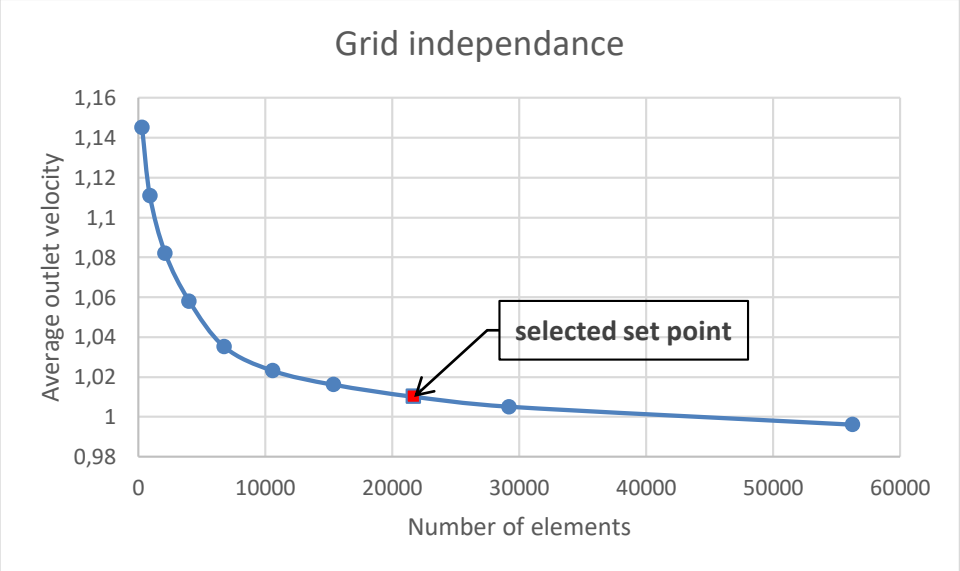

Figure III.9: Grid independence test

Figure III .9 shows that there is no significant change in average velocity at the outlet beyond the grid size of (21708 elements, 95247 nodes). Therefore, for the present study, this grid size is used to perform all the simulations.

V.3. Set up the physical model and solver

The CFD code (ANSYS FLUENT) solves the turbulent flow and heat transfer models by the discretization of the continuous space and time (if transient, steady in this study) into finite intervals. A finite volume solver solves the governing equations of mass, momentum and energy on a staggered grid. The variables are computed at only the grid points; this means that discrete values replace the continuous information contained in the solution of the differential equations.

V.4. Material properties and operation conditions

All the properties of used materials, air as a working fluid and walls (steel and glass), are available in the Fluent® database. The Boussinesq approximation is used to consider the buoyancy driven force and get faster convergence. The thermal expansion coefficient of air is 0.0034 (k^{-1})

V.5. Boundary conditions

The computational domain is the space between the glazing and absorber wall with inlet and outlet openings, any CFD problem is defined in terms of initial and boundary conditions. It is important to specify these correctly and understands their role in the numerical algorithm. The initial values of all the variables need to be specified at all solution points in the flow domain. This involves no special measures other than initializing the appropriate data arrays in the CFD code. The present section describes the implementation of the boundary conditions at the:

- Inlet
- outlet
- walls

The following boundary conditions are adopted (similar boundary conditions have been adopted in [26]

V.5.1. Inlet

At the inlet section of the solar chimney, Pressure inlet boundary condition is set to define the fluid pressure, Pressure inlet boundary conditions is used since the flow rate and velocity are not known. This situation may arise in many practical situations, including buoyancy-driven flows **[75].** The total (gauge) pressure is set to zero at the inlet, and the inflow is normal to the inlet. The incoming air is at the reference temperature.

The pressure field obtained by solving the pressure correction equation does not give absolute pressures (Patankar, 1980). It is common practice to fix the absolute pressure at one inlet node and set the pressure correction to zero at that node. Having specified a reference value, the absolute pressure field inside the domain can now be obtained **[83].**

In order to have an accurate simulation, the system should be supplied by a realistic inlet values of turbulent kinetic energy k its and dissipation rate ε. because the inlet values of turbulence parameters can significantly affect the downstream flow.

V.5.2. Outlet

At the outlet area, we consider the pressure outlet boundary condition; it is assumed that the stream wise variations of all velocity components and temperature are negligible. The fluid pressure at the exit becomes equal to the ambient pressure. In case of a backflow at the exit, his velocity is supposed to be normal to the exit boundary and the backflow temperature is at the reference temperature.

V.5.3. Walls

A rigid no-slip wall condition is used on all walls (including the vertical absorber wall and the inclined glazing wall). In addition, a constant heat flux is imposed at the absorber wall; thermal efficiency is introduced to calculate values of imposed heat flux from the captured solar irradiation. We supposed that all the other walls are adiabatic.

VI. Numerical Solution

The pressure based solver is selected and the SIMPLE scheme (Patankar, 1980) **[82]** is used to enforce mass conservation through coupling the velocity and pressure. The sequence of operations in the SIMPLE algorithm is given in **Figure III.10**

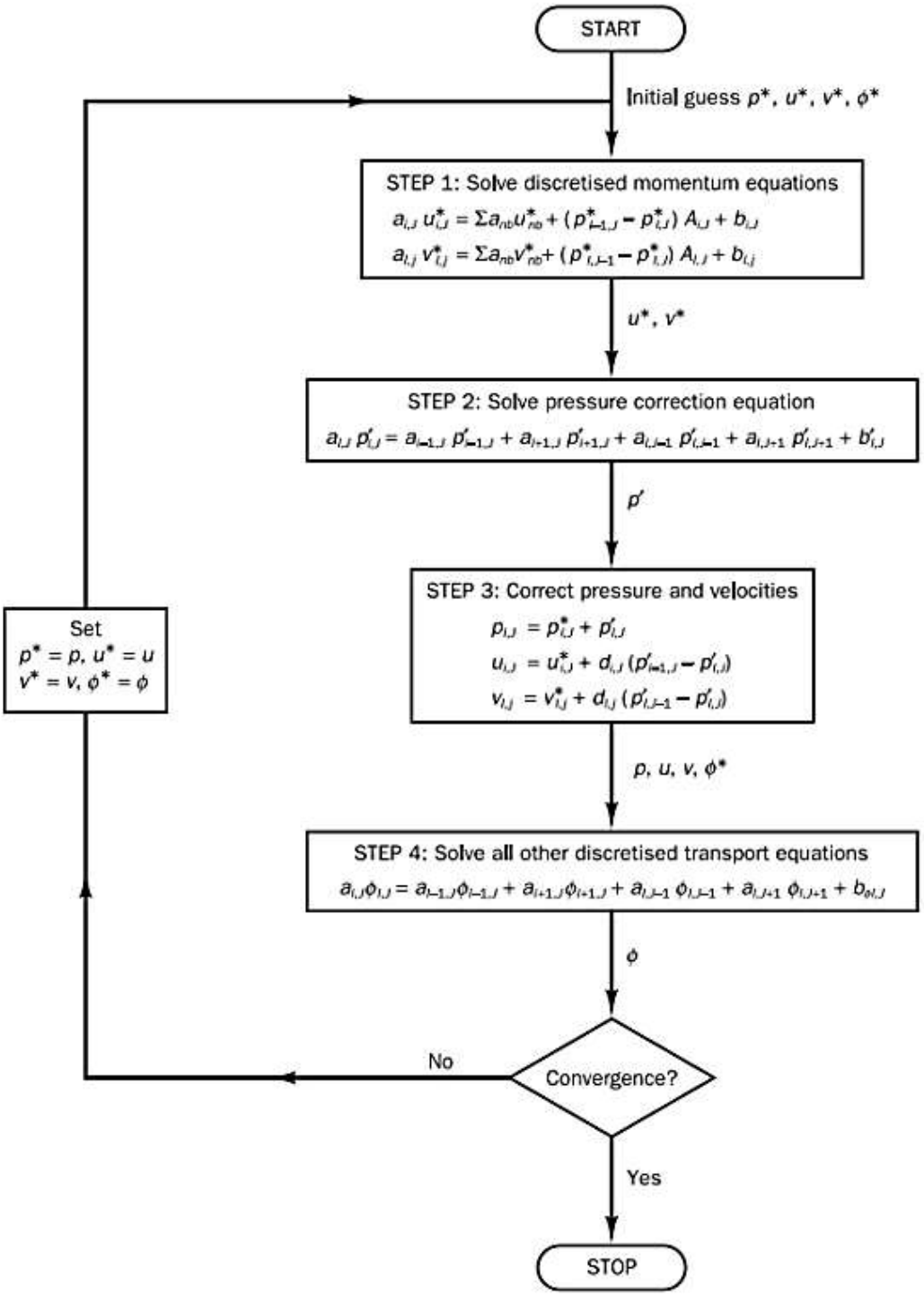

Figure III .10: The SIMPLE algorithm [83]

For spatial discretization, the second order scheme is used for pressure terms; for the momentum and turbulence variables, the second order upwind scheme is adopted. The least squares cell based is selected for gradients. however; the QUICK scheme is used for the energy.

Numerical stability is improved by the introduction of so-called under-relaxation factors.

VII. Solution convergence

For numerical solution, the algorithm is iterative; in a converged solution, residuals should be very small. Progress towards a converged solution require careful selection of the settings of various relaxation factors. In the present work, residuals should drop 10^{-15} or after 1000 iterations. **Figure III .11** indicates the convergence behavior, it show that residuals of the computed variables become stable after 800 iterations ($\approx 10^{-5}$ for momentum and turbulence variables and approximatively 10^{-7} for the energy).

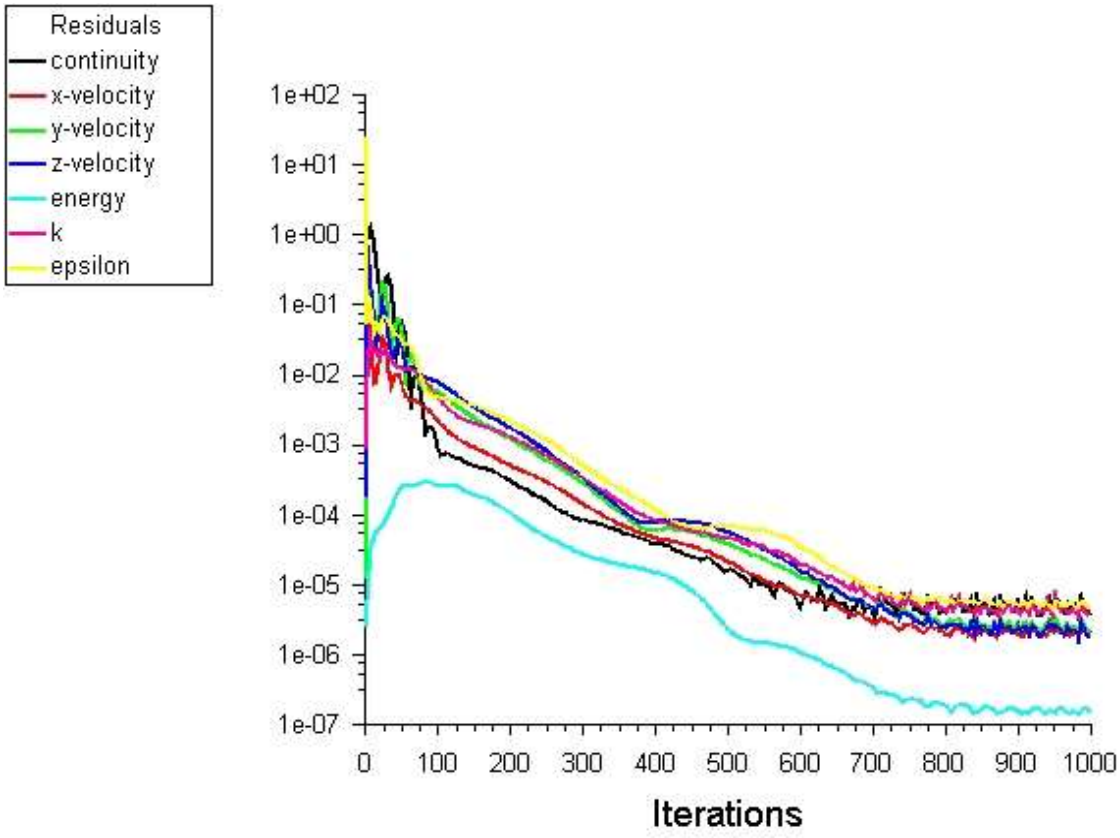

Figure III.11: Residuals

VIII. Validation

CFD process solves systems of non-linear partial differential equations in discretized form on meshes of finite control volumes that cover the domain of interest and its boundaries. This gives rise to uncertainty and errors:

a. Uncertainty

- Physical model uncertainty: differences between real flows and CFD due to inadequate representation of physical model or by simplifying assumptions in the modelling process (e.g. incompressible flow, steady flow)
- Input uncertainty: (caused mainly by lack of knowledge) inaccuracies due to limited information or approximate representation of geometry, boundary conditions, material properties etc.

b. Errors

Recognized numerical errors are:

- Discretization error: The discretization error is associated with the neglected higher-order terms, which gives rise to errors in CFD results. Discretization errors can be minimized by careful mesh design in high-quality CFD.
- Roundoff error: named the machine accuracy, it is the result of the computational representation of real numbers by a finite number of significant digits.
- Iterative convergence error: the iterative process is essential for numerical solution of fluid flow problems. If the iteration sequence is convergent, the difference between the final solution and the current solution after n iterations reduces as the number of iterations increases. But, in practice, we cut the sequence by fixing the number of iterations, this is due to the available resources of computing power and time when the solution is sufficiently close to the final solution. This truncation generates numerical error in the CFD solution.

Once errors and uncertainty are inevitable aspects of CFD, it becomes necessary to validate the simulation tool in order to quantify the level of confidence in its results. For this raison, CFD and experimental results were compared; key parameters selected for the comparison are average outlet velocity and temperature.

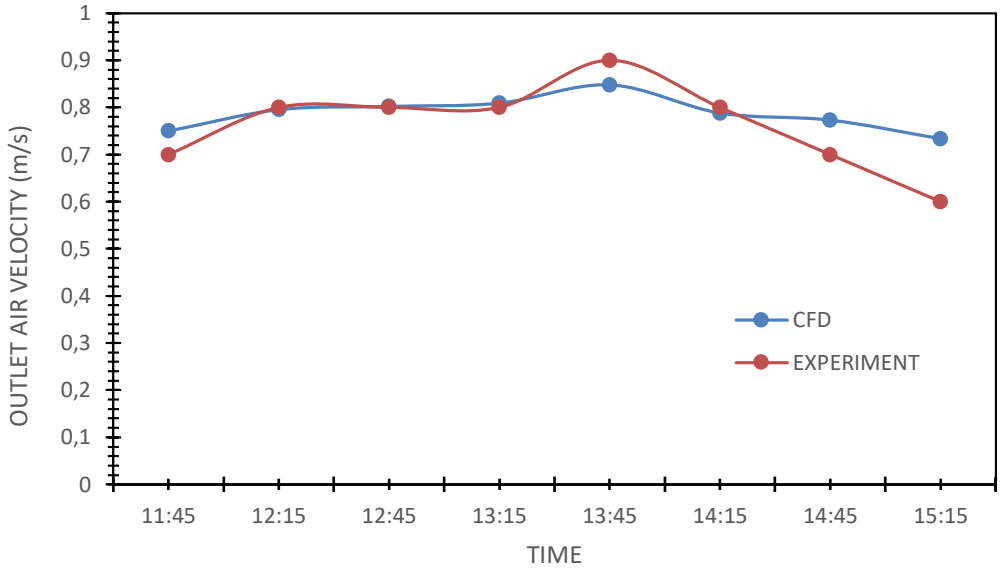

Figure III.12: Experimental and numerical results for the outlet air velocity; Comparison to validate the numerical code

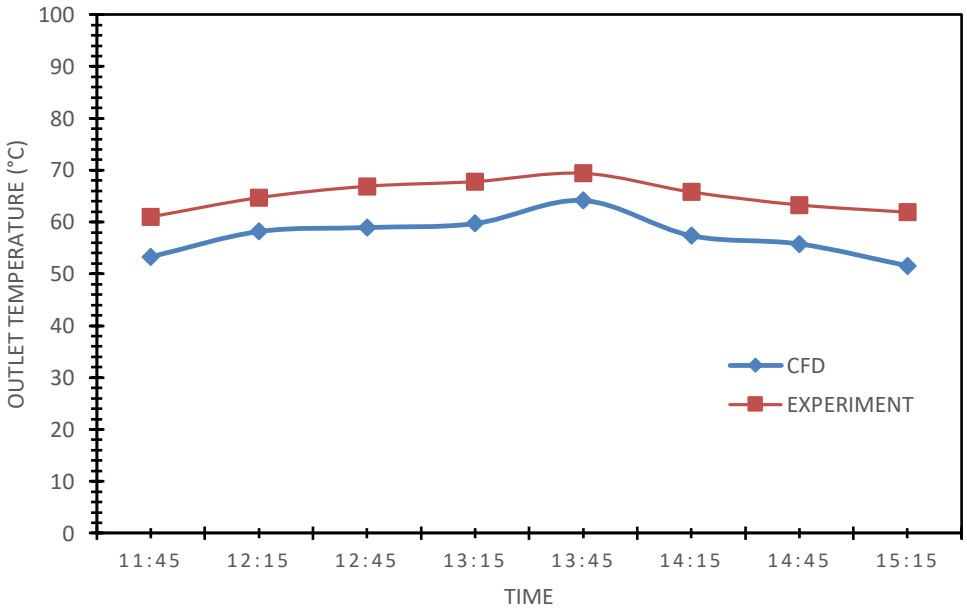

Figure III.13: Experimental and numerical results for the outlet air temperature; Comparison to validate the numerical code

Figure III.12 and III.13 show the behavior of velocity and temperature at the outlet of the h/l=1.5 solar chimney. The figures indicate that the results obtained with numerical model

show
a smaller difference regarding the experimental results.

The values indicate that the model underestimates the temperature behavior by 7.5% to 12%. Regarding the velocity, the model sometimes underestimate and sometimes overestimate the value during the test period. Hence, numerical results show a very good agreement with the experimental results.

IX. Results and discussion

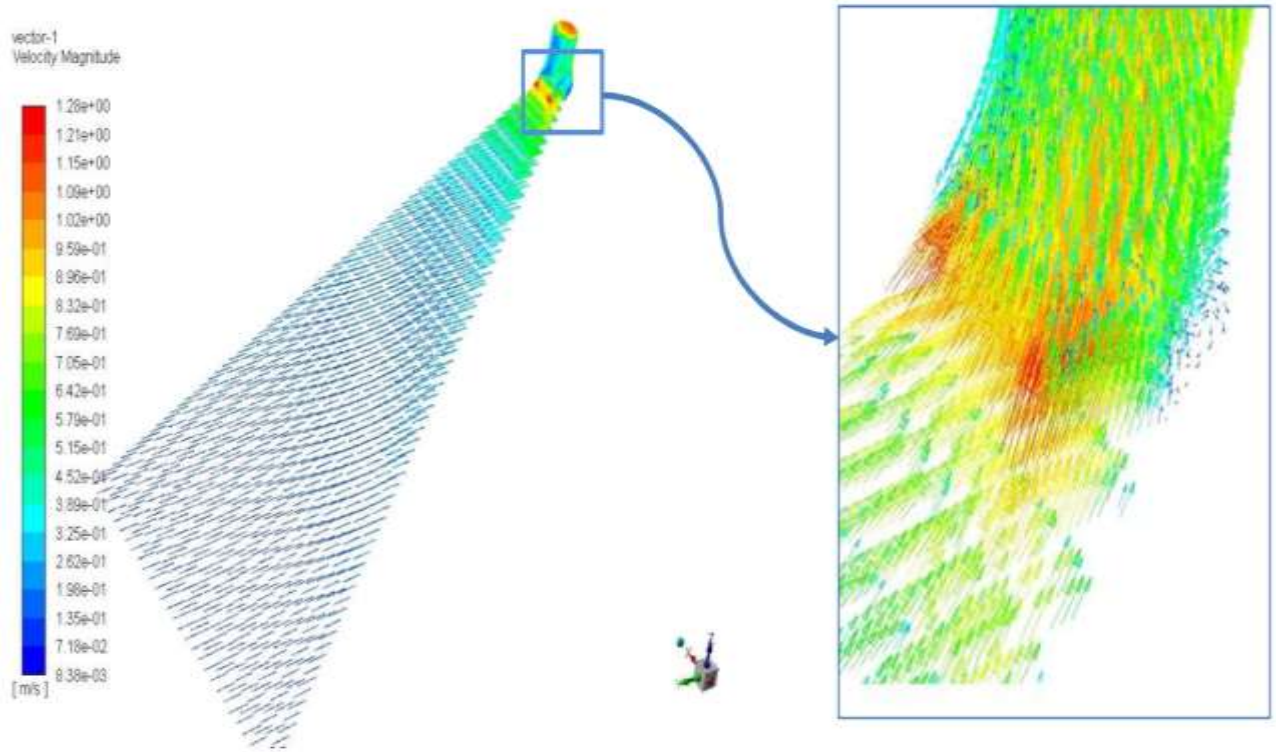

Figure III.14: Velocity vectors in the chimney domain

Figure III.14 shows the velocity vectors in the solar chimney domain, Fresh air come into the chimney with small kinetic and thermal energy and take thermal energy by different modes of heat transfer. Through the system, a part of thermal energy is converted into kinetic energy. Near the outlet, higher velocity of air result because of the passage narrowing. At the elbow, a recirculation is generated**;** this is a configuration that should be avoided in solar chimney systems in order to eliminate energy loses.

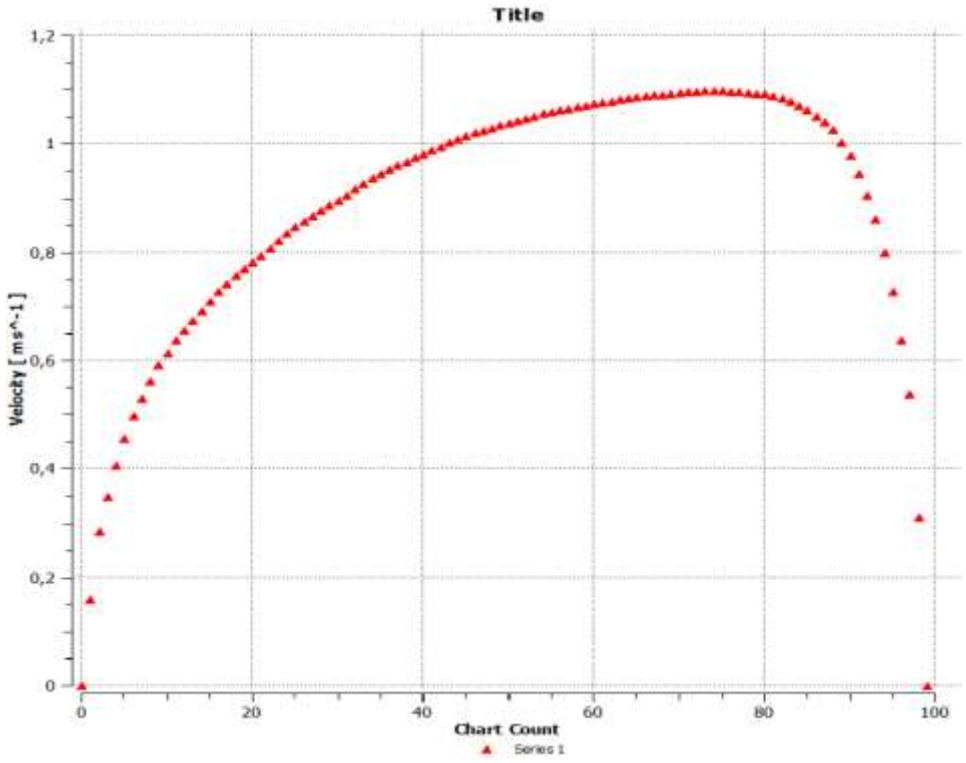

Figure III.15: Velocity profile at the outlet

The velocity profile in **figure III.15** is located at the outlet area; it is plotted to show the maximum magnitude in this section. The velocity reaches 1.1 m/s beside the opposite wall of the flow direction. In this side, the profile is logarithmic; it means that the flow is fully turbulent. In the other side, the turbulence seems not developed according to the velocity profile.

The same conclusion is drawn from the velocity contours in **figure III.16**. High velocity magnitude in this section is not only the result of the heat transfer and density differences but mainly by the geometry. This geometry is carefully selected to simplify the velocity and then the flow rate measurement and minimize relative errors in the experiment task. Subsequently, good agreement attained with experimental results when comparing velocity profiles.

Upon a careful observation at the mid-plan of the SC, we notice that the velocity near both sides is greater than at the middle section. This imbalance is due to the turbulence. By identifying the gradient in the contour plot, we ensure that large-scale vortexes are generated.

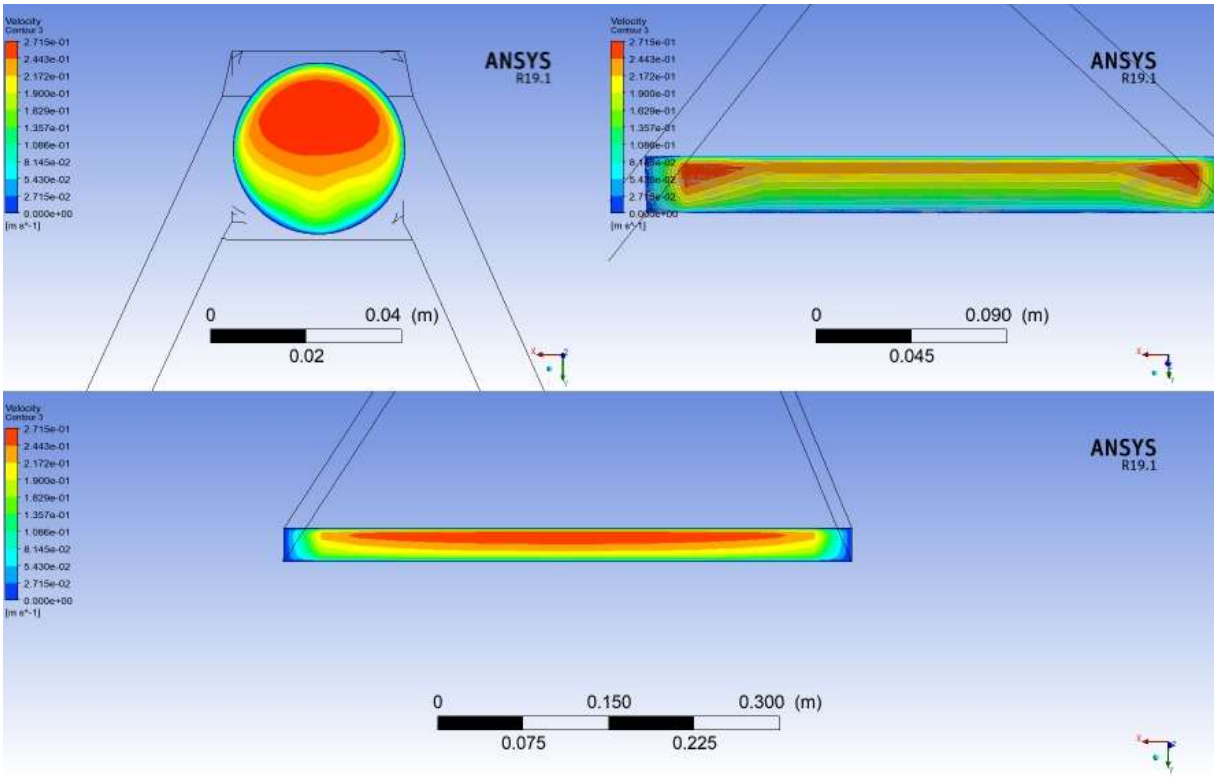

Figure III.16 : Velocity contours at the inlet, mid-plane and outlet

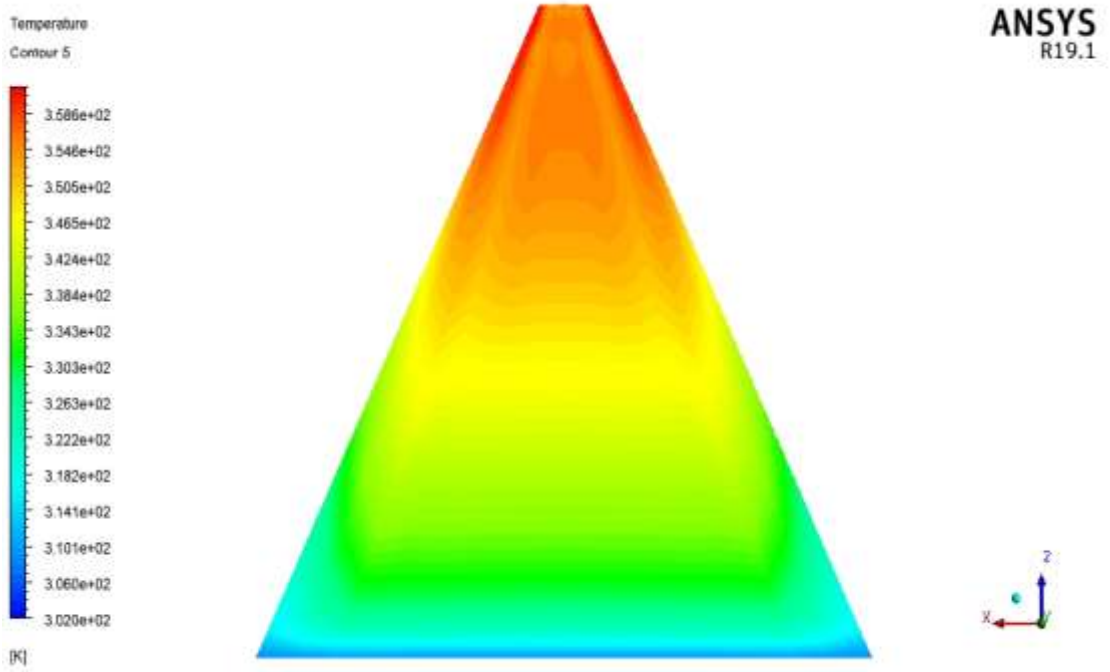

Figure III.17 : Temperature contours at the glazing

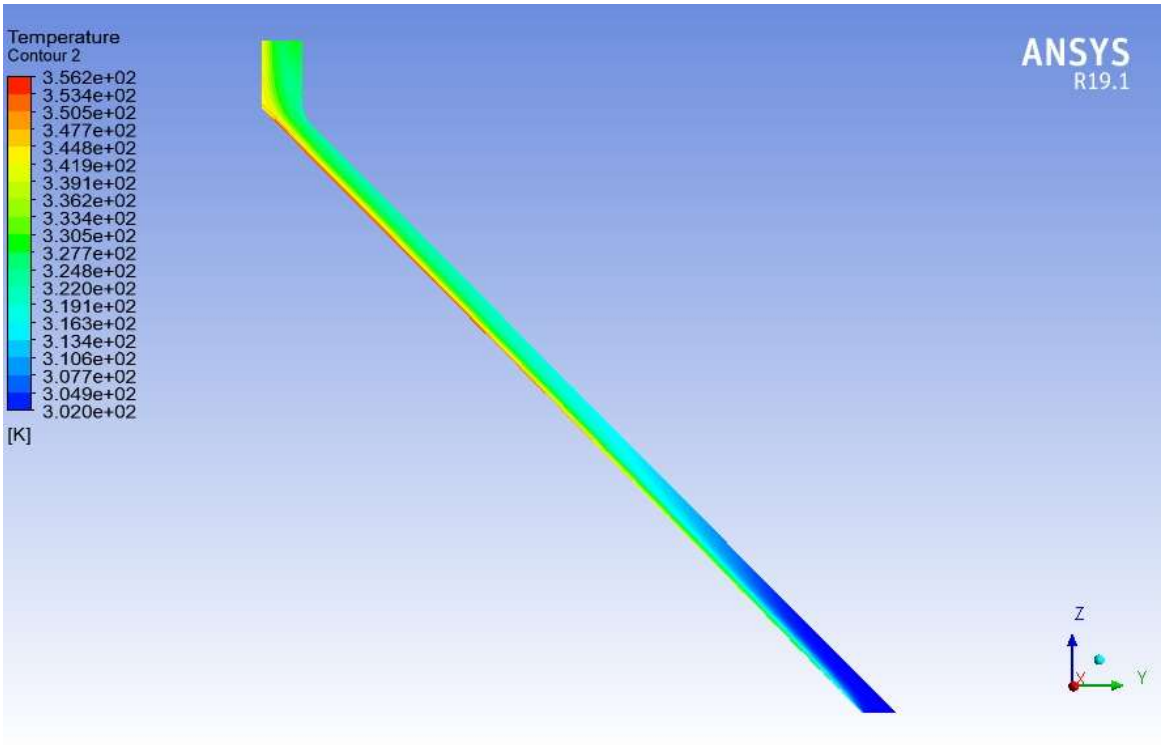

Figure III.18: Temperature contours at the longitudinal mid-plan YZ

Figure III.18 is the temperature distribution contours at the longitudinal mid-plan; with a closer look at the temperature distribution, we observe that there is a large change in air temperature between the inlet and the outlet. Fresh air comes into the chimney and began to take thermal energy by different modes of heat transfer, the same tendency is noticeable in the glazing temperature contours (**Fig. III.17**). This tendency is the required process using the solar chimney; it has direct impact on the air density that will decrease and then assist air to move out the system improving the ventilation mechanism. A temperature gradient is also happen from the absorber in perpendicular direction; this is due to the heat exchange process between the absorber and the air mainly by convection, this is evidently shown in **figure III.19**.

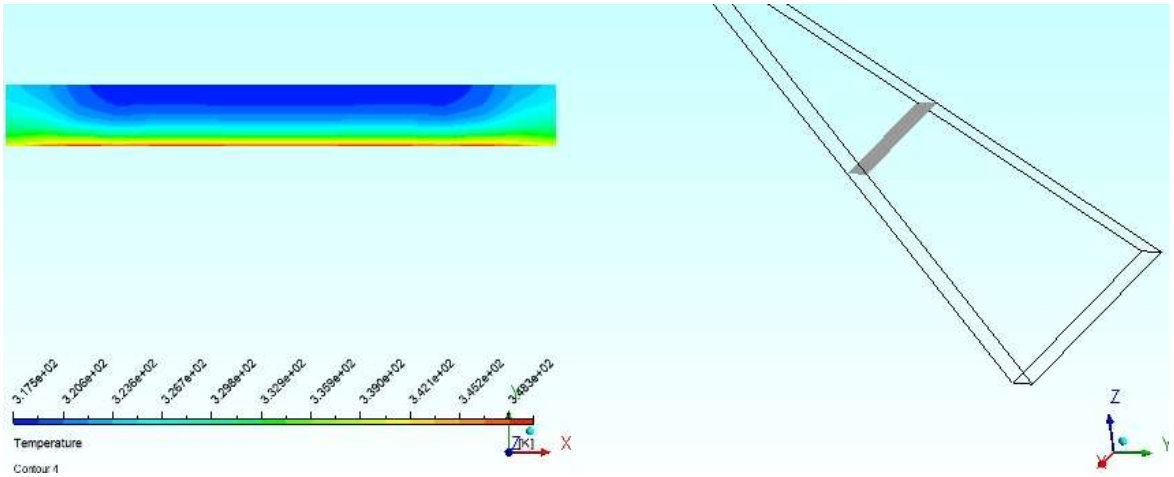

Figure III.19: Temperature contours at the transversal mid-plan

X. Wind effect on the solar chimney exhaust

X.1. Introduction

The wind can have a significant impact on building ventilation. It creates a fascinating phenomenon known as "pressure drop" between the windward side and the leeward side of a building. This pressure difference plays a crucial role in ensuring proper airflow and ventilation inside buildings known as wind-driven ventilation. By harnessing this natural force, we can optimize indoor air quality and create a healthy and comfortable indoor environment. By understanding how wind affects ventilation, we can optimize our buildings to maximize energy efficiency and improve occupant well-being.

X.2. Description

In this section, we try to boost the ventilation system using the wind impact on the chimney exhaust. The task is to define how wind interacts with the chimney exhaust to enhance air circulation. When wind blows, with an appropriate geometry at the chimney exhaust, such as the venturi, it creates a pressure drop that can boost the flow go across the chimney and gives better ventilation. Moreover, the adopted system can serves the following purposes

- Improve the solar chimney performance
- Extend the ventilation process during night-time or cloudy days
- serves as a chimney cap keeping out rainwater, snow and debris going down the chimney

- Prevent animals mainly birds from building nests inside the chimney
- Prevent undesirable wind interference

In order to catch advantageous contribution of wind and prevent undesirable wind interference, the chimney top should be strategically positioned. A vane tail is designed to allow the device caches the wind direction (**Figure III.20**). When mounted on the system, the vane rotates under the influence of the wind such that its center of pressure to leeward and the vane directs the assembly into the wind direction.

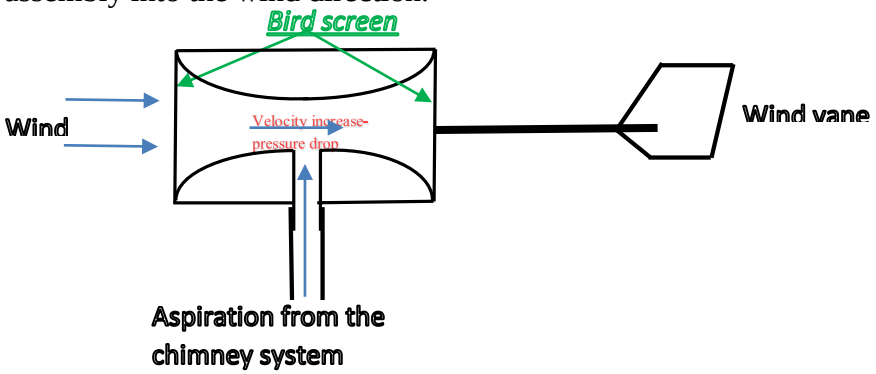

Figure III.20: Chimney cap arrangement for wind assistance

X.3. CFD model

The numerical simulation for this section is done using a 2D computational fluid dynamics model. For the natural ventilation prediction, the fluid is Newtonian; the flow is considered incompressible and turbulent, standard k-ε model with a standard wall functions is used. Material properties are independent of temperature except the density in buoyancy term; Density variation caused by temperature rise is expressed using Boussinesq approximation.

X.4. Boundary conditions

X.4.1. Inlet

At the inlet section of the solar chimney, Pressure inlet boundary condition is set to define the fluid pressure, Pressure inlet boundary conditions is used since the flow rate and velocity are not known. The total (gauge) pressure is set to zero at the inlet, and the inflow is normal to the inlet. The incoming air is at the reference temperature.

Differently, at the wind channel inlet, the incoming velocity value is imposed normal to the inlet as the wind velocity.

X.4.2. Outlet

At the outlet area, we consider the pressure outlet boundary condition; it is assumed that the stream wise variations of all velocity components and temperature are negligible. In case of a backflow at the exit, his velocity is supposed to be normal to the exit boundary and the backflow temperature is at the reference temperature.

X.4.3. Walls

No slip boundary conditions are adopted on solid boundaries. A constant heat flux is imposed at the absorber wall. All the other walls are adiabatic.

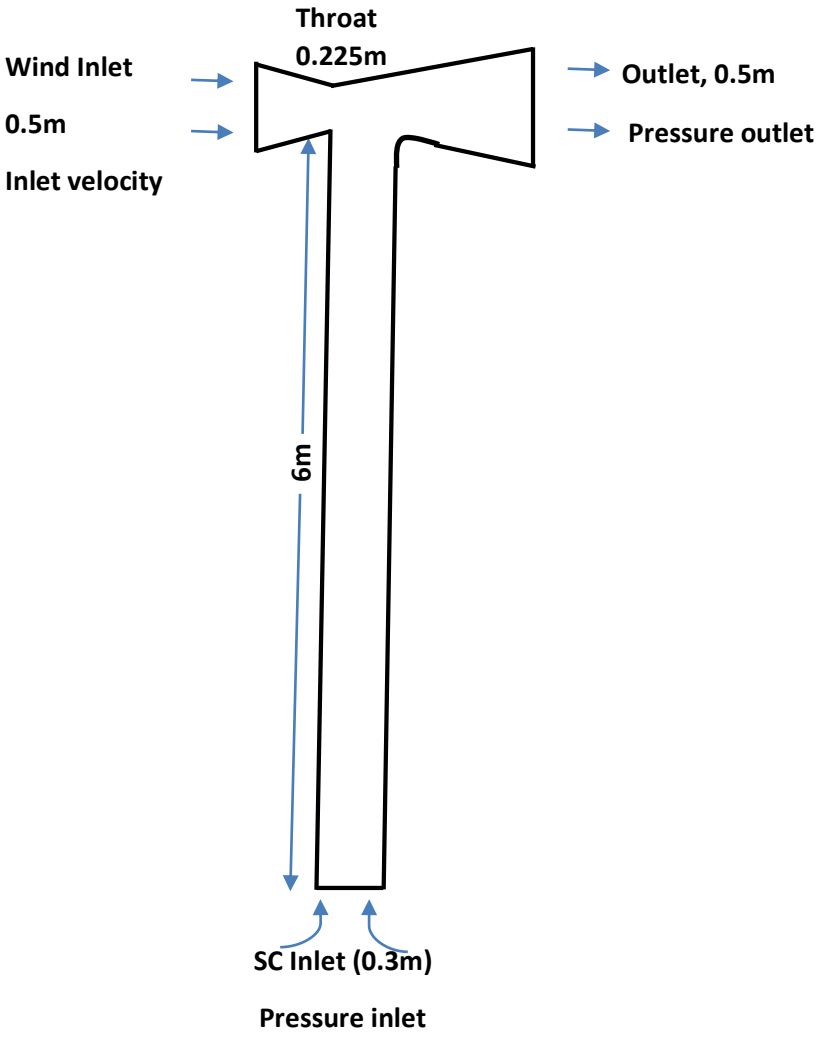

Figure III.21: Geometry and boundary conditions

X.5. Computational grid

The computational domain is divided into 9057 elements and 9389 nodes which is sufficient to get appropriate results. The Quadrilateral method is used. Detail of the meshing is presented in **table X.1**

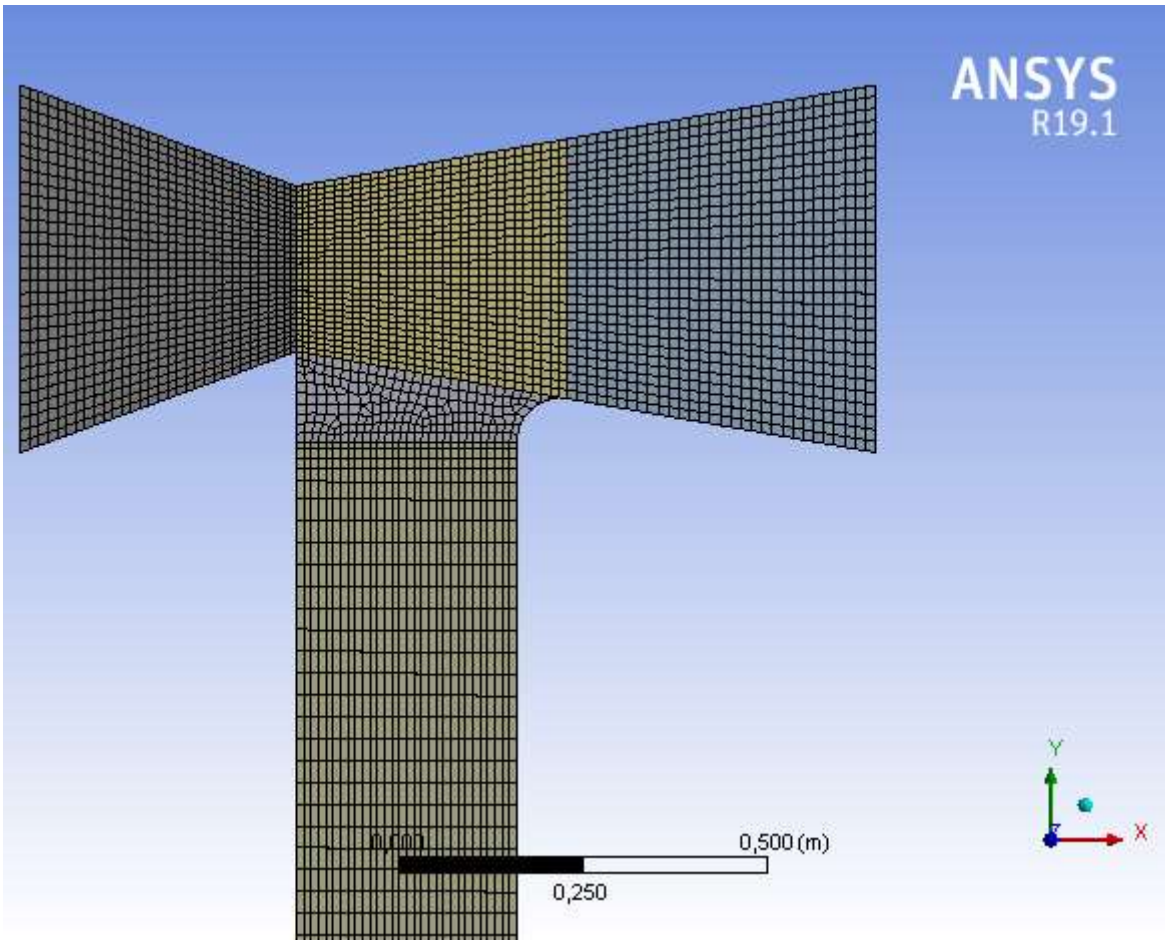

Figure III.22. Mesh generated

Object Name	*Corps surfacique*	*Corps surfacique*	*Corps surfacique*	*Corps surfacique*	*Corps surfacique*
State	Meshed				
Graphics Properties					
Visible	Yes				
Transparency	1				
Definition					
Suppressed	No				
Coordinate System	Default Coordinate System				

Thickness	1,e-003 m				
Thickness Mode	Refresh on Update				
Behavior	None				
Reference Frame	Lagrangian				
Material					
Assignment					
Fluid/Solid	Defined By Geometry (Solid)				
Bounding Box					
Length X	0,41887 m	0,36922 m		0,3 m	0,37564 m
Length Y	0,5 m	0,35379 m	0,12262 m	5,8774 m	0,5 m
Properties					
Volume	1,7881e-004 m³	1,0684e-004 m³	3,0058e-005 m³	1,7632e-003 m³	1,3615e-004 m³
Centroid X	0,59061 m	0,19831 m	0,14315 m	0,15 m	-0,21158 m
Centroid Y	6,1125 m		5,9269 m	2,9387 m	6,1125 m
Centroid Z	0, m				
Surface Area(approx.)	0,17881 m²	0,10684 m²	3,0058e-002 m²	1,7632 m²	0,13615 m²
Statistics					
Nodes	961	992	244	6324	992
Elements	900	930	207	6090	930
Mesh Metric	None				

Table III.1: Geometry and mesh characteristics

X.6. Results and discussion

The pressure distribution in a solar chimney is the key factor that drives the airflow within the chimney. A solar chimney operates on the principle of buoyancy-driven natural convection. The sun's energy heats the air trapped in the channel, causing it to become warmer and less dense as shown in **figures III.23**. This warm, low-density air is lighter than the surrounding cooler air, creating a pressure difference between the base of the chimney and the outside environment.

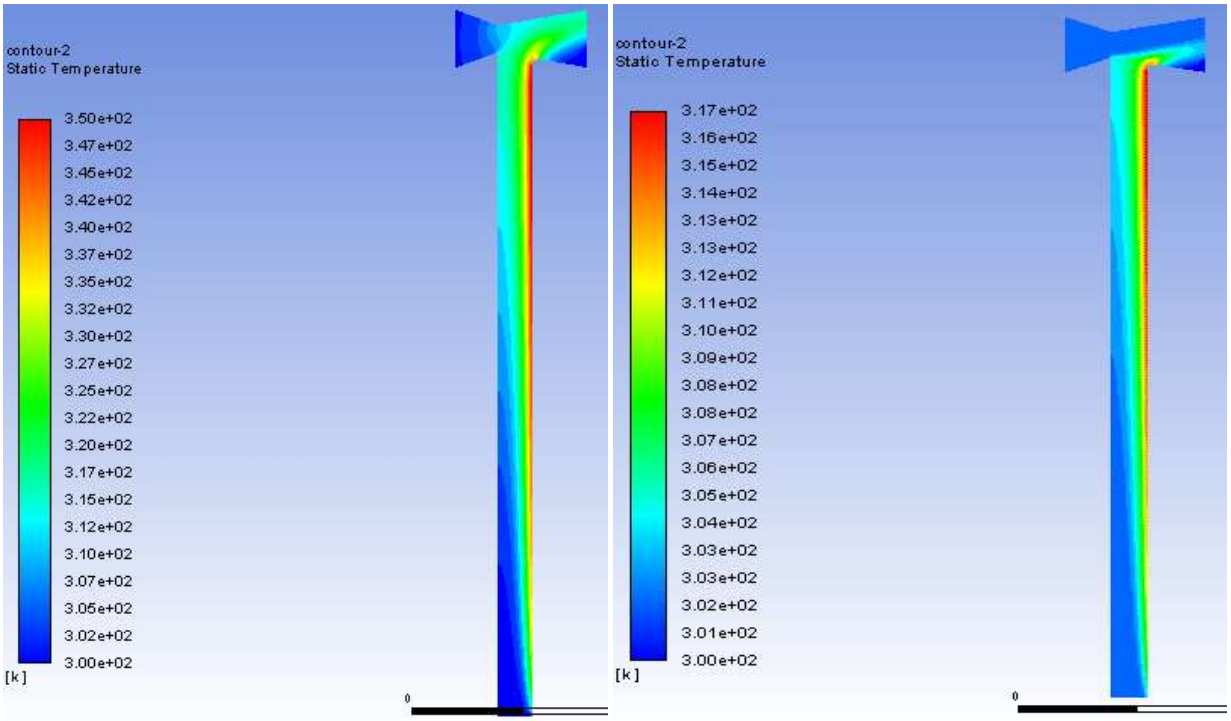

(V_{wind}=0 m/s) **(V_{wind}=0.1 m/s)**

Figure III.23: Temperature contours in the CFD domain

As the heated air rises, it flows upward through the chimney. The air's buoyancy causes it to move from the high-pressure area at the base (cooler ambient air) to the low-pressure area at the top (warmer rising air). As the air ascends, it maintains a pressure gradient along the height of the chimney, with higher pressure at the base and lower pressure at the top **(Figure III.24)**.

In the convergent-divergent (CD) channel, the pressure contours vary along the length of the channel due to changes in the channel's geometry and the fluid's behavior. The pressure contours in a CD channel depend on the flow regime, fluid properties, and the specific design of the channel. Here, the CD channel is used to create a pressure drop in the SC exhaust using the wind power. **Figure III.24** shows the pressure distribution in the SC and the CD as a wind channel.

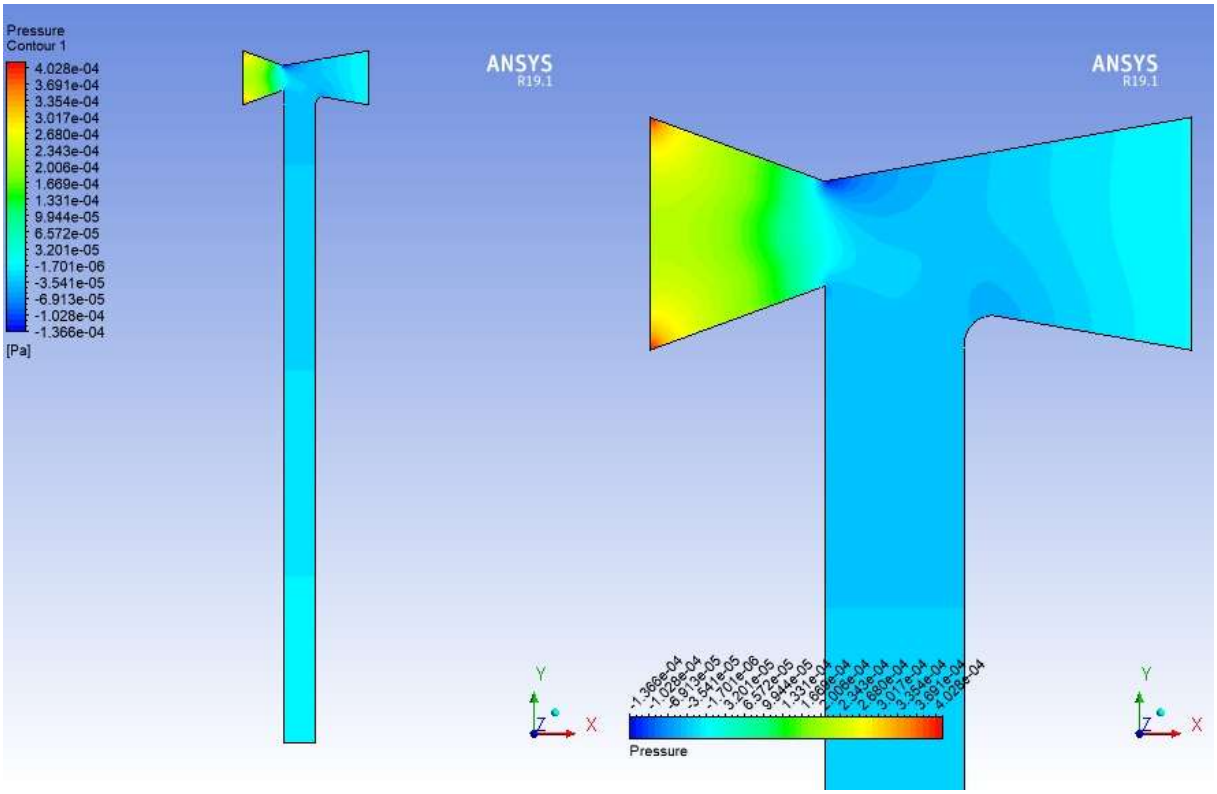

Figure III.24: Pressure distribution in the SC and wind channel CD (V_{wind}=0.1m/s)

In the convergent section of the channel, the flow is accelerated as the cross-sectional area of the channel decreases. According to Bernoulli's principle, as the fluid velocity increases, the pressure decreases. The pressure contours in the convergent section typically show a gradual decrease in pressure from the inlet towards the throat.

The throat is the narrowest part of the channel. At this point, the flow reaches its highest velocity **(Figure III.25)**, and the pressure is at its lowest value. The pressure contours at the throat show the lowest pressure value along the channel **(Figure III.24)**. This decrease in pressure is a result of the fluid's acceleration through the converging section providing a favorable pressure gradient inside the SC and an increase in flow rate driven by the SC.

As the fluid exits the throat and enters the divergent section, the channel widens, and the flow begins to decelerate. The pressure contours in the divergent section typically show an increase from the throat to the exit.

It is important to note that the actual pressure contours can be influenced by factors such as the shape of the channel, the angle of divergence, the Mach number of the flow, and the presence of shocks.

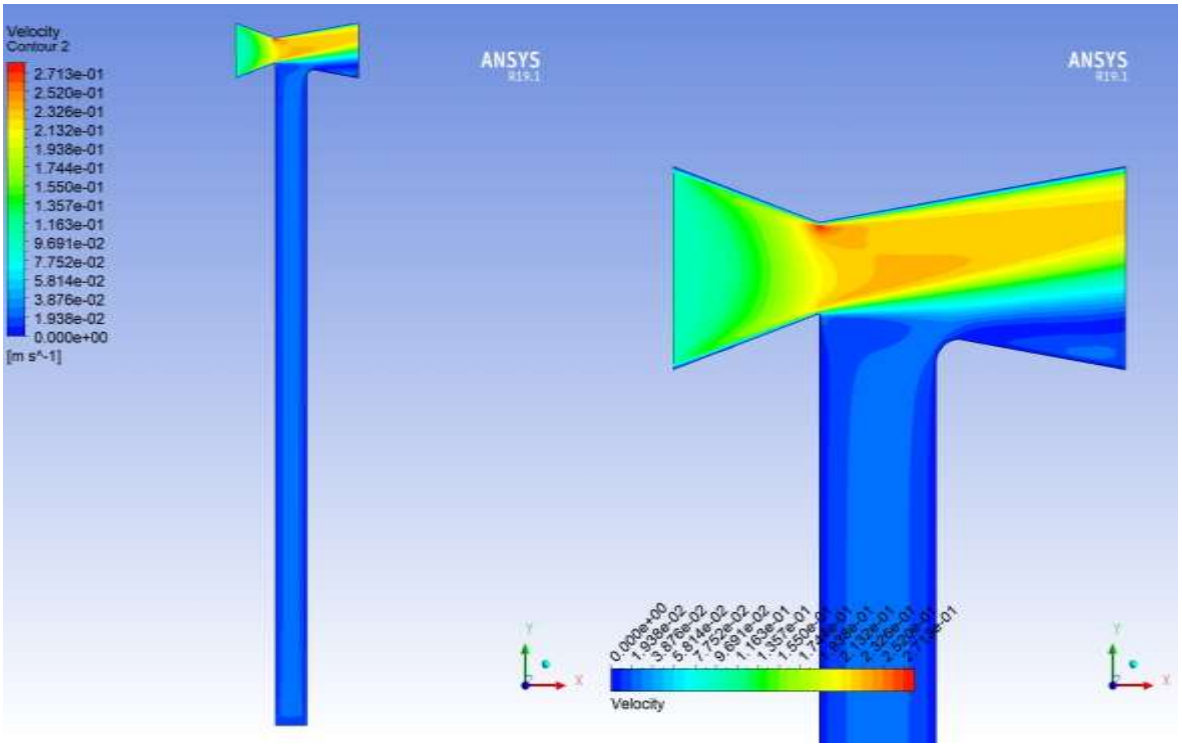

Figure III.25: Velocity contours in the CFD domain (V_{wind}=0.1m/s)

The velocity and pressure distribution in a solar chimney can be affected by various factors, such as the height and other dimensions of the chimney, the solar irradiation, the surrounding environment, and weather conditions. In this simulation, we consider only the wind effect by varying its velocity and set a constant heat flux at the absorber.

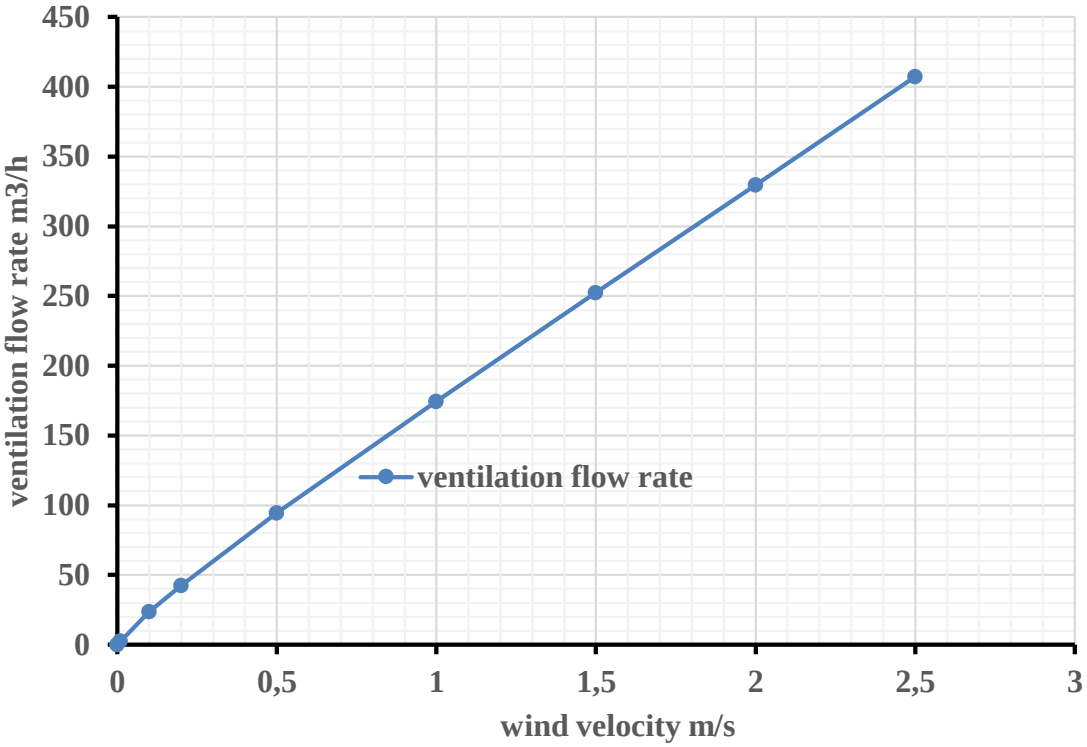

Figure III.26: Ventilation flow rate variation with wind velocity

In this case, especially under certain assumptions and simplifications, the relationship between wind speed and chimney flow rate can be approximated as linear as shown in **figure III.26.** This means that if the wind speed doubles, the flow rate would also approximately double, assuming other factors remain constant.

X.7. Conclusion

In summary, understanding the pressure distribution is crucial for designing and optimizing the efficiency of solar chimneys. Clearly, create a pressure drop at the chimney discharge area can improve significantly its performances for sunny and low or no insolation days as well as at night. As the wind is noted to have a significant effect on the chimney, the design can be done with considering the wind effect without the solar assistance.

In practice, detailed models and calculations are often used to account for these complexities and provide accurate predictions of chimney draft and flow rate under various conditions. Therefore, while a linear relationship between wind speed and chimney flow rate can serve as a basic approximation, it might not capture the full complexity of the phenomenon.

CHAPTER IV

Environmental and Economic Impact

CHAPTER IV: ENVIRONMENTAL AND ECONOMIC IMPACT

I. Introduction

Solar chimneys offer several potential benefits that can positively affect energy consumption, operational costs, and carbon dioxide emissions, thereby helping to mitigate their negative environmental impact. In solar chimneys, sun's energy create a temperature difference between the air inside the chimney and the surrounding air. This temperature difference drives the flow of air, which can be used for ventilation, cooling, or even for power generation. By utilizing solar energy, solar chimneys reduce the dependence on traditional energy sources, such as electricity or fossil fuels, this leads to lower energy consumption and decrease the demand of traditional energy sources like coal, oil, and natural gas

As a result, Using solar chimneys contribute to mitigating climate change by reducing carbon dioxide and other greenhouse gas emissions into the atmosphere.

II. Costs

An important factor to consider when deciding how much money to earmark toward each investment is the risk profile. Some investments entail more risk than others **[84].**

While solar chimneys have lower operational costs, there can be a significant initial investment required for their construction and installation. This cost might be a barrier to adoption for some projects, despite the long-term benefits. Any solar system has many cost components; the total cost is the sum of all the following individual costs:

Engineering cost: it is the cost of the study carried out by a design office

Equipment cost: Sometimes equipment costs are spread out over many suppliers, the equipment cost is the sum of the costs of all the procurement.

Installation costs: Depending on the complexity of the job, the cost of installation is fixed even If you are a do-it-yourselfer.

Maintenance costs: is the servicing cost that may occur, as cleaning or retrofitting. Solar chimneys, like any other infrastructure, require maintenance to ensure their continued efficiency. Proper maintenance is essential to prevent degradation over time and to maximize their lifetime.

III. Energy save

The solar chimney was simulated in RETScreen4 to estimate the thermal energy gain during a year; it shows the technical evaluation and an outlook of economic and environmental benefits.

The solar chimney system performance was simulated as a non-operating fan during the solar radiated period. The economic inputs were based on cost estimated and suggested values.

The selected location of climate data in RETScreen database Tlemcen/Zenata in figure 8 (is near the experiment location 10Kilometers).

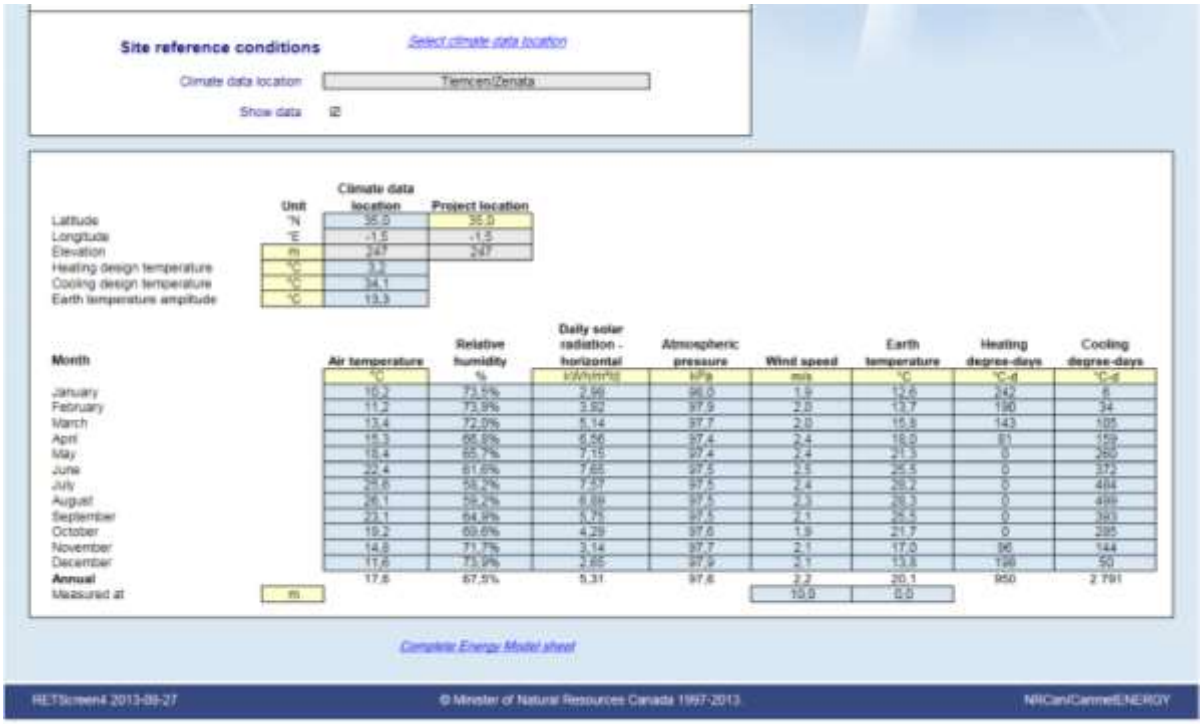

Figure IV.1: Climate data in RETScreen database (Tlemcen/Zenata)

The power of the fan was calculated by using the experimental data, The air flow is given from (Eq. II.6) and measured air velocity and then converted into the power of electrical motor driving the fan using a rule-of-thumb of 475 L/s per kilowatt (750 cfm/hp) of fan motor capacity [85]. The required airflow is that given in table IV.1 [1].

Table IV.1: Total Ventilation Air Requirements

Area Based	Occupancy Based
0.10 L/s per square meter of floor space	8 L/s per person, based on normal occupancy

IV. payback

The RETScreen model is capable to perform a detailed economic analysis using some cost and interest parameters such as discount and inflation rates, GHG (greenhouse gases) emission reduction credit, project life, energy cost, escalation rate, etc. The inflation rate of 4% and 30 years project life are used. An estimated initial cost is also used; the electricity price is given from the national electricity provider invoice.

In term of GHG emission, the results show that using an efficient solar chimney in ventilation system in a 120 m2 floor space house save the equivalent of 23.9 liters of gasoline (Fig. IV.2).

The economic analysis show that the payback period is 16.3 years; it means a desirable investment.

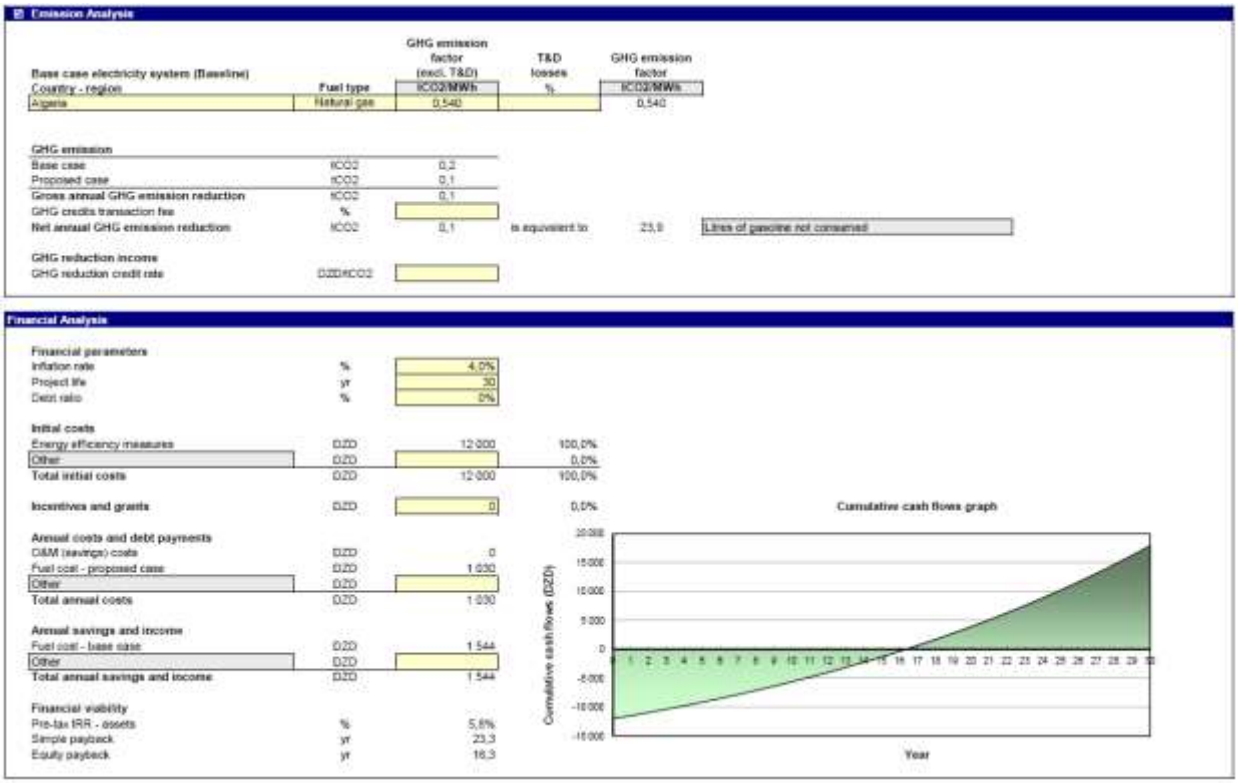

Figure IV.2: Emission and financial analysis

V. Conclusions

Solar chimney has a potential benefits in terms of: energy requirement, operational cost and carbon dioxide emission, which has a negative environment impact. An approach using RETScreen4 software with experimental input data was carried out, it confirmed that 1m² of solar chimney installed in favorable conditions could cover 37m² of living space in term of ventilation. For a medium building (120m²) ventilated by a solar chimney system saves an equivalent of 23.9 liters of gasoline per year.

Conclusion

Conclusion

Energy efficiency in buildings becomes increasingly an important strategy to reduce energy use and pollution. Natural ventilation can offer significant benefits in term of thermal comfort and energy consumption. Solar chimney is one of the simplest and efficient system used to improve natural ventilation. As well as building characteristics, the design of solar chimney depends on several factors. A review of scientific researches on the topic reveal several aspects and gives very useful feedback.

The main factors examined in this work are the geometry and the wind effect. Encouraging result is obtained; it show that solar chimney can significantly contribute in natural ventilation rate.

Experimental study is used to investigate trapezoidal-prism solar chimney behavior; three chimneys with different height to base length ratio h/l (1, 1.5 and 2) are used. Two correlations were developed to predict air velocity and thermal efficiency; it was found that:

- Air velocity increase by increasing h/l in a logarithmic tendency
- The optimum thermal efficiency can be taken by h/l=1.65

The wind contribute considerably not only in cross ventilation but also on stack ventilation by acting on the chimney exhaust. An adopted geometry helps create a depression at the outlet of the chimney. By using an appropriate geometry at the top of the solar chimney, the wind can significantly improve the solar chimney performances. Clearly, create a pressure drop at the chimney discharge area can improve its performances for sunny and low or no insolation days as well as at night. Considering the wind effect on the chimney, the design can be done even without the solar assistance.

The economic and environment benefits were also studied with retscreen4 software. It shows that:

- Using an efficient solar chimney in ventilation system in a 120 m^2 floor space house saves the equivalent of 23.9 liters of gasoline
- The payback period is 16.3 years

Finally, as a perspective, we propose as an interesting research axis related to studying experimentally and numerically the effects of various factors on solar chimney and investigate how different modifications impact the performance of the system. The proposed study aspects are:

Effect of Fins in the Absorber: Adding fins to a heat-absorbing surface is a common technique to enhance heat transfer. Fins increase the surface area exposed to the heat source,

which can lead to more efficient heat transfer. You could experiment with fins of different dimensions (length, thickness, and spacing) and study how they impact the ventilation rate.

Effect of Ribs: The addition of ribs or baffles in fluid flow systems can influence the flow patterns, pressure drop, and heat transfer. By studying this case, we explore how different rib shapes, sizes, and arrangements affect fluid flow distribution and heat exchange. This could involve measuring pressure drops and temperature variations across chimney, as well as using numerical simulations to visualize flow patterns.

Each of these aspects requires careful experimental setup and numerical modeling to ensure accurate and reliable results. Combining experimental data with numerical simulations allows to validate and refine the model and provide valuable insights into improving the efficiency and effectiveness of the systems in various cases.

References

[1] American Society of Heating, Refrigeranting and Air-conditioning Engineers (ASHRAE) "Chapter 26: Ventilation and Infiltration",
In: 2001 ASHRAE Fundamentals Handbook, ASHRAE, Atlanta, GA, USA, 2001, pp. 26.1–26.32 ASHRAE Handbook 2001, chapter 26 ventilation and infiltration

[2] Rakesh, K., Chengwang, L. Solar chimney—"A passive strategy for natural ventilation", Energy and Buildings, 43, pp. 1811–1819, 2011.
https://doi.org/10.1016/j.enbuild.2011.03.035

[3] Chan, H.-Y., Riffat, S. B., Zhu, J. "Review of passive solar heating and cooling technologies", Renewable and Sustainable Energy Reviews, 14(2), pp. 781–789, 2010. https://doi.org/10.1016/j.rser.2009.10.030

[4] C. Jiménez-Xamán, J. Xamáná, M. Gijon-Rivera, I. Zavala-Guillén, F. Noh-Pat, E. Simá, "Assessing the thermal performance of a rooftop solar chimney attached to a single room" Journal of Building Engineering 31 (2020) 101380
https://doi.org/10.1016/j.jobe.2020.101380

[5] Afonso, C., Oliveira, "A. Solar chimneys: simulation and experiment", Energy and Buildings, 32, pp. 71–79, 2000.
https://doi.org/10.1016/S0378-778899)00038-9

[6] Karima E. A., Saif W. M. "Experimental and numerical studies of solar chimney for natural ventilation in Iraq", Energy and Buildings, 47, pp.450–457, 2012. https://doi.org/10.1016/j.enbuild.2011.12.014

[7] Wenting, D., Yuji, H., Tokiyoshi, Y. "Natural ventilation performance of a double-skin façade with a solar chimney", Energy and Buildings, 37, pp.411–418, 2005.
https://doi.org/10.1016/j.enbuild.2004.08.002

[8] Ong, K.S. "A mathematical model of a solar chimney", Renewable Energy, 28, pp. 1047–1060, 2003.
https://doi.org/10.1016/S0960-148102)00057-5

[9] Xinyu Zha, Jun Zhang, and Menghao Qin. "Experimental and Numerical Studies of Solar Chimney for Ventilation in Low Energy Buildings", Procedia Engineering 205 pp. 1612–1619, 2017
https://doi.org/10.1016/j.proeng.2017.10.294

[10] https://urbanecologycenter.org/ (accessed December 2022)

[11] G. Gan, S.B. Riffat "A numerical study of solar chimney for natural ventilation of buildings with heat recovery" Applied Thermal Engineering 18 (1998) 1171–1187
https://doi.org/10.1016/S1359-4311(97)00117-8

[12] Kwang Ho Lee, Richard K. Strand "Enhancement of natural ventilation in buildings using a thermal chimney" Energy and Buildings 41 (2009) 615–621
doi:10.1016/j.enbuild.2008.12.006

[13] B. Zamora, A.S. Kaiser " Optimum wall-to-wall spacing in solar chimney shaped channels in natural convection by numerical investigation" Applied Thermal Engineering 29 (2009) 762–769
doi:10.1016/j.applthermaleng.2008.04.010

[14] Guohui Gan "Simulation of buoyancy-driven natural ventilation of buildings-Impact of computational domain" Energy and Buildings 42 (2010) 1290–1300
doi:10.1016/j.enbuild.2010.02.022

[15] Wenting Ding, Yoshikazu Minegishi, Yuji Hasemi, Tokiyoshi Yamada, "Smoke control based on a solar-assisted natural ventilation system" Building and Environment 39 (2004) 775–782
doi:10.1016/j.buildenv.2004.01.002

[16] Evangellos Bacharoudis, Michalis Gr. Vrachopoulos, Maria K. Koukou, Dionysios Margaris, Andronikos E. Filios, Stamatis A. Mavrommatis, " Study of the natural convection phenomena inside a wall solar chimney with one wall adiabatic and one wall under a heat flux" Applied Thermal Engineering 27 (2007) 2266–2275
doi:10.1016/j.applthermaleng.2007.01.021

[17] Yicun Hou, Huang Li, Angui Li, " Experimental and theoretical study of solar chimneys in buildings with uniform wall heat flux" Solar Energy 193 (2019) 244–252
https://doi.org/10.1016/j.solener.2019.09.061

[18] Wei, D., Qirong, Y., Jincui, Z. "A study of the ventilation performance of a series of connected solar chimneys integrated with building", Renewable Energy, 36, pp.265-271, 2011 https://doi.org/10.1016/j.renene.2010.06.030

[19] Ramadan, B., Nader, S.A. K. "Effect of solar chimney inclination angle on space flow pattern and ventilation rate", Energy and Buildings, 41, pp.190–196, 2009. https://doi.org/10.1016/j.enbuild.2008.08.009

[20] Mathur, J., Mathur, S., Anupma,. "Summer-performance of inclined roof solar chimney for natural ventilation", Energy and Buildings, 38, pp1156-1163, 2006. https://doi.org/10.1016/j.enbuild.2006.01.006

[21] Jing, K., Jianlei, N., Chengwang, L. "A CFD based approach for determining the optimum inclination angle of a roof-top solar chimney for building ventilation", solar energy, 198, pp. 555-569 2020. https://doi.org/10.1016/j.solener.2020.01.017

[22] Sakonidou, E.P., Karapantsios, T.D., Balouktsis , A.I., Chassapis, D. "Modeling of the optimum tilt of a solar chimney for maximum air flow", Solar Energy, 82, pp.80–94, 2008 . https://doi.org/10.1016/j.solener.2007.03.001

[23] Chen, Z.D., Bandopadhayay, P., Halldorsson, J., Byrjalsen, C., Heiselberg, P., Lic, Y. "An experimental investigation of a solar chimney model with uniform wall heat flux", Building and Environment, 38, pp.893 – 906, 2003. https://doi.org/10.1016/S0360-132303)00057-X

[24] Saifi , N., Settou , N. ,Dokkar , B., Negrou, B., Chennouf, N. "Experimental study and simulation of airflow in solar chimneys", Energy Procedia, 18, pp.1289 – 1298, 2012 . https://doi.org/10.1016/j.egypro.2012.05.146

[25] https://broadtechengineering.com/cfd-flow-analysis/solar-chimney (accessed December 2022)

[26] Rakesh Khanal and Chengwang Lei, Flow reversal effects on buoyancy induced air flow in a solar chimney, Solar Energy 86 (2012) 2783–2794 http://dx.doi.org/10.1016/j.solener.2012.06.015

[27] Long Shi, Guomin Zhang, Wei Yang, Dongmei Huang, Xudong Cheng, Sujeeva Setunge. "Determining the influencing factors on the performance of solar chimney in buildings" Renewable and Sustainable Energy Reviews · volume 88 Pages 223-238, May 2018 https://doi.org/10.1016/j.rser.2018.02.033

[28] Hussein J. Mohammed, Abbas J. Jubear, Haddi Obaid "Natural Ventilation in Passive System of Vertical Two-Stores Solar Chimney" Journal of Advanced Research in Fluid Mechanics and Thermal Sciences, Volume 69, Issue 2 (2020) 130-146 https://doi.org/10.37934/arfmts.69.2.130146

[29] T V Nguyen and Y Quoc Nguyen, "Performance of a solar chimney configuration to achieve equal flow rate for ventilation of three-story building" IOP Conf. Series: Materials Science and Engineering 1109 (2021) 012001 doi:10.1088/1757-899X/1109/1/012001

[30] Duen-Sheng Lee, Tzu-Chen Hung, Jaw-Ren Lin, Jun Zhao, "Experimental investigations on solar chimney for optimal heat collection to be utilized in organic Rankine cycle" Applied Energy 154 (2015) 651–662 http://dx.doi.org/10.1016/j.apenergy.2015.05.079

[31] D.J. Harris , N. Helwig "Solar chimney and building ventilation", Applied Energy 84 (2007) 135–146 doi:10.1016/j.apenergy.2006.07.001

[32] Bansal N.K, Mathur R, Bhandari M.S. Solar chimney for enhanced stack ventilation. Build Environ. 1993;28:373-7. https://doi.org/10.1016/0360-1323(93)90042-2

[33] Pillai, P. K. C., & Agarwal, R. C. (1981). Factors influencing solar energy collector efficiency. Applied Energy, 8(3), 205–213. doi:10.1016/0306-2619(81)90018-0

[34] Nouanégué, H. F, & Bilgen, E. (2009). Heat transfer by convection, conduction and radiation in solar chimney systems for ventilation of dwellings. International Journal of Heat and Fluid Flow, 30(1), 150–157. doi:10.1016/j.ijheatfluidflow.2008.08.006

[35] Dordelly, J.C.F.; El Mankibi, M.; Roccamena, L.; Remiona, G.; Landa, J.A. "Experimental analysis of a PCM integrated solar chimney under laboratory conditions". Solar Energy 2019, 188, 1332–1348 https://doi.org/10.1016/j.solener.2019.06.065

[36] Tiji, M. E., Eisapour, M. Yousefzadeh, R., Azadian, M., & Talebizadehsardari, P. (2020). A numerical study of a PCM-based passive solar chimney with a finned absorber. Journal of Building Engineering, 32, 101516. https://doi.org/10.1016/j.jobe.2020.101516

[37] Bernardo Buonomo, Lucia Capasso, Alessandra Diana, Oronzio Manca1 and Sergio Nardini "A Numerical Analysis on a Solar Chimney with an Integrated Latent Heat Thermal Energy Storage" 74th ATI National Congress AIP Conf. Proc. 2191, 020029-1–020029-10; https://doi.org/10.1063/1.5138762

[38] Souayfane, F., Fardoun, F., & Biwole, P.-H. "Phase change materials (PCM) for cooling applications in buildings: A review". Energy and Buildings, 129, 396–431. http://dx.doi.org/10.1016/j.enbuild.2016.04.006

[39] Faraj, K., Khaled, M., Faraj, J., Hachem, F., & Castelain, C. (2019). Phase change material thermal energy storage systems for cooling applications in buildings: A review. Renewable and Sustainable Energy Reviews, 109579. doi:10.1016/j.rser.2019.109579

[40] Miyazaki, T., Akisawa, A., & Kashiwagi, T. (2006). The effects of solar chimneys on thermal load mitigation of office buildings under the Japanese climate. Renewable Energy, 31(7), 987–1010. doi:10.1016/j.renene.2005.05.003

[41] Arce, J., Xamán, J. P., Álvarez, G., Jiménez, M. J., Enríquez, R., & Heras, M. R. (2012). A Simulation of the Thermal Performance of a Small Solar Chimney Already Installed in a Building. Journal of Solar Energy Engineering, 135(1), 011005. doi:10.1115/1.4007088

[42] Abdullahi, S. Ayegba, Musa Abdul, and Adejoh Joshua "Impacts of Relative Humidity and Mean Air Temperature on Global Solar Radiations of Ikeja, Lagos, Nigeria" International Journal of Scientific and Research Publications, Volume 7, Issue 2, February 2017

[43] O. T. Kolebaje, a. Ikusika & P. Akinyemi "Estimating solar radiation in ikeja and port harcourt via correlation with relative humidity and temperature" int. j. of energy prod. & mgmt., vol. 1, no. 3 (2016) 253–262 DOI: 10.2495/EQ-V1-N3-253-262

[44] Yang, K., & Koike, T. (2002). Estimating surface solar radiation from upper-air humidity. Solar Energy, 72(2), 177–186. doi:10.1016/s0038-092x(01)00084-6

[45] https://www.carboun.com/sustainable-design/a-damascus-school-revives-traditional-cooling-techniques (accessed December 2022)

[46] Tariq Ahmed , Prashant Kumar , Laetitia Mottet, "Natural ventilation in warm climates: The challenges of thermal comfort, heatwave resilience and indoor air quality". Renewable and Sustainable Energy Reviews 138 (2021) 110669 https://doi.org/10.1016/j.rser.2020.110669

[47] Mahnoosh Eghtedari, Abbas Mahravan. "evaluation a hybrid passive cooling system for a building using experimental and commercial software (design builder)" journal of renewable energy and environment Vol. 8, No. 2, (2021) 74-80 https://doi.org/10.30501/jree.2021.239940.1131

[48] Gao, N.; Yan, Y.; Sun, R.; Lei, Y. Natural Ventilation Enhancement of a Roof Solar Chimney with Wind-Induced Channel. Energies 2022, 15, 6492. https://doi.org/10.3390/en15176492

[49] Ammar Bouchair, PhD, Pr "The effect of the altitude on the performance of a solar chimney" Energy 249 (2022) 123704

https://doi.org/10.1016/j.energy.2022.123704
[50] Zhang, H.; Tao, Y.; Shi, L. Solar Chimney Applications in Buildings. Encyclopedia 2021, 1, 409–422. https://doi.org/10.3390/encyclopedia1020034
[51] Asfour, O. Natural ventilation in buildings: An overview. In Natural Ventilation: Strategies, Health Implications and Impacts on the environment; Nova Science Pub Inc.: New York, NY, USA, 2015; pp. 1–26.
[52] Lal, S., Kaushik, S.C. and Bhargav, P.K. (2013), "Solar chimney: A sustainable approach for ventilation and building space conditioning", International Journal of Development and Sustainability, Vol. 2 No. 1, pp. 277-297
[53] Shiv Lal, Subhash Chand Kaushik. CFD Simulation Studies on Integrated Approach of Solar Chimney and Earth Air Tunnel Heat Exchanger for Building Space Conditioning. International Journal of Economy, Energy and Environment. Vol. 2, No. 3, 2017, pp. 32-39. doi: 10.11648/j.ijeee.20170203.11
[54] Li, Y., Long, T., Bai, X., Wang, L., Li, W., Liu, S., … Huang, S. (2021). An experimental investigation on the passive ventilation and cooling performance of an integrated solar chimney and earth–air heat exchanger. Renewable Energy, 175, 486–500. doi:10.1016/j.renene.2021.05.004
[55] Maerefat, M., Haghighi, A.P. "Passive cooling of buildings by using integrated earth to air heat exchanger and solar chimney", Renewable Energy, 35, pp.2316-2324, 2010. https://doi.org/10.1016/j.renene.2010.03.003
[56] Maerefat, M., Haghighi, A.P. "Natural cooling of stand-alone houses using solar chimney and evaporative cooling cavity", Renewable Energy, 35, pp.2040–2052, 2010. https://doi.org/10.1016/j.renene.2010.02.005
[57] Raman, P., Mande, S. & Kishore, V. V. . (2001). A passive solar system for thermal comfort conditioning of buildings in composite climates. Solar Energy, 70(4), 319–329. doi:10.1016/s0038-092x(00)00147-x
[58] Zhai, X.Q., Song, Z.P., Wang, R.Z. "A review for the applications of solar chimneys in buildings", Renewable and Sustainable Energy reviews, 15, pp.3757–3767, 2011. https://doi.org/10.1016/j.rser.2011.07.013
[59] Linden, P.F. "The fluid mechanics of natural ventilation", Annual Review on Fluid Mechanics, 31, pp.201–238, 1999. https://doi.org/10.1146/annurev.fluid.31.1.201
[60] Kumar, S. J., Sinha, S., Kumar, N. "experimental investigation of solar chimney assisted bioclimatic architecture", Energy Convers. Mgmt, 39 5/6, pp.441-44, 1998. https://doi.org/10.1016/S0196-890497)00024-1
[61] **https://www.google.dz/maps/**
[62] ANSYS Fluent Theory Guide
[63] Roland Schiestel ; *"*Modélisation et simulation des écoulements turbulent*"* Edition HERMES, PARIS 1993
[64] Roland Schiestel ; *"Les écoulements turbulents"* Edition HERMES, PARIS 1998
[65] Thomas B. Gatski, M. Yousuff Hussaini, and John L. Lumley "Simulation and Modeling of Turbulent Flows" Oxford University Press; 1st edition (July 11, 1996)
[66] Pijush Kundu, Ira Cohen "fluid mechanics" second edition - August 30, 2001 ISBN: 9780080545585
[67] Alexandre J. Chorin, Jerrold E. Marsden "A mathematical introduction to fluid mechanics-Third Edition" Springer New York, NY 1993, ISBN 978-0-387-97918-2 https://doi.org/10.1007/978-1-4612-0883-9
[68] Jiyuan Tu, Chaoqun Liu, Guan-Heng Yeoh "computational fluid dynamics a practical approach-second edition" Elsevier, 2013; ISBN 978-0-08-098243-4 https://doi.org/10.1016/C2010-0-67980-6
[69] J. Blazek "Computational fluid dynamics principles and application" Elsevier 2001 ISBN: 0 08 043009 0.

[70] Steve T. Hoffmann, Klaus A.; Chiang "Computational Fluid Dynamics", Volume 2. Engineering Education System august 2000 USA. ISBN:0-9623731-3-3

[71] H. Lomax , Thomas H. Pulliam, David W. Zingg "Fundamentals of Computational Fluid Dynamics-Springer-Verlag Berlin and Heidelberg GmbH & Co. K 1999 ISBN-3540416072

[72] Hirsch C. Numerical Computation of Internal and External Flows. v1 (Elsevier, 2007)(ISBN 0750665947)

[73] Roland Schiestel "Modeling and Simulation of Turbulent Flows" Wiley-ISTE January 2010 ISBN: 978-0-470-39346-8

[74] John C. Tannehill, Richard H. Pletcher, Dale A. Anderson "Computational Fluid Mechanics And Heat Transfer" Taylor & Francis; 2e édition (15 avril 1997) ISBN-10 : 156032046X

[75] https://www.cfd-online.com/ (accessed (february2022)

[76] ANSYS Fluent Users Guide

[77] B. E. Launder and D. B. Spalding. Lectures in Mathematical Models of Turbulence. Academic Press, London, England. 1972.

[78] Wall functions | Introduction to CFD (upv.es) accessed (february2022)

[79] Fluid Mechanics 101 - YouTube accessed (february2022)

[80] B. E. Launder and D. B.Spalding. "The Numerical Computation of Turbulent Flows". Computer Methods in Applied Mechanics and Engineering. 3. 269–289. 1974.

[81] von Kármán "Mechanical Similitude and Turbulence" Tech. Mem. NACA, no. 611, 1931

[82] S. V. PATANKAR ; '' Numerical heat transfer and fluid flow '' 1980. CRC Press.

Series in computational methods in mechanics and thermal sciences, Hemisphere Publishing Corporation & Mc Graw Hill B. C. 1980

[83] H. K. Versteeg and W. Malalasekera, An introduction to computational fluid dynamics: The finite volume method, 2nd e (2007), Harlow, Pearson Prentice Hall (1995).

[84] DeGunther, Rik. Solar Power Your Home For Dummies. Hoboken, N.J., Wiley, 2008

[85] RETScreen International, Available from http://www.retscreen.net/ [Accessed: 27 August 2013]

[86] J. Baranger ; " Introduction à l'analyse numérique" Hermann. PARIS 1987

[87] B. Démidovitch, I. Maron ; "Elément de calcul numérique" Edition MIR, MOSCOU 1979